

Electronic Thesis and Dissertation Repository

9-28-2017 1:30 PM

Synthesis and Photophysical Studies of Pyrrolocytosine Derivatives

Atefeh Rouhi, *The University of Western Ontario*

Supervisor: Robert H. E. Hudson, *The University of Western Ontario*

A thesis submitted in partial fulfillment of the requirements for the Master of Science degree in Chemistry

© Atefeh Rouhi 2017

Follow this and additional works at: <https://ir.lib.uwo.ca/etd>

 Part of the [Nucleic Acids, Nucleotides, and Nucleosides Commons](#)

Recommended Citation

Rouhi, Atefeh, "Synthesis and Photophysical Studies of Pyrrolocytosine Derivatives" (2017). *Electronic Thesis and Dissertation Repository*. 5020.

<https://ir.lib.uwo.ca/etd/5020>

This Dissertation/Thesis is brought to you for free and open access by Scholarship@Western. It has been accepted for inclusion in Electronic Thesis and Dissertation Repository by an authorized administrator of Scholarship@Western. For more information, please contact wlsadmin@uwo.ca.

Abstract

Pyrrolocytosine (pC) derivatives are used in the study of nucleic acid structure, function and in the design of the hybridization probes. They have unique properties including small size and Watson-Crick base pairing capability and impressive fluorescent properties. However, they exhibit variation in the fluorescence properties upon incorporation into single-stranded DNA and double-stranded DNA.

This study analyzes the effect of the nearest neighbours on the fluorescence properties of phenylpyrrolocytosine (PhpC) and provides a guide to the proper design of the PhpC containing fluorescent probes. Moreover, the possibility of photoinduced electron transfer (PET) as the underlying mechanism of the unusual photophysical behavior of PhpC in response to different nearest neighbours is investigated by measurement of the redox potentials of the PhpC. Furthermore, the possibility of the fluorescence resonance energy transfer (FRET) between PhpC and *p*-NO₂-PhpC for potential utilization in the design of molecular beacons is investigated by fluorescence studies.

Keywords

Pyrrolocytosine (pC) derivatives, DNA, photoinduced electron transfer (PET), Fluorescence resonance energy transfer (FRET), cyclic voltammetry, Rehm-Weller equation, Stern-Volmer constant

Co-Authorship Statement

In chapter 2, the effect of the nearest neighbours on the photophysical properties of PhpC is analyzed and electrochemical studies were performed to investigate the underlying mechanism of PhpC's unusual photophysical properties.

The photophysical data has appeared in Azizi, F. *Photophysical Properties of Single- and Double-Stranded DNA containing 6-Phenylpyrrolocytosine (PhpC)*. M.Sc. Thesis, 2012 and was shared with me for further analysis.

Moreover, Dr. S. Barbon assisted me with the electrochemical studies and Prof. Gilroy kindly helped me with the basics of the electrochemistry.

Dedication and Acknowledgement

I would like to express my deepest gratitude to my supervisor; Dr. Hudson who gave me the opportunity to work under his supervision. I thank him for his consistent help, support, and valuable comments during my M.Sc. studies and I will always remember him for his immense knowledge, kindness, and patience.

I would like to thank my committee members; Prof. Wisner, Prof. O'Donoghue, Prof. Rogan for their invaluable comments.

I would like to thank all the past and present members of Hudson research group; David Park, Dr. Rachael Wang, Dr. Sung Ju Cho, Timothy Martin-Chan, Prof. Yoshio Saito, Ali Heidari, Dr. Augusto Matarazzo, Dr. Mojmir Suchy, Anastasiya Vinokurtseva, Mason Hermann, Santiago Giron, Amer El-Samman, Yimin Liang, Serina Fossett, Simona Milijanc, and Meredith Allen for all their friendship and help during my M.Sc. studies.

I would like to thank Members of other groups; Prof. Gilroy, Dr. Stephanie Barbon, Prof. Damha, and Fereshteh Azizi.

I would like to thank all my friends in Iran and Canada for all the good memories and friendship.

I would like to thank my parents, Maryam and Yahya who I cannot imagine myself here without their unconditional love, support, and help.

And last but not least, I would like to thank my brilliant husband, Peyman, who has supported and loved me since the first day we met and I wish to dedicate this thesis to him.

Table of Contents

Abstract.....	i
Co-Authorship Statement.....	ii
Dedication and Acknowledgement.....	iii
Table of Contents.....	iv
List of Tables.....	vii
List of Figures.....	ix
List of Schemes.....	xiii
List of Appendices.....	xiv
List of abbreviations.....	xv
Chapter 1.....	1
1 Introduction.....	1
1.1 Nucleic acid chemistry.....	1
1.2 Fluorescence.....	5
1.3 Fluorescence resonance energy transfer (FRET) and fluorescence quenching.....	7
1.3.1 Fluorescence resonance energy transfer (FRET).....	8
1.3.2 Intersystem crossing or the heavy atom effect.....	9
1.3.3 Electron exchange or Dexter interactions.....	9
1.3.4 Photoinduced electron transfer (PET).....	10
1.4 Fluorescently labeled nucleosides.....	12
1.4.1 Chromophoric base analogs.....	13
1.4.2 Pteridines.....	14
1.4.3 Expanded nucleobases.....	15
1.4.4 Extended nucleobases.....	17
1.4.5 Isomorphous nucleobases.....	18

1.5	Pyrrolocytosine (pC) derivatives	20
1.5.1	Synthesis of the pC derivatives.....	23
1.5.2	Sonogashira cross-coupling; the key reaction in the synthesis of pC derivatives	24
1.5.3	Applications of the pC derivatives.....	26
1.6	Solid phase oligonucleotide synthesis	29
1.7	Objectives of the thesis	31
	Chapter 2.....	32
2	Analysis of the effect of the nearest neighbours on the quantum yield of PhpC upon incorporation into ssDNA and dsDNA and investigation of the underlying mechanism.....	32
2.1	Introduction.....	32
2.2	Results and discussions.....	33
2.2.1	Investigation of the effect of the nearest neighbours on the quantum yield of the ssDNA and dsDNA containing PhpC.....	33
2.2.1.1	Fluorescence quantum yield of the ssDNA containing PhpC.....	34
2.2.1.2	Fluorescence quantum yield of the dsDNA containing PhpC	37
2.2.1.3	Optimum design of the fluorescent probes containing PhpC.....	44
2.2.2	Investigation of the photoinduced electron transfer (PET) of some pC derivatives	44
2.2.2.1	Synthesis of the d-PhpC and d- <i>p</i> -NO ₂ -PhpC	45
2.2.2.2	Cyclic voltammetry	46
2.2.2.3	Ground state redox potentials.....	47
2.2.2.4	Excited state redox potentials.....	49
2.2.2.5	Estimation of photoinduced electron transfer free energies.....	50
2.2.2.6	Discussion	51
2.3	Conclusion	56
	Chapter 3.....	58

3	Study of the possibility of FRET by pC derivatives as fluorescent donor and acceptor	58
3.1	Introduction.....	58
3.2	Results and discussion	62
3.2.1	Spectroscopic Properties of d- <i>p</i> -NO ₂ -PhpC, and d-PhpC.....	62
3.2.2	Quenching studies of d-PhpC and pyrene by d- <i>p</i> -NO ₂ -PhpC.....	62
3.3	Conclusion	65
	Chapter 4.....	66
4	Future studies	66
	Experimental.....	67
	References.....	71
	Appendices.....	77
	Curriculum Vitae	88

List of Tables

Table 1-1: Double helical parameters of A-, B-, and Z-DNA.	5
Table 1-2: Selected examples of Chromophoric base analogs and their photophysical properties, R'= ribose/ 2'-deoxyribose/ -CH ₂ COOH.	14
Table 1-3: Selected examples of pteridine analogs and their photophysical properties, R'= ribose/ 2'-deoxyribose/ -CH ₂ COOH.	15
Table 1-4: Selected examples of the expanded nucleobases and their photophysical properties, R'= ribose/ 2'-deoxyribose/ -CH ₂ COOH.	17
Table 1-5: Selected examples of the extended nucleobases and their photophysical properties, R'= ribose/ 2'-deoxyribose/ -CH ₂ COOH.	18
Table 1-6: Selected examples of the isomorphous nucleobases and their photophysical properties, R'= ribose/ 2'-deoxyribose/ -CH ₂ COOH.	20
Table 1-7: Selected examples of pC derivatives and their photophysical properties, R'= ribose/ 2'-deoxyribose/ -CH ₂ COOH.	21
Table 2-1: The fluorescence quantum yield of the ssDNA and dsDNA containing PhpC. The highest and the lowest numbers in each column are bolded.	33
Table 2-2: Ground state oxidation and reduction potentials in DMF and MeCN	48
Table 2-3: Excited state oxidation and reduction potentials in DMF and MeCN. The bolded numbers are used for the estimation of the photoinduced electron transfer.	50
Table 2-4: The oxidation and the reduction potentials of the natural nucleosides	51
Table 2-5: The estimation of the free energy of electron transfer ($\Delta G_{NOX/NRED}^{\circ}$ in eV) for pC derivatives calculated using Rehm-Weller equation	51

Table 2-6: Revised ground state and excited state redox potentials of d- <i>p</i> -NO ₂ -PhpC and <i>p</i> -OMe-PhpC are highlighted.....	53
Table 2-7: The revised free energy changes ($\Delta G_{NOX/NRED}^{\circ}$ in eV) of d- <i>p</i> -NO ₂ -PhpC and <i>p</i> -OMe-PhpC are highlighted.....	53
Table 2-8: The estimation of the free energies ($\Delta G_{NOX/NRED}^{\circ}$ in eV) of the 2-AP, 8-VA, 6-MAP, DMAP, 3-MI, and 6-MI.....	54
Table 2-9: The computational values of the redox potentials of d-MepC and 2-AP and the estimation of the free energy changes ($\Delta G_{NOX/NRED}^{\circ}$ in eV).....	55
Table 2-10: The revised estimation of the free energy changes of ($\Delta G_{NOX/NRED}^{\circ}$ in eV) d-MepC and 2-AP and comparing with the free energy change ($\Delta G_{NOX/NRED}^{\circ}$ in eV) of pC derivatives of the study.	56
Table 3-1: The K_{SV} and K_{SV}^{-1} of the d-PhpC and d- <i>p</i> -NO ₂ -PhpC, and pyrene and d- <i>p</i> -NO ₂ -PhpC as FRET pairs.	65

List of Figures

Figure 1-1: A) Chemical structure and numbering of purine and pyrimidine bases, B) Nomenclature of nucleoside and nucleotide, C) The structure of 2-deoxy-D-ribose and D-ribose sugars.....	1
Figure 1-2: Central dogma of molecular biology	3
Figure 1-3: The chemical structure and the names of the DNA and RNA nucleosides.	3
Figure 1-4: The phosphodiester bond and the base pairing of the nucleotides in the dsDNA. The hydrogen bond donors are shown in green and hydrogen bond acceptors in red.	3
Figure 1-5: The side view of the different DNA structures. The picture is adapted with permission from: Arnott, S. Trends Biochem. Sci. 2006 , <i>31</i> , 349-354.	4
Figure 1-6: Jablonski diagram.	6
Figure 1-7: Fluorescence resonance energy transfer diagram.	8
Figure 1-8: A) Proximity, and B) spectral overlap between the donor and acceptor.	9
Figure 1-9: Intersystem crossing diagram.....	9
Figure 1-10: Electron exchange or Dexter interaction diagram.....	10
Figure 1-11: Photoinduced electron transfer diagram: A) when fluorophore is an acceptor, and B) when fluorophore is a donor.	11
Figure 1-12: Energy diagram of PET.....	12
Figure 1-13: Hydrogen bonding of the pC derivatives with G and the orientation of the R group towards the major groove of the duplex. The hydrogen bond donors are shown in green and hydrogen bond acceptors in red. R= Me, Ph, etc.	22

Figure 1-14: The picture is reproduced with permission from: Wahba, A. S.; Esmaili, A.; Damha, M. J.; Hudson, R. H. <i>Nucleic Acids Res.</i> 2010 , <i>38</i> , 1048-1056.....	26
Figure 1-15: BoPhpC in hydrogen bonding with G. The additional hydrogen bonding with G increases the duplex stability. The hydrogen bond donors are shown in green and hydrogen bond acceptors in red.	27
Figure 1-16: Two 2-PypC and two silver ions in parallel stranded DNA constructs.	28
Figure 1-17: Hydrogen bonding of the pC derivative containing alkylamino side chain tethered via triazole linker with iso-G in parallel stranded DNA constructs. The hydrogen bond donors are shown in green and hydrogen bond acceptors in red.	28
Figure 1-18: PypC in hydrogen bonding with guanine. The hydrogen bond donors are shown in green and hydrogen bond acceptors in red.....	29
Figure 2-1: The fluorescence quantum yield of the ssDNA (orange) in decreasing order from left to right in conjunction with the quantum yield of the dsDNA (teal) and the quantum yield difference of ssDNA and dsDNA (purple). The red line shows the quantum yield of the free d-PhpC in water ($\Phi_f = 0.31$).....	34
Figure 2-2: Fluorescence quantum yield of ssDNA containing PhpC in decreasing order and the observed trends where: A) X= A; B) Y= A; C) X= C; D) Y= C; E) X= G; F) Y= G; G) X= T; H) Y= T.....	36
Figure 2-3: Summary of the structure activity relationship of the change in quantum yield of the PhpC upon incorporation into ssDNA with different neighbours	36
Figure 2-4: Fluorescence quantum yield of the ssDNA containing PhpC flanked by A) 5'-A and 3'-A. B) 3'-T and 5'-T. C) 5'-C and 3'-C. D) 5'-G and 3'-G. The sequences with no significant difference are shown with star (*).....	37
Figure 2-5: Fluorescence quantum yield of dsDNA containing PhpC (5'-XPhpCY-3') to decreasing order and the observed trends where: A) X= A; B) Y= A; C) X= C; D) Y= C; E) X= G; F) Y= G; G) X= T; H) Y= T.	38

Figure 2-6: Summary of the structure-activity relationship of the change in quantum yield of the PhpC upon hybridization into dsDNA having different neighbours.	38
Figure 2-7: Fluorescence quantum yield of the dsDNA containing PhpC flanked by: A) 5'-A and 3'-A. B) 5'-T and 3'-T. C) 5'-C and 3'-C. D) 3'-G and 5'-G.....	39
Figure 2-8: Change in the quantum yield of dsDNA containing PhpC with respect to the placement of the nucleosides on the same strand VS. the complementary strand where: A) Y/Y'= A/T; B) Y/Y'= C/G; C) X/X'= A/T; X/X'= C/G. The sequences with no significant difference are shown with star (*).....	40
Figure 2-9: Quantum yield of the dsDNA containing PhpC based on the number of guanines around PhpC	41
Figure 2-10: The observed trend for the dsDNA sequences containing PhpC based on the influence of neighbouring A) Guanine, and B) Adenine.....	42
Figure 2-11: The revised trend for the dsDNA sequences by including the effect of the neighbouring guanine and adenine on the quantum yield	43
Figure 2-12: Normalized change in quantum yield of ssDNA upon hybridization into dsDNA	44
Figure 2-13: A) Oxidation side and B) reduction side of the CV of the d-PhpC in [nBu ₄ N][PF ₆]/DMF.....	48
Figure 2-14: A) Oxidation side and B) Reduction side of the CV of d-PhpC in [nBu ₄ N][PF ₆]/MeCN.....	48
Figure 2-15: A) Oxidation side and B) Reduction side of the CV of the <i>p</i> -OMe-PhpC in [nBu ₄ N][PF ₆]/DMF.....	49
Figure 2-16: A) Oxidation side and B) reduction side of the CV of the d- <i>p</i> -NO ₂ -PhpC in [nBu ₄ N][PF ₆]/DMF.....	49

Figure 3-1: A) Molecular beacons in the absence of target sequence and B) in the presence of target sequence.	58
Figure 3-2: A) The structure of the first molecular beacon designed by Kramer and Tyagi. B) The spectral overlap between EDANS and DABCYL.....	59
Figure 3-3: The structure of the molecular beacon containing 2-AP and MepC in A) unhybridized state and B) hybridized state.....	61
Figure 3-4: The designed molecular beacon containing PhpC and <i>p</i> -NO ₂ -PhpC.....	62
Figure 3-5: Quenching spectra of d-PhpC by d- <i>p</i> -NO ₂ -PhpC in EtOH.....	63
Figure 3-6: Stern-Volmer plot for the quenching of d-PhpC by d- <i>p</i> -NO ₂ -PhpC.....	63
Figure 3-7: Quenching spectra of Pyrene by d- <i>p</i> -NO ₂ -PhpC in EtOH.....	64
Figure 3-8: Stern-Volmer plot for the quenching of pyrene by d- <i>p</i> -NO ₂ -PhpC.....	64
Figure 4-1: Chemical structure of some examples of the insulators.....	66

List of Schemes

Scheme 1-1: Schematic overview of the synthesis of the pC derivatives.....	24
Scheme 1-2: Proposed catalytic cycle of the Sonogashira cross-coupling.....	25
Scheme 1-3: Schematic overview of the chemical synthesis of the oligonucleotide on universal support III.....	30
Scheme 2-1: Synthesis of the d-PhpC and d- <i>p</i> -NO ₂ -PhpC.....	46

List of Appendices

Appendix 1: ^1H NMR spectra 3',5'-di- <i>O</i> -acetyl-2'-deoxycytidine (2).....	77
Appendix 2: ^1H NMR spectra 5-iodo-3',5'-di- <i>O</i> -acetyl-2'-deoxycytidine (3).....	78
Appendix 3: ^1H NMR spectra N^4 -benzoyl-5-iodo-3',5'-di- <i>O</i> -acetyl-2'-deoxycytidine (4)	79
Appendix 4: ^1H NMR spectra 3',5'-di- <i>O</i> -acetyl-2'-deoxy-6-phenylpyrrolocytidine (5) ..	80
Appendix 5: ^1H NMR spectra 2'-deoxy-6-phenylpyrrolocytidine (6)	81
Appendix 6: ^1H NMR spectra 1-ethynyl-4-nitrobenzene	82
Appendix 7: ^1H NMR spectra 3',5'-di- <i>O</i> -acetyl-2'-deoxy-6-(<i>p</i> - nitro)phenylpyrrolocytidine (7)	83
Appendix 8: ^{13}C NMR spectra 3',5'-di- <i>O</i> -acetyl-2'-deoxy-6-(<i>p</i> - nitro)phenylpyrrolocytidine (7)	84
Appendix 9: ^1H NMR spectra 2'-deoxy-6-(<i>p</i> -nitro)phenylpyrrolocytidine (8).....	85
Appendix 10: The copyright permission.....	86
Appendix 11: The copyright permission.....	87

List of abbreviations

A	adenine
AcOH	acetic acid
aq.	aqueous
br	broad (spectral)
Bz	benzoyl
°C	degrees Celsius
C	cytosine
cat.	catalyst
cDNA	complementary deoxyribonucleic acid
CV	cyclic voltammetry
d	doublet
δ	chemical shift in parts per million downfield from tetramethylsilane
DABCYL	4-[4-(dimethylamino)phenylazo] benzoic acid
DCM	dichloromethane
DFT	density functional theory
DMF	<i>N,N</i> -dimethylformamide
DMSO	dimethyl sulfoxide
DMT	4,4'-dimethoxytrityl
DNA	deoxyribonucleic acid
dsDNA	double stranded DNA
EDTA	ethylenediaminetetraacetic acid
EtOAc	ethyl acetate
Et	ethyl
equiv.	equivalent
EtOH	ethanol
FCC	flash column chromatography
FRET	Fluorescence resonance energy transfer
g	grams
G	guanine

h	hours
Hex	Hexane
Hz	hertz
J	coupling constant
λ	wavelength
k_q	bimolecular quenching constant
K_{sv}	Stern-Volmer quenching constant
K_{sv}^{-1}	inverse of the Stern-Volmer quenching constant
L	liter
μ	micro
m	multiplet
MeCN	acetonitrile
MeOH	methanol
min	minutes
Et ₃ N	triethylamine
NMR	nuclear magnetic resonance
ODN	oligodeoxynucleotide
PET	Photoinduced electron transfer
Ph	phenyl
PhCCH	phenylacetylene
PNA	peptide nucleic acid
ppm	parts per million
q	quartet
R_f	retention factor
RNA	ribonucleic acid
RT	room temperature
s	singlet
ssDNA	single stranded DNA
T	thymine
t	triplet
THF	tetrahydrofuran

TLC	thin layer chromatography
T_m	melting temperature for a nucleic acid complex
TMS	trimethylsilyl
U	uracil
UV	ultraviolet
vis	visible
Φ_f	fluorescence quantum yield

Chapter 1

1 Introduction

1.1 Nucleic acid chemistry

Studying nucleic acids goes back to 1869 when Swiss chemist Friedrich Miescher isolated DNA from pus in surgical bandages. Even though the isolated DNA had some protein impurities, he recognized the unique nitrogen/phosphorous ratio and high molecular weight of the molecule and called it “nuclein”.¹ Later in 1889, Richard Altmann isolated the protein-free form of the nuclein and recognized the acidic character of it and used the term “nucleic acid” for the first time.² Other advancements until 1929, include isolation and identification of the heterocyclic components of nuclein known today as the canonical nucleobases (adenine, cytosine, guanine, and thymine (Figure 1-1)) by Albrecht Kossel in 1879,³ and isolation and identification of D-ribose (Figure 1-1) from plant nucleic acids in 1911⁴ and 2-deoxy-D-ribose (Figure 1-1) from animal nucleic acids in 1929,⁵ both by Phoebus Levene. Later, in 1954 Alexander R. Todd proved the nucleotide structure and stereochemistry by chemical synthesis.⁶

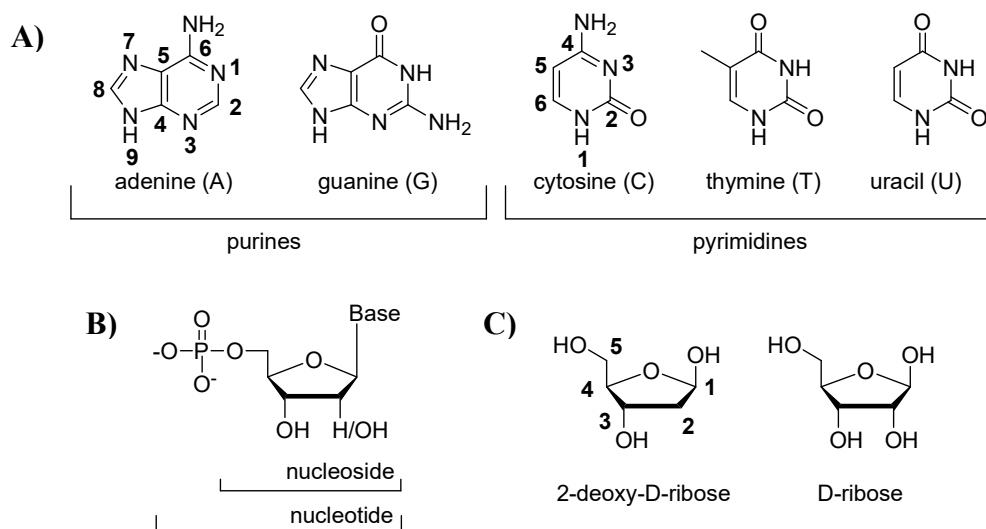


Figure 1-1: A) Chemical structure and numbering of purine and pyrimidine bases, B) Nomenclature of nucleoside and nucleotide, C) The structure of 2-deoxy-D-ribose and D-ribose sugars.

During the period of 1928-1952, one of the most important advancements in the field of nucleic chemistry was achieved. Up until then, it was believed that proteins were the molecules of heredity, rationalized by the notion that a 20-letter alphabet of proteins provides more diversity than the 4-letter alphabet of nucleic acids. However, further research on transformation ability of bacterial DNA led to the conclusion that DNA was the molecule of genetic inheritance.⁷

In 1952 Erwin Chargaff proposed two rules appropriately named Chargaff's rules. 1) In natural DNA, the number of guanine units equals the number of cytosine units and the number of adenine units equals the number of thymine units. 2) The composition of DNA varies from one species to another.⁸

The stage was now ready for the structural proposal of DNA. With the proved primary structure of DNA in single-stranded, and the DNA fiber X-ray diffraction data collected by Maurice Wilkins and Rosalind Franklin, and the correct use of the keto form of the bases instead of enol tautomer, James D. Watson and Francis H. C. Crick proposed the double-helix structure of the DNA in 1953 and discovered the secret of life.⁹

With the discovery of the double helical structure of DNA, a new area of study called molecular biology came into the world. The scientists already knew that almost all of the information required for almost all of the biological functions of a cell are coded in the sequences of nucleotide bases in the DNA of the cell, however, the question of how DNA works within the body remained unresolved for years. This question was answered by Francis Crick in 1970 when he solved the mystery.¹⁰ What he proposed was called "the central dogma of molecular biology" and it demonstrates that genetic information is stored, accessed and replicated from the DNA duplex structure as a linear nucleotide code. DNA is transcribed into RNA, which is the biopolymer responsible for the transportation of genetic information from DNA to the ribosome. The RNA utilizes D-ribose sugar instead of 2-deoxy-D-ribose sugar and uracil (U) instead of thymine (T) as the complementary base for adenine (A). In the ribosome, which is the site of protein manufacturing, the RNA is translated into proteins of different functions (Figure 1-2).



Figure 1-2: Central dogma of molecular biology.

Our DNA is made of four different nucleosides. Each nucleoside consists of a base connected to the 2-deoxy-D-ribose sugar via β -N-glycosidic bond (Figure 1-3). The nucleosides are connected together via the phosphodiester bond between sugars and make one strand of the DNA. The second strand is connected to the first strand by hydrogen bonding between the bases. This hydrogen bonding is in a way that always A and T with two hydrogen bonds, and C and G with three hydrogen bonds, pair with each other (Figure 1-4).

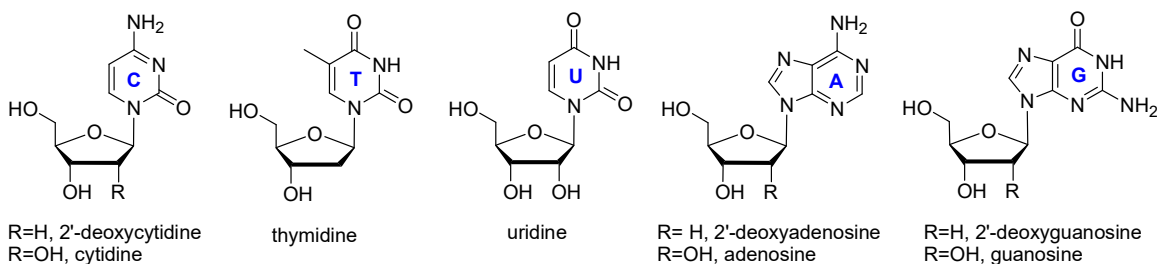


Figure 1-2: The chemical structure and the names of the DNA and RNA nucleosides.

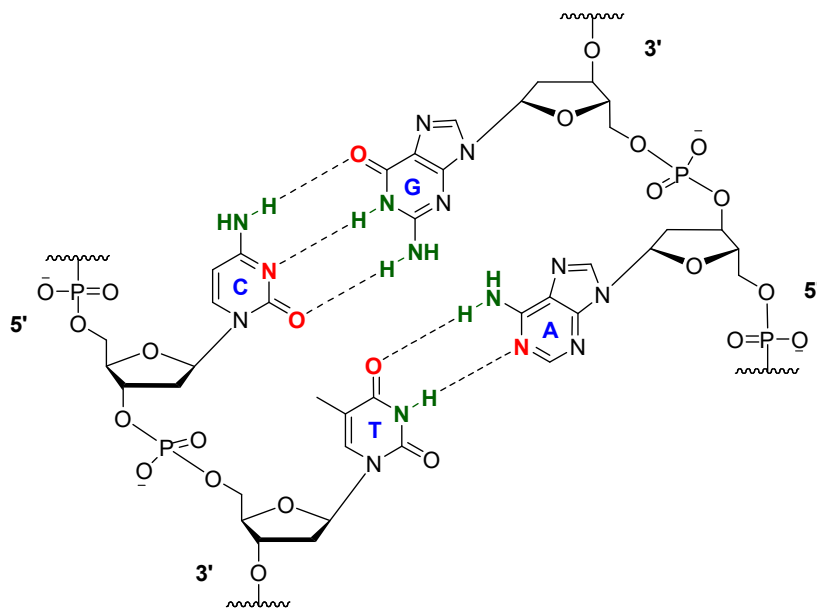


Figure 1-4: The phosphodiester bond and the base pairing of the nucleotides in the dsDNA. The hydrogen bond donors are shown in green and hydrogen bond acceptors in red.

The strands are running in opposite direction (anti-parallel) and coil around a central axis and have right-handed helical sense. Moreover, the helical shape of the DNA molecule makes two grooves in the structure, a major groove with 12 Å width and 8.5 Å depth, and a minor groove with 6 Å width and 7.5 Å depth. This form of double-stranded DNA is called B-DNA.¹¹

The study of the x-ray diffraction of dehydrated DNA fibers revealed different forms of DNA structure. For instance, when the relative humidity is reduced to less than about 75% A-DNA is formed. The A-DNA's structure is wider and shorter than that of B-DNA, and its base pairs are tilted rather than perpendicular to the helix axis. Also, in A-DNA sugar pucker is C3'-endo while in B-DNA is C2'-endo (Table 1-1).¹¹⁻¹⁴

Later, Alexander Rich and his associates discovered the Z-DNA as the third type of DNA helix. The Z-DNA is anti-parallel strand held together by Watson-Crick base-pairing with the left-handed screw sense. Furthermore, the phosphates in the backbone zigzagged; hence, they called it Z-DNA. The Z-DNA is adopted by short oligonucleotides that have sequences of alternating pyrimidines and purines with high salt concentrations to minimize electrostatic repulsion between the backbone phosphates, which are closer to each other than in A- and B-DNA.¹¹

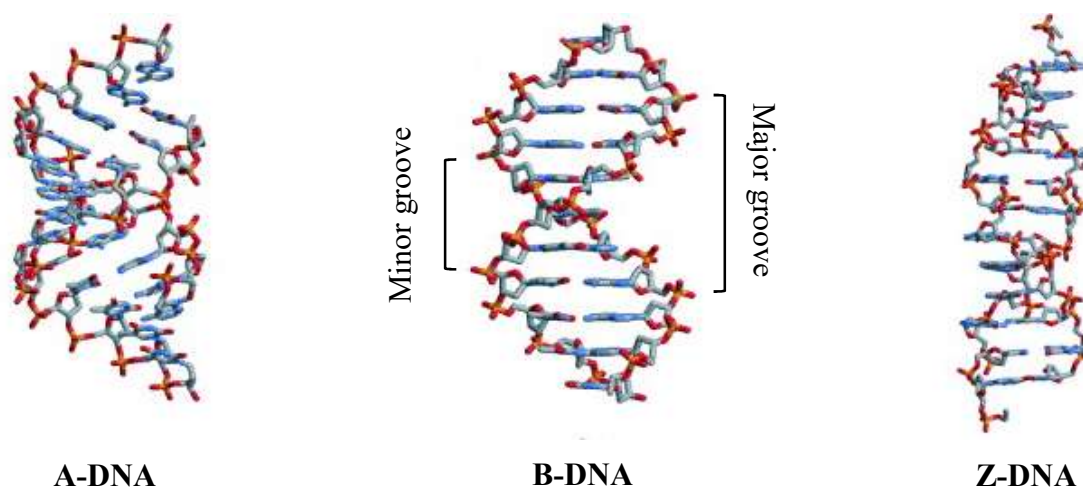
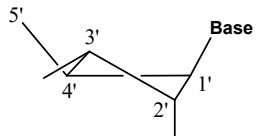
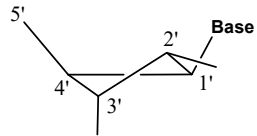


Figure 1-3: The side view of the different DNA structures. The picture is adapted with permission from: Arnott, S. Trends Biochem. Sci. 2006, 31, 349-354.

Table 1-1: Double helical parameters of A-, B-, and Z-DNA.

	Helix Type		
	A	B	Z
Shape	Broadest	Intermediate	Narrowest
Rise per base pair	2.3 Å	3.4 Å	3.8 Å
Helix diameter	25.5 Å	23.7 Å	18.4 Å
Screw sense	Right-handed	Right-handed	Left-handed
Glycosidic bond	anti	anti	A, T, C : anti G : syn
Sugar pucker	C3'-endo 	C2'-endo 	A, T, C : C2'-endo G : C3'-endo
Base pairs per turn	11	10.4	12
Pitch per turn	25.3 Å	35.4 Å	45.6 Å
Tilt of base pairs from normal to helix axis	19 °	1 °	9 °
Major groove	Narrow & very deep	Wide & quite deep	Flat
Minor groove	Very broad & shallow	Narrow & quite deep	Very deep & narrow

1.2 Fluorescence

Fluorescence is a photophysical process in which absorption of a photon by a chromophore is followed by emission of a photon. This process and its difference to phosphorescence can be well explained using Jablonski diagram in Figure 1-6. This diagram shows that upon absorption of light by a chromophore and excitation of electrons to first excited electronic singlet state (S_1), several pathways are possible for transition back to the ground electronic singlet state (S_0). From the lowest vibrational energy level of S_1 , the molecule can undergo internal conversion (IC) to the various vibrational energy levels of S_0 followed by vibrational relaxation (VR) resulting in nonradiative decay (VR + IC). Fluorescence is also possible, resulting in radiative decay from the lowest vibrational energy level of S_1 to the various vibrational energy levels of S_0 . Furthermore, intersystem crossing (ISC) from S_1 to

first excited electronic triplet state (T_1) can be followed by nonradiative decay (IC + VR) or radiative decay (phosphorescence) from the lowest vibrational energy level of T_1 .¹⁵

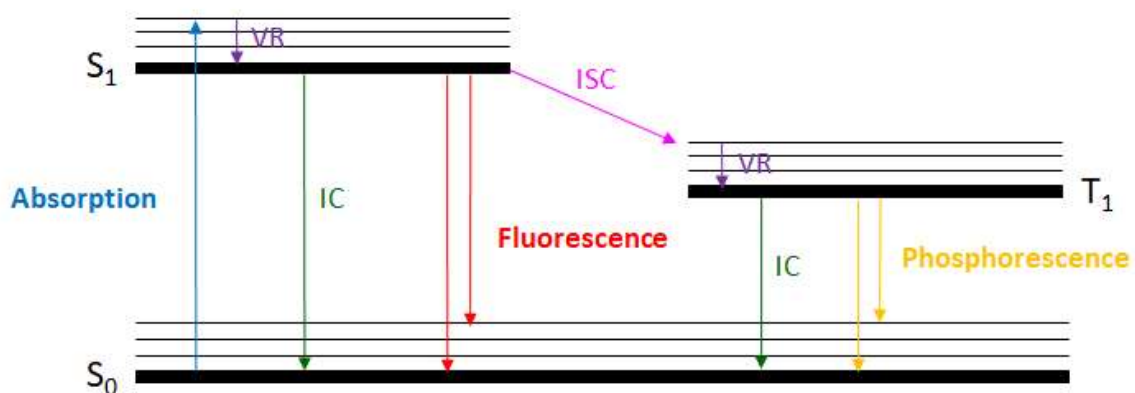


Figure 1-4: Jablonski diagram.

The fluorescence properties of a system are determined by measurement of the excitation and emission wavelengths, the fluorescence quantum yield, and the lifetime of the excited state. Simply, the excitation wavelength is a wavelength in which the fluorophore has the maximum absorption, and the emission wavelength is a wavelength in which the fluorophore emits the absorbed energy. The difference (in wavelength or frequency units) between the band maxima of the excitation and emission spectra is called Stokes shift.¹⁵

The fluorescence quantum yield (Φ) is the number of emitted photons relative to the number of absorbed photons. The emitted photons have the rate constant of Γ , and the absorbed photon is the sum of the fluorophore rate constant Γ and nonradiative rate constant k_{nr} . Therefore, the quantum yield, is given by following equation.¹⁵

$$\Phi = \frac{\Gamma}{\Gamma + k_{nr}} \quad \text{Equation 1}$$

The quantum yield can be close to unity if the non-radiative decay rate is much smaller than the rate of radiative decay ($k_{nr} < \Gamma$). However, the quantum yield of fluorescence is always less than unity because of Stokes shifts.¹⁵

The fluorescence lifetime (τ) is defined as the average time the molecule spends in the excited state before returning to the ground state. In practice, it is the time available for the

fluorophore to interact with or diffuse in its environment, and hence the time the information available from its emission. Generally, fluorescence lifetimes are near 10 ns and are calculated by following equation.¹⁵

$$\tau = \frac{1}{\Gamma + k_{nr}}$$

Equation 2

1.3 Fluorescence resonance energy transfer (FRET) and fluorescence quenching

Fluorescence resonance energy transfer (FRET) is a process in which a fluorophore as a donor transfers its energy into an acceptor. The acceptor may be fluorescent or non-fluorescent, in both cases, the fluorescent intensity of the fluorophore is decreased. The resonance energy transfer does not require molecular contact, therefore, it is not sensitive to steric factors and electrostatic interactions.¹⁵

Fluorescence quenching is any process in which the fluorescence intensity is decreased. Quenching can result in the partially or fully dissipation of the fluorophore's electronic energy as non-radiative decay or heat. Quenching, unlike FRET, requires molecular contact between the fluorophore and the quencher. The extent of quenching is sensitive to molecular factors that affect the rate and probability of contact, including steric and shielding and charge-charge interactions.¹⁵

There are two types of fluorescence quenching; static quenching and dynamic (collisional) quenching. Dynamic quenching is due to diffusive encounters of the excited state fluorophore upon contact with a quenching substance and static quenching is due to the complex formation between the fluorophore and the quencher in the ground state. There are at least three mechanisms for quenching: intersystem crossing, electron exchange, and photoinduced electron transfer (PET). It is often difficult to know the mechanism of quenching. The mechanisms are not mutually exclusive, and many reports indicate that sometimes quenching occurs by a combination of these mechanisms.¹⁵

The fluorescence resonance energy transfer and three underlying mechanisms of quenching including intersystem crossing, electron exchange, and photoinduced electron transfer will be discussed in the following section.

1.3.1 Fluorescence resonance energy transfer (FRET)

In fluorescence resonance energy transfer, absorption of light by a donor (D) results in excitation of one electron from the highest occupied molecular orbital (HOMO) to the lowest-unoccupied molecular orbital (LUMO) (D^* in Figure 1-7). Then, the electron in the excited electron returns to the ground state and simultaneously an electron in the acceptor (A) goes into a higher excited-state orbital. If the acceptor is fluorescent it may then emit. If the acceptor is non-fluorescent the energy is dissipated as heat. The distance in which RET is 50% efficient is 30 Å and is called Förster distance. This distance compared to the size of the molecules is very large and makes the direct interaction of the electron clouds of the donor and acceptor impossible.¹⁵

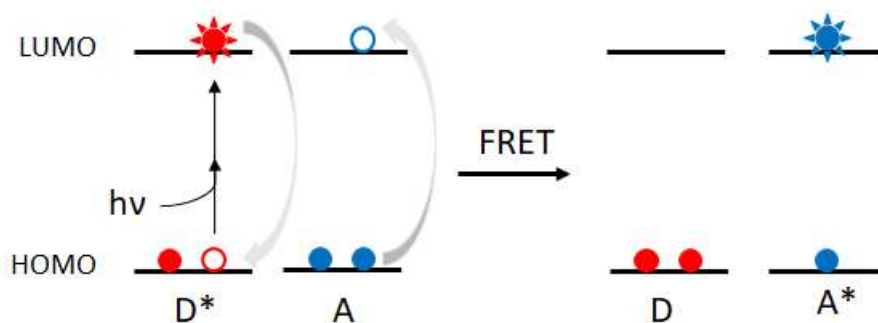


Figure 1-5: Fluorescence resonance energy transfer diagram.

FRET has been utilized in the design of the molecular beacons which are hairpin form single-stranded oligonucleotides containing donor and acceptor of FRET on each end. Molecular beacons report presence or absence of a target sequence based on the presence or absence of the FRET. For the efficient FRET, the donor and the acceptor must be in close proximity to each other and the emission of the donor must overlap the absorption of the acceptor. Therefore, a good FRET pair for a molecular beacon is the one that has optimum overlap between the emission of the donor and absorption of the acceptor when they are placed in close proximity (Figure 1-8).

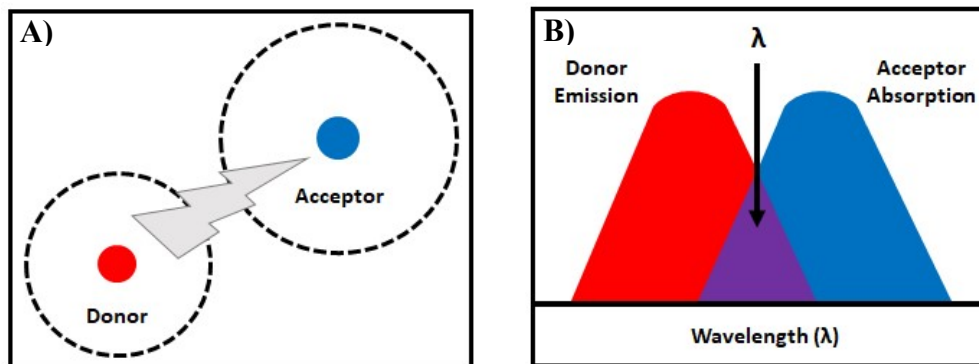


Figure 1-6: A) Proximity, and B) spectral overlap between the donor and acceptor.

1.3.2 Intersystem crossing or the heavy atom effect

The intersystem crossing is believed mostly to occur in the quenching by heavy atoms, halogens, and oxygen. In intersystem crossing, the excited singlet state becomes an excited triplet state by an encounter with a heavy atom or a triplet oxygen molecule. The triplet states are usually long-lived and quenched by oxygen, therefore, the fluorophore is likely to be quenched to the ground state by the same quencher, or return to the ground state by non-radiative decay. This mechanism might not be the only mechanism involved in the quenching by oxygen or halogens. The electron exchange or photoinduced electron transfer might be involved as well. However, it is not always clear which mechanism is dominant in each case.¹⁵

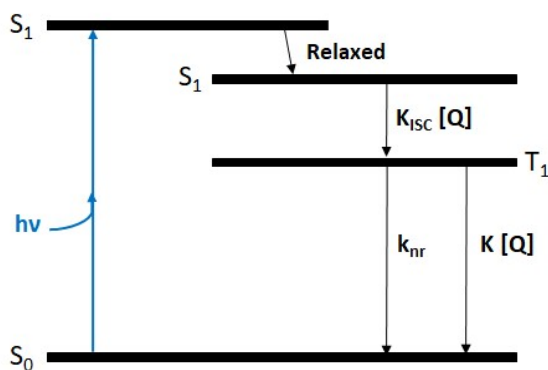


Figure 1-7: Intersystem crossing diagram.

1.3.3 Electron exchange or Dexter interactions

In electron exchange (Figure 1-10), the excited electron of the donor in the LUMO is transferred to the acceptor. The acceptor then transfers an electron from the HOMO back

to the donor, so the acceptor is left in an excited state. The exchange can be sequential or concerted. Electron exchange has some similarities to FRET and some differences. In both energy is transferred to an acceptor, and both depend on spectral overlap of the donor and acceptor. However, FRET is well known to result in an excited acceptor and the Dexter interaction is usually associated with quenching.¹⁵

Both Dexter interaction and FRET require spectral overlap, but when a fluorophore and a quencher have a spectral overlap which one happens? If the distance is large, the transfer occurs by FRET before Dexter transfer can occur. If the distance is short, the donor will be completely quenched by FRET or Dexter transfer, and thus non-observable. Dexter transfer can be observed if the spectral overlap is small, and Dexter rate of exchange is large. Additionally, high concentrations are needed for significant Dexter transfer (1 M gives 6.5 Å distance), whereas FRET occurs at much lower concentrations (10^{-2} M gives 30 Å distance).¹⁵

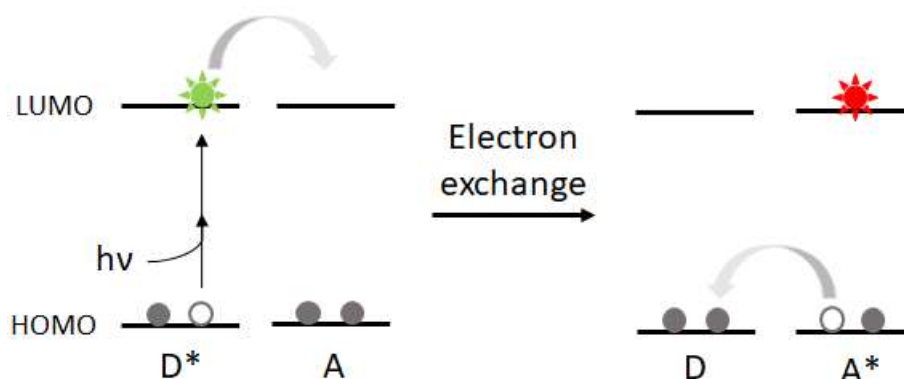


Figure 1-8: Electron exchange or Dexter interaction diagram.

1.3.4 Photoinduced electron transfer (PET)

PET is an excited state electron transfer process in which an electron is transferred from an electron donating species (D) to an electron accepting species (A). The fluorophore can be either electron donor or electron acceptor and the direction of electron transfer in the excited state is determined by the oxidation and reduction potential of ground and excited states. The more common situation is when the excited state of a fluorophore acts as an electron acceptor (Figure 1-11A). In this case, upon excitation of an electron from HOMO to LUMO of the acceptor, one electron is transferred from the HOMO of the donor to the

HOMO of the acceptor and a complex is formed between the electron donor (D) and the electron acceptor (A). It is often difficult to predict the efficiency of quenching by intersystem crossing and electron exchange, however, PET can be predicted because the possibility of electron transfer can be predicted from the redox potentials of the fluorophore and the quencher.¹⁵

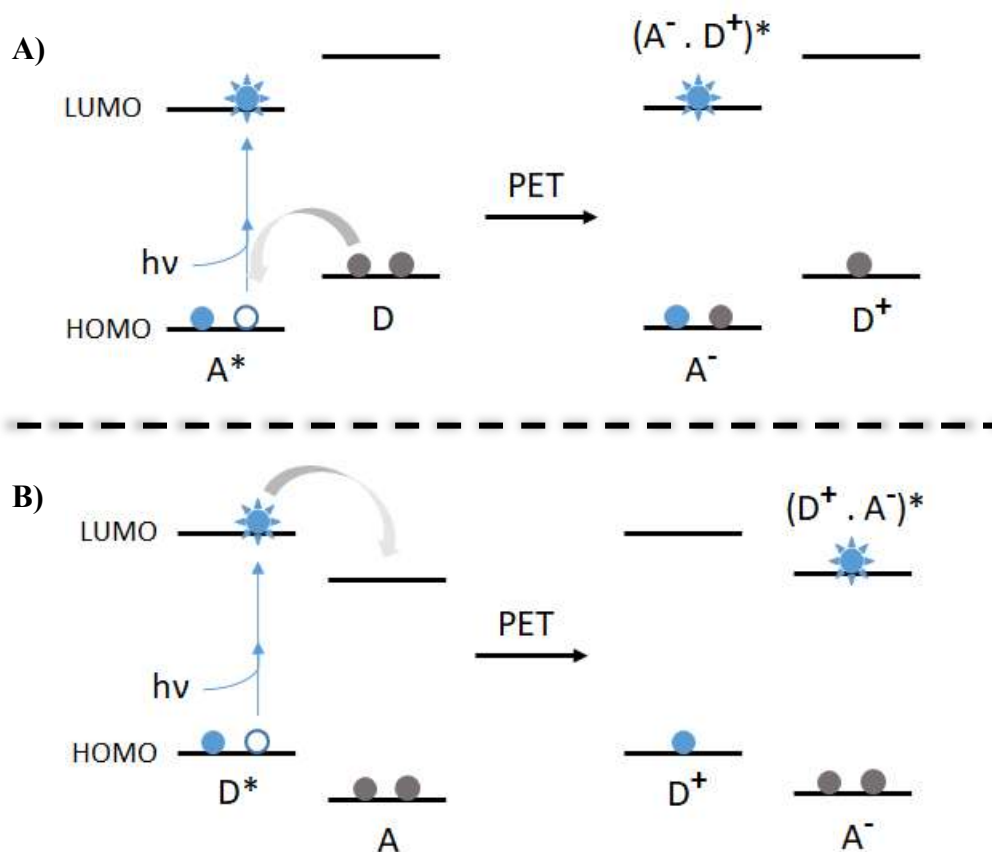


Figure 1-9: Photoinduced electron transfer diagram: A) when fluorophore is an acceptor, and B) when fluorophore is a donor.

The energy diagram of PET with the excited molecule being electron donor is shown in Figure 1-12. It shows that upon excitation, the first event is charge separation in which the electron donor transfers the electron to the acceptor with a rate (k_p) and forms the charge transfer complex ($[D^+ A^-]^*$). This charge transfer complex can be quenched and returned to the ground state through non-radiative decay (k_{nr}) without emission of a photon, or can emit as an exciplex ($h\nu_E$) or loses some energy and makes ($D^+ + A^-$). Through the charge recombination step, the extra electron on the acceptor is transferred back to the donor and

returned to the ground state ($D + A$). The most important part of this process is the decrease in total energy of the charge transfer complex. The energy decreases because the ability of the fluorophore to accept or donate an electron decreases when a fluorophore is in the excited state.¹⁵

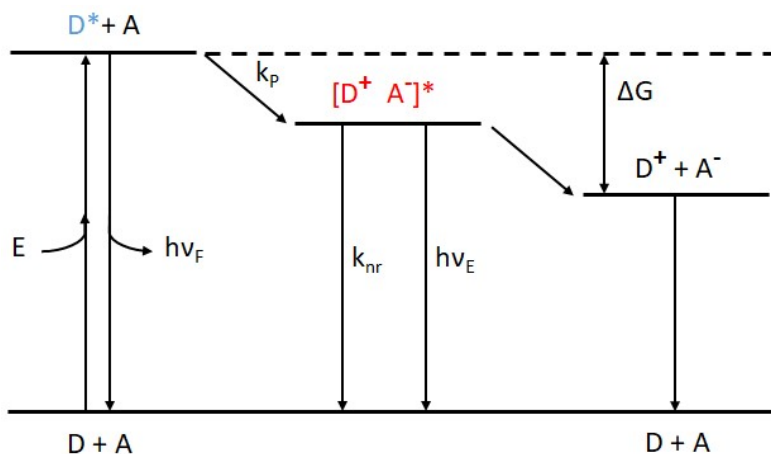


Figure 1-10: Energy diagram of PET.

The energy change for PET is given by Rehm-Weller equation:

$$\Delta G = E(D^+/D) - E(A/A^-) - \Delta G_{00} - \frac{e^2}{\epsilon d} \quad \text{Equation 3}$$

In this equation, the reduction potential $E(D^+/D)$ describes the process: $D^+ + e \rightarrow D$ and the reduction potential $E(A/A^-)$ describes the process: $A + e \rightarrow A^-$. This equation shows that both donor and acceptor are reduced, however in the PET process one component is reduced and the other is oxidized. ΔG_{00} is the energy of the $S_0 \rightarrow S_1$ transition of the fluorophore and the last term on the right is the coulombic attraction energy experienced by the ion pair following the electron transfer reaction. ϵ is the dielectric constant of the solvent and d is the distance between the charges.¹⁵

1.4 Fluorescently labeled nucleosides

As mentioned earlier, years of research have resulted in understanding the chemical and 3D structure of the DNA. In order to understand the function, dynamics, interactions and microenvironment of the DNA, several biophysical and theoretical tools developed. Most of these tools rely on electrophoresis, circular dichroism, calorimetry, nuclear magnetic

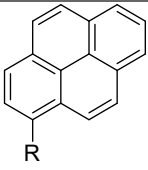
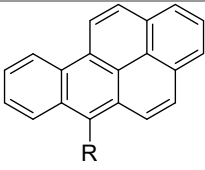
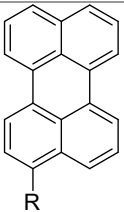
resonance (NMR) spectroscopy, X-ray crystallography, etc. Among these methods, fluorescence spectroscopy is appealing, as it is easily accessible, versatile, and provides information in real time with great sensitivity. While there are a couple of emissive naturally occurring nucleosides, the purines and pyrimidines are virtually non-emissive in neutral aqueous solution. The natural nucleosides have extremely low quantum yield ($0.5 - 3 \times 10^{-4}$) and lifetime (0.5 – 1 picosecond). Therefore, fluorescently labeled nucleosides must be designed in order to study the function, dynamics, interactions and microenvironment of the DNA. Furthermore, they can be incorporated into hybridization probes for the diagnosis of the genetic disorders and viral and microbial infections. A perfect fluorescently labeled nucleoside has red-shifted absorption band compared to the natural nucleosides and amino acids, emission band near or in the visible region and high quantum efficiency. There are five major types of fluorescently labeled nucleosides based on the modifications on the nucleobase. Each type will be discussed in the following section and some examples and some of their applications will be explained. For the complete review of the fluorescently labeled nucleosides refer to the cited references.¹⁶⁻²³

1.4.1 Chromophoric base analogs

In this type of modification, natural bases are replaced with established fluorophores, typically polycyclic aromatic hydrocarbons (PAH). This type of fluorescence nucleoside has an isolated absorption band and high quantum efficiency approaching unity; however, they lack the Watson-Crick (WC) hydrogen bonding face.

Recently, Kool and coworkers synthesized a DNA-like chain containing different PAH fluorophores called oligodeoxyfluorosides (ODFs). These poly-chromophoric oligomers are closely packed emissive assemblies that exhibit complex energy transfer phenomena between the chromophores, making them highly sensitive to their environment. This complexity results in fluorescence emission across the visible spectrum, and optical responses including not only quenching but also lighting up and color changes. ODFs have been implemented in the detection of toxic gases and metal ions, and in multiplexed imaging of live cells.²⁴⁻³⁰ Recently it has been used to distinguish 14 different structurally varied insecticides and herbicides as micromolar level contaminants in water.³¹

Table 1-2: Selected examples of Chromophoric base analogs and their photophysical properties, R'= ribose/ 2'-deoxyribose/ -CH₂COOH.

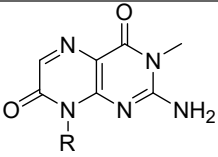
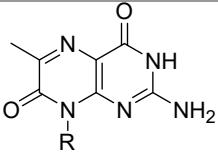
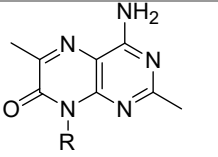
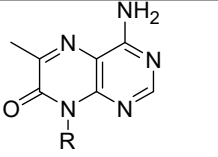
Structure	Name	Solvent	λ_{abs} (nm)	λ_{em} (nm)	Φ_f	τ_0 (ns)	Ref.
	pyrene	MeOH	241, 345	375, 395	0.12		17
	benzopyrene	MeOH	394	408	0.98		17
	perylene	MeOH	440	433, 472	0.88		17

1.4.2 Pteridines

Pteridines are naturally occurring highly emissive heterocycles whose have a structural resemblance to the purines. Like purines, they can have Watson-Crick hydrogen bonding with C or T and because of the similarity in size, they can make stable DNA duplexes. Pteridines have isolated absorption band (≥ 300 nm) and high quantum efficiency ($\Phi = 0.39-0.88$).

Hawkins and coworkers almost exclusively worked on the pteridine derivatives and showed that pteridines can be utilized in hybridization probes and tracking the DNA uptake in cells.^{32,33}

Table 1-3: Selected examples of pteridine analogs and their photophysical properties, R'= ribose/ 2'-deoxyribose/ -CH₂COOH.

Structure	Name	solvent	λ_{abs} (nm)	λ_{em} (nm)	Φ_f	τ_0 (ns)	Ref.
	3-MI	Tris buffer (pH= 7.5)	254, 350	430	0.88	6.5	17
	6-MI	Tris buffer (pH= 7.5)	340	431	0.70	6.4	17
	DMAP	Tris buffer (pH= 7.5)	250, 333	430	0.48	4.8	17
	6-MAP	Tris buffer (pH= 7.5)	248, 329	430	0.39	3.8	17

1.4.3 Expanded nucleobases

Extending the conjugation system of the natural nucleobases by fusing or inserting aromatic or heterocyclic rings into pyrimidines and purines generates a diverse group of expanded nucleobases. Expanded nucleobases mostly retain their hydrogen bonding face and have relatively high quantum yields, although their large surface area could potentially perturb the DNA duplex stability.

One of the most interesting members of this group is tC nucleoside which was initially synthesized by Matteucci and coworkers in 1995 as a helix stabilizing modification for the potential use as antisense therapeutics.³⁴ In 2001, Wilhelmsson and coworkers have incorporated tC into PNA and noticed the uniqueness of the tC in preserving fluorescence quantum yield upon incorporation into the oligonucleotide, duplex formation and the environment polarity.³⁵ Later they developed two more derivatives of this family, tC^O and tC_{nitro}. The tC derivatives can form a WC-like base pairing with guanine and have relatively low quantum yields.³⁶⁻⁴⁰

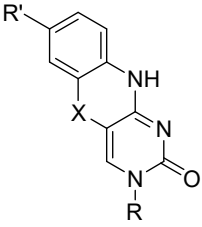
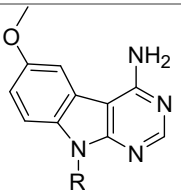
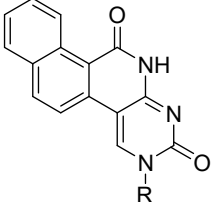
The studies showed that tC without any perturbation, adopts the B-DNA structure⁴¹ and unlike most of the fluorescent nucleosides its quantum yield is insensitive to the neighbouring nucleosides in ssDNA and dsDNA.⁴² Moreover, its enzymatic incorporation into oligonucleotides was investigated and showed that tC and tC^O are polymerized with slightly higher efficiency opposite guanine than cytosine triphosphate and bind with nanomolar affinity to the DNA polymerase active site.⁴³⁻⁴⁶

It is observed that tC under intense long-term illumination and in the presence of oxygen is degraded to form the sulfoxide form of tC which has a blue-shifted absorption and a less intense fluorescence compared to that of tC. Moreover, conversion of tC to its photoproduct within the dsDNA greatly reduces the duplex stability. It is speculated that this property can be implemented in the photo-switchable probes.⁴⁷

Another member of this family, tC^O, has higher quantum yield and introduces minimal perturbations to the normal secondary structure of DNA⁴⁸ and RNA⁴⁹. It is shown that tC^O and tC_{nitro} are good FRET pairs⁵⁰ and have been used in several biological studies.⁵¹⁻⁵³ Moreover, it is shown that tC^O specifically binds to a type of the monoclonal antibody and was found to raise its fluorescence intensity by a factor of five. This unique feature makes it a valuable tool in fluorescence dependent immunoassays.⁵⁴

As another example of the size expanded nucleoside family, Saito and coworkers have synthesized several modified nucleosides like MDA and NPP and incorporated into oligonucleotides. They noticed the unique characteristic of this nucleosides in distinguishing between natural nucleosides opposite to them. Saito named this group of molecules base discriminating fluorescent (BDF) nucleosides and utilized them in single nucleotide polymorphism detection.⁵⁵

Table 1-4: Selected examples of the expanded nucleobases and their photophysical properties, R'= ribose/ 2'-deoxyribose/ -CH₂COOH.

Structure	Name	Solvent	λ_{abs} (nm)	λ_{em} (nm)	Φ_f	τ_0 (ns)	Ref.
	X= S, R'= H tC	Phosphate buffer (pH= 7.5)	377	513	0.13	3.2	42
	X= O, R'= H tC ^O	Phosphate buffer (pH= 7.5)	359	461	0.30	3.4	37
	X= S, R'= NO ₂ tC _{nitro}		375-525	530	≈ 0		39,40
	^{MD} A	Phosphate buffer (pH= 7.0)	327	397, 427	0.118		56
	NPP	MeOH	365	395	0.26		57

1.4.4 Extended nucleobases

Extended nucleobase analogs are typically synthesized by tethering known fluorophores to the natural nucleobases via a rigid or flexible linker. Depending on the conjugating or non-conjugating nature of the linker, the extended fluorophore could generate new chromophore with new photophysical properties or could preserve the photophysical properties of the parent fluorophore. These nucleosides normally retain their hydrogen bonding face, and because of the linker, they do not perturb the double helical structure of DNA. However, due to the distance between the reporter and the site of the modification they are not able to accurately report the microenvironment of the DNA.

Recently Hocek and coworkers have synthesized a cytosine linked to a meso-substituted BODIPY fluorescent molecular rotor (C^{bdp}) to sense changes in DNA microenvironment both in vitro and in vivo. It was shown that in living cells, DNA containing C^{bdp} can be

visualized in real time and can respond to interactions with DNA-binding proteins and lipids by changes in the fluorescence lifetimes in the range of 0.5–2.2 ns. These features can make this probe suitable for analysis of DNA-associated processes, cellular structures, and also DNA-based nanomaterials.^{58,59}

As another example, Saito and coworkers recently synthesized 8-aza-3,7-dideaza-2'-deoxyadenosine tethered with naphthalene in position 3 which showed environmentally sensitive intramolecular charge transfer (ICT) emission because of electron transition in the coplanar conformer formed by nucleobase and naphthalene moieties. Since the naphthalene group is oriented towards the minor groove it makes this modified nucleoside a powerful tool for monitoring the DNA minor groove.⁶⁰

Table 1-5: Selected examples of the extended nucleobases and their photophysical properties, R'= ribose/ 2'-deoxyribose/ -CH₂COOH.

Structure	Name	Solvent	λ_{abs} (nm)	λ_{em} (nm)	Φ_f	τ_0 (ns)	Ref.
	C ^{bdp}	Phosphate buffer (pH= 7.4)	495	512	0.03		⁵⁹
	^{3n7z} A	1,4-Dioxane MeOH	351 351	398 422	0.68 0.06		⁶⁰

1.4.5 Isomorphous nucleobases

Isomorphous nucleobases closely resemble the size, structure and WC base pairing of the natural nucleosides; therefore, they do not perturb the overall structural stability of the DNA while having desirable fluorescence properties. Furthermore, their quantum yields strongly depend on the sequence they are incorporated into and their microenvironment,

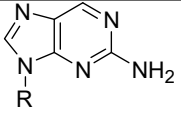
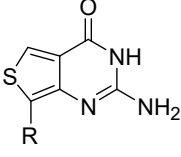
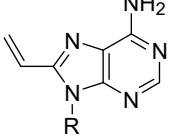
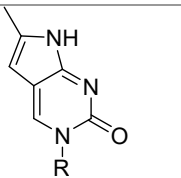
thus most of them are good reporters of the state of hybridization and their microenvironment.

The most famous member of this family and the fluorescently labeled nucleosides entirely is 2-aminopurine (2-AP). It is a constitutional isomer of adenine with largely enhanced photophysical properties. Since its introduction in 1969 by Stryer et al.,⁶¹ it has been extensively used in vastly different areas of fluorescence spectroscopy research. 2-AP seems to be the ideal fluorescent because of its size and structural resemblance to natural bases, ability to form WC base pairing, high quantum yield, isolated absorption band, minimal sensitivity to pH changes and importantly sensitivity to environmental polarity. Moreover, 2-AP perfectly pairs with T/U and does not disturb the double helical structure of DNA/RNA. However, 2-AP is significantly quenched upon incorporation into oligonucleotides with a sequence-dependent manner.⁶²

Recently Tor and coworkers have introduced a novel nucleobase thienoguanine (thG) which is believed to resolve 2-AP's deficiencies.⁶³ In one example replacement of thG with a guanine residue on an 18-mer stem-loop oligonucleotide required for the completing HIV-1 DNA synthesis, provided more relevant structural and dynamical information of the 18-mer than that of 2-AP. The thG nucleoside allowed for the first time, to selectively and faithfully monitor the conformations and dynamics of a given G residue in a DNA sequence.⁶⁴ Moreover, Park and coworkers demonstrated that thG enables the visual detection of the transition of B-DNA to Z-DNA based on different π -stacking of B- and Z-DNA.⁶⁵

Another member of this family is MepC which will be discussed in next section.

Table 1-6: Selected examples of the isomorphous nucleobases and their photophysical properties, R'= ribose/ 2'-deoxyribose/ -CH₂COOH.

Structure	Name	Solvent	λ_{abs} (nm)	λ_{em} (nm)	Φ_f	τ_0 (ns)	Ref.
	2-AP		303	370	0.68	7.0	¹⁷
	th G	water	321	453	0.46	14.8	⁶³
	8-VA	HEPES buffer (pH= 7.5)	290	382	0.66	4.7	¹⁷
	MepC	water	342	461	0.05		⁶⁶

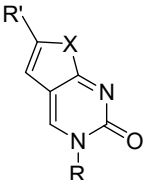
1.5 Pyrrolocytosine (pC) derivatives

Pyrrolocytosine derivatives are isomorphous nucleobases, first described in 1987 by Inoue and coworkers.⁶⁷ They synthesized 2'-deoxy-pyrrolocytidine (d-pC) and 2'-deoxy-6-butylpyrrolocytidine (d-BupC) (Table 1-7) and incorporated the d-pC into dodecadeoxyribonucleotides using the phosphotriester solid phase synthesis. Later in 1996, Gamper et al., tried to incorporate the p-dC into an oligonucleotide using phosphoramidite method.⁶⁸ However, phosphite oxidation step caused degradation of the pyrrolocytosine ring presumably by oxidation of the 6 position by iodine. Although the synthesis of the modified oligonucleotides containing pyrrolocytosine was done by incorporation of the 2'-deoxy-furanouracil (d-fU) into DNA, an then in situ conversion of furanouracil to pyrrolocytosine upon treatment with ammonium hydroxide in the last step of the oligonucleotide synthesis where all the nucleotides are deprotected and the oligonucleotides are cleaved from the solid support (refer to Scheme 1-3 for the oligonucleotide synthetic cycle).

For years, due to the commercial availability of the d-fU, the synthesis of the d-pC labeled oligonucleotides was done by incorporation of d-fU into oligonucleotides and in situ conversion of fU to pC. Then, in 2004 Berry and co-workers synthesized 2'-deoxy-6-methylpyrrolocytidine (d-MepC) and successfully incorporated it into DNA.⁶⁹ Two things were done in order to avoid the oxidative degradation of the pyrrolocytosine ring. One is the presence of the methyl group at 6 position of the ring and the other one is using a more dilute iodine oxidizer (0.02 M). Interestingly, MepC hybridized selectively with G ($G \gg T > A > C$) and the melting temperature (T_m) of fully complementary oligonucleotides and the ones with one to four MepC was identical, indicating that MepC pairs with G exactly similar to C. Moreover, the PCR experiments showed that MepC residues can be recognized and incorporated by polymerase enzymes.

Because of the interesting properties of MepC including quenching upon hybridization and commercial availability despite its low quantum yield in ssDNA (0.03), it was extensively used in several areas of research.²⁰

Table 1-7: Selected examples of pC derivatives and their photophysical properties, R'= ribose/ 2'-deoxyribose/ -CH₂COOH.

Structure	Name	Solvent	λ_{abs} (nm)	λ_{em} (nm)	Φ_f	τ_0 (ns)	Ref.
	X= NH, R'= H pC	water	336	450			67
	X= NH, R'= CH ₃ (CH ₂) ₃ BupC	water	340	460			67
	X= O, R'= H fU	Phosphate buffer (pH= 7)	322				68
	X= NH, R'= Me MepC	water	342	461	0.05		66
	X= NH, R'= Ph PhpC	EtOH	369	447	0.31		70

In line with this type design, Hudson's group synthesized 6-phenylpyrrolocytosine (PhpC) and incorporate it into PNA,^{71,72} DNA,⁷³ and RNA⁷⁴ (Table 1-7). Later, this group synthesized a handful of 6-substituted pyrrolocytosine derivatives and incorporated some of them into DNA, RNA, and PNA backbones.^{70,75}

The pC derivatives are intrinsically fluorescent, meaning the pyrimidine ring is a part of the conjugation system, allowing to have reasonable fluorescence without a drastic increase in the size of the natural nucleoside compared to the conventional polyaromatic hydrocarbons (PAH). Their red-shifted absorption maxima at 360 nm allow selective excitation over the natural nucleosides and amino acids and they retain their hydrogen bonding face with their complementary base (G). Moreover, they can be derivatized through functionalization at the 6 position of the bicyclic ring. This position is easily accessible through the synthetic route of pC and more importantly, it is oriented away from the hydrogen bonding face and it is towards the major groove of the DNA double helix in which DNA duplex can accept substitutions more easily (Figure 1-13). Therefore, pC derivatives do not disturb the duplex stability in the dsDNA due to the small size of the molecule and the hydrogen bonding ability of it.^{69,73} Moreover, they are able to report changes in their microenvironment, oligonucleotide's structure and dynamics, and its state of hybridization.⁷⁴

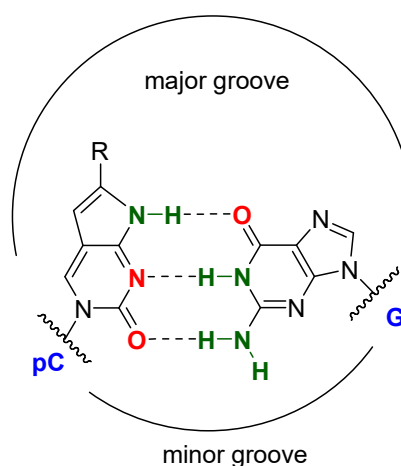


Figure 1-11: Hydrogen bonding of the pC derivatives with G and the orientation of the R group towards the major groove of the duplex. The hydrogen bond donors are shown in green and hydrogen bond acceptors in red. R= Me, Ph, etc.

1.5.1 Synthesis of the pC derivatives

Generally, pC derivatives can be synthesized by three different routes of synthesis shown in Scheme 1-1.

A) Route A

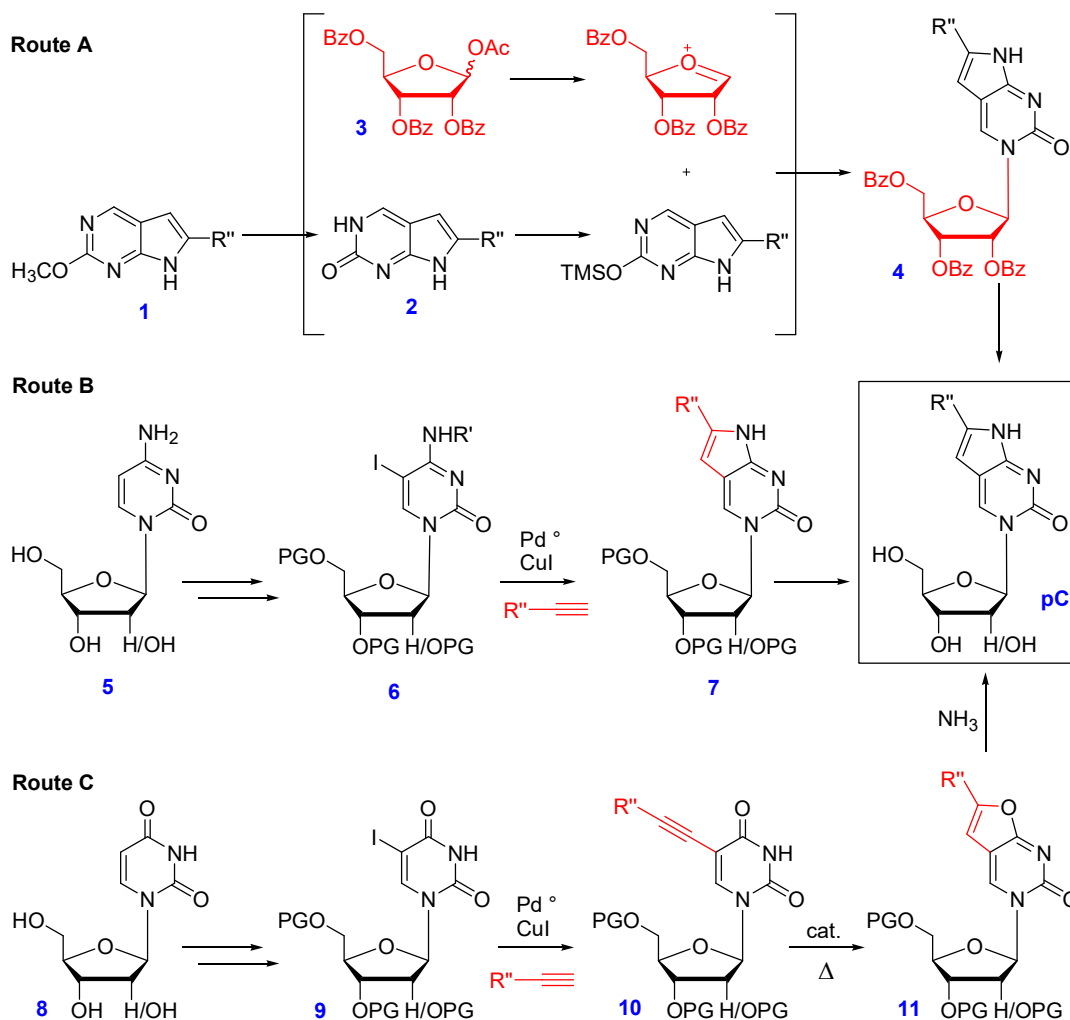
This method takes advantage of the low nucleophilicity of the pyrrole nitrogen. The key reaction in this route is the reaction of compound **2** and **3**. In this step first the silylation of the compound **2** takes place and then the acylated sugar (compound **3**) in the presence of trimethylsilyltriflate (TMSOTf) as catalyst (one-pot Vorbrüggen reaction) affords the protected nucleoside (compound **4**). Finally, deprotection of the nucleoside affords the pyrrolocytidine. This method has only been used for the synthesis of the pyrrolocytosine ring ($R''=H$) and only for RNA monomer.⁷⁶⁻⁷⁸

B) Route B

After iodination at the C5 position of the cytosine and protection of the exocyclic amine, Sonogashira cross-coupling and annulation takes place sequentially (**6**→**7**). Then, the benzoyl group is removed under mild basic conditions right after Sonogashira cross coupling and cyclization. After that, the purified cyclized product is deprotected under basic conditions to afford pC derivative.

C) Route C

Using properly protected and iodinated uridine (compound **9**), the Sonogashira cross-coupling is carried out (**9**→**10**). Then 5-endo dig cyclization of the 5-alkynyluracil gives the furanouridine ring (compound **11**). There are several methods to push the cyclization reaction forward. It can be metal mediated including Ag^+ ,⁷⁹ Cu^+ ,⁶⁷ Zn^+ ,⁸⁰ and base-catalyzed,⁸¹ and electrophile catalyzed.⁸² Finally, substitution of oxygen with nitrogen and deprotection is done one-pot using concentrated ammonia (**11**→pC).

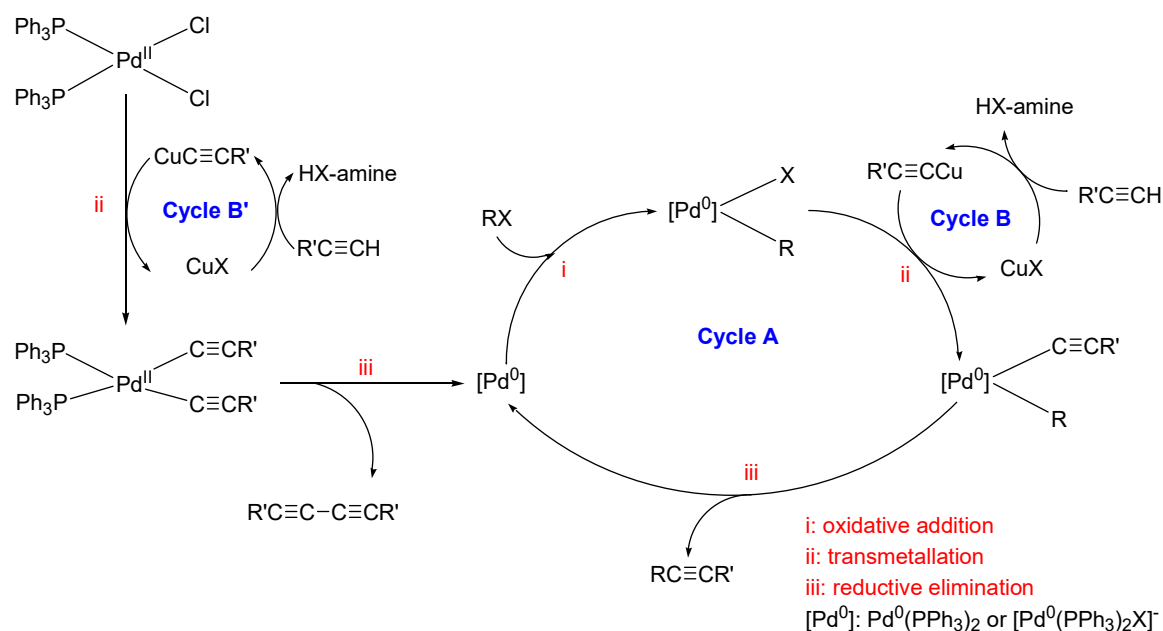


Scheme 1-1: Schematic overview of the synthesis of the pC derivatives.

1.5.2 Sonogashira cross-coupling; the key reaction in the synthesis of pC derivatives

The key reaction in the synthesis of pC derivatives is Sonogashira cross-coupling. It is a palladium(Pd)-copper(Cu) catalyzed reaction, first time introduced in 1975 by Kenkichi Sonogashira.⁸³ This reaction was developed based on combining Cu-catalyzed alkylation of Pd complexes (Cycle B and B' in Scheme 1-2) and Pd-catalyzed cross-coupling of sp^2 -C halides with terminal acetylenes (Cycle A in Scheme 1-2). At that time this reaction was considered as an improved substitution for Stephens-Castro reaction for synthesis of acetylenes, in which sometimes might be limited by the vigorous reaction conditions and also by the difficulties in the preparation of cuprous acetylides.⁸⁴

The proposed mechanism of the catalytic cycle for this reaction involves three cycles of A, B, and B', shown in the Scheme 1-2. The $[\text{Pd}^0]$ is considered as an active form of the catalyst and it may be neutral $\text{Pd}^0(\text{PPh}_3)_2$ or anionic $[\text{Pd}^0(\text{PPh}_3)_2\text{X}]^-$ species. The $[\text{Pd}^0]$ is generated from the $\text{Pd}(\text{PPh}_3)_2\text{Cl}_2$ pre-catalyst (Cycle B' in Scheme 1-2) and gives the $[\text{Pd}^{\text{II}}]$ intermediate by the oxidative addition of the sp^2 -C halide (Cycle A in Scheme 1-2). The transmetalation of the transient copper acetylide species, generated via cycle B, leads to the formation of alkynylpalladium(II) derivative. Lastly, reductive elimination gives the coupled product and regenerates the active $[\text{Pd}^0]$ species.⁸⁴



Scheme 1-2: Proposed catalytic cycle of the Sonogashira cross-coupling.

There are several Pd sources to be used in different cross-coupling reactions. $\text{Pd}(\text{PPh}_3)_2\text{Cl}_2$ and $\text{Pd}(\text{PPh}_3)_4$ are two of the most commonly available sources. In the case of $\text{Pd}(\text{PPh}_3)_2\text{Cl}_2$, the active species must be produced by reductive elimination of the Pd-acetylide complex generated from $\text{Pd}(\text{PPh}_3)_2\text{Cl}_2$ and the terminal acetylene (Cycle B' in Scheme 1-2) which leads to consumption of terminal acetylene and generation of the homo-coupled by-product. However, in the case of $\text{Pd}(\text{PPh}_3)_4$, the active species is generated after the endergonic loss of triphenylphosphine. Nevertheless, this Pd source is very sensitive to air which could be problematic.⁸⁴

1.5.3 Applications of the pC derivatives

It has been shown that PhpC containing DNA oligonucleotides have lower fluorescence intensity upon hybridization into matched sequence containing G than mismatched sequences containing A, C, T. Therefore, PhpC can fluorometrically discriminate between guanosine containing complementary strands from other strands. This property can be used in the single nucleotide polymorphism (SNP) detection of guanine.^{73,85}

Moreover, it is shown that small interfering RNA (siRNA) containing PhpC possess thermal stability and gene silencing activity similar to natural siRNA which provides an ideal system for fluorescence-based monitoring of siRNA uptake, accumulation, and activity.⁸⁶

Furthermore, incorporation of a single PhpC into RNA:DNA duplex, quenches its fluorescence (quenched state), and upon cleavage of the PhpC containing segment by HIV-1 RNase H, fluorescence increases (emissive state) by 14-fold. This system provides molecular beacon-like response reporting HIV-1 RNase H activity. Figure 1-14 shows the concept of HIV-1 RNase H assay. The PhpC is in the quenched state in RNA:DNA hybrid and upon treatment with RNase H, it goes to emissive state.⁸⁷

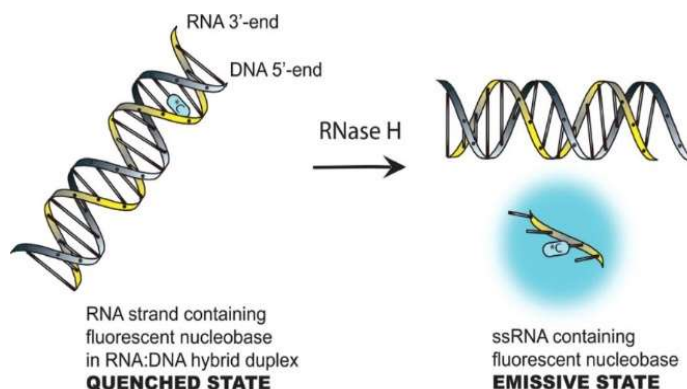


Figure 1-12: The picture is reproduced with permission from: Wahba, A. S.;

Esmaeili, A.; Damha, M. J.; Hudson, R. H. *Nucleic Acids Res.* **2010**, *38*, 1048-1056.

Another derivative of the pC family is [bis-*o*-(aminoethoxy)-phenyl]pyrrolocytosine (BoPhpC) which is designed to have additional hydrogen bonding with guanine. The PNAs containing this derivative have a higher melting temperature (T_m) showing high duplex stabilization effect which can be attributed to the additional hydrogen bonding. Moreover,

they offer good discrimination against binding to mismatched sequences with the decrease in fluorescence quantum yield.^{88,89}

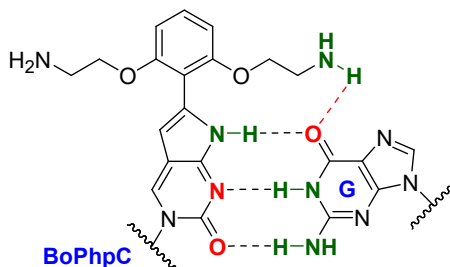


Figure 1-13: BoPhpC in hydrogen bonding with G. The additional hydrogen bonding with G increases the duplex stability. The hydrogen bond donors are shown in green and hydrogen bond acceptors in red.

The RNA containing BoPhpC complementary to the mRNA encoding the protein huntington (HTT) which is responsible for the Huntington's disease, selectively inhibited mutant HTT expression. Moreover, through fluorescence activity of the BoPhpC, cellular localization and trafficking can be monitored without any disturbances.⁹⁰

In another example, BoPhpC was incorporated into a PNA sequence complementary to miRNA-122. The miRNA-122 is required for hepatitis C virus (HCV) replication, therefore anti-miRNA-122 can lead to suppression of HCV. The results showed that PNA containing BoPhpC could enter liver cells in the absence of the transfection agents and inhibit miRNA-122. Moreover, it allowed monitoring of PNA without substantial compromise of the PNA activity in inhibition of miRNA, providing interesting information regarding cell delivery and trafficking of the miRNA-122.⁹¹

Another derivative of the pC family, 2-pyridinyl-pyrrolocytosine (2-PypC) was utilized in the parallel-stranded DNA. Duplexes with parallel stranded orientation are resistant to nucleolytic enzymes and their potential applications are antisense therapeutics or diagnostics. The parallel-stranded DNA is thermally less stable than the anti-parallel stranded DNA and several methods have been utilized to stabilize it. Seela and co-workers were able to enhance the stability of the parallel-stranded DNA by silver mediated base pairing between two pairs of the 2-PypC.⁹² It was shown that the stability enhanced with 2 equivalents of the silver ions. The binding of metal ions can give the DNA molecule unique

chemical and physical characteristics including electrical conductivity, single-molecule magnetism, or charge transfer properties which are another potential application of pC derivatives.

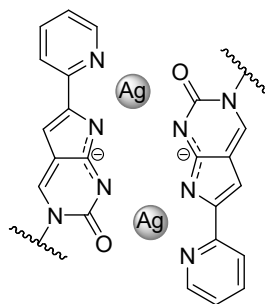


Figure 1-14: Two 2-PypC and two silver ions in parallel stranded DNA constructs.

In order to increase the stability of the parallel-stranded DNA, in another attempt, Seela and co-workers, synthesized a pC derivative containing alkylamino side chain tethered via a triazole linker to the 5 position of pC (Figure 1-17). This derivative was designed to have extra hydrogen bonding with iso-G in parallel-stranded DNA. However, the studies showed that the oligonucleotides containing this derivative does not increase the melting temperature and therefore does not increase the stability of the parallel-stranded DNA.⁹³

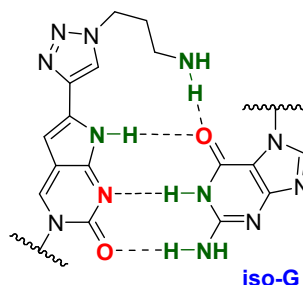


Figure 1-15: Hydrogen bonding of the pC derivative containing alkylamino side chain tethered via triazole linker with iso-G in parallel stranded DNA constructs.

The hydrogen bond donors are shown in green and hydrogen bond acceptors in red.

Saito and coworkers synthesized the pyrene-labeled pyrrolocytosine (PyrpC) and utilized it in the design of the quencher free molecular beacons. The quencher free molecular beacons utilize guanine as the natural quencher of most of the fluorophores. PyrpC was incorporated into the stem of the molecular beacons and the modified molecular beacons showed higher duplex stability than the fully-matched sequence and the fluorescence of the pyrene-labeled pyrrolocytidine was efficiently quenched by the opposite G. Moreover,

the designed MBs could detect the target DNA with an excellent efficiency, irrespective of the sequence, length and the position in the stem. It is worth noting that the pyrene-labeled pC containing oligonucleotide was synthesized by attaching the pyrene post-synthetically onto the methylamino derivative of pC (Figure 1-18) and the guanine as the quencher was in hydrogen bonding with the pyrrolocytosine.⁹⁴

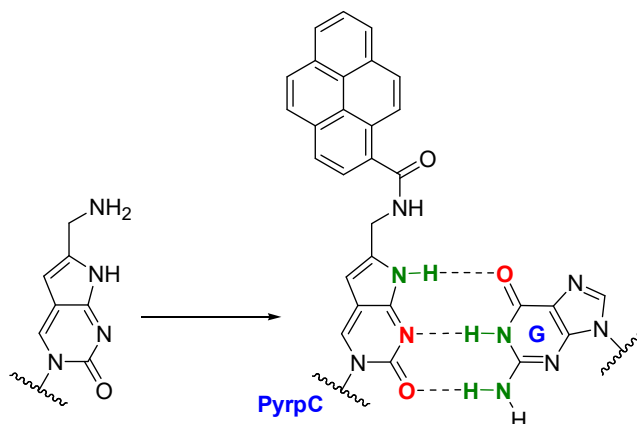


Figure 1-16: PyrC in hydrogen bonding with guanine. The hydrogen bond donors are shown in green and hydrogen bond acceptors in red.

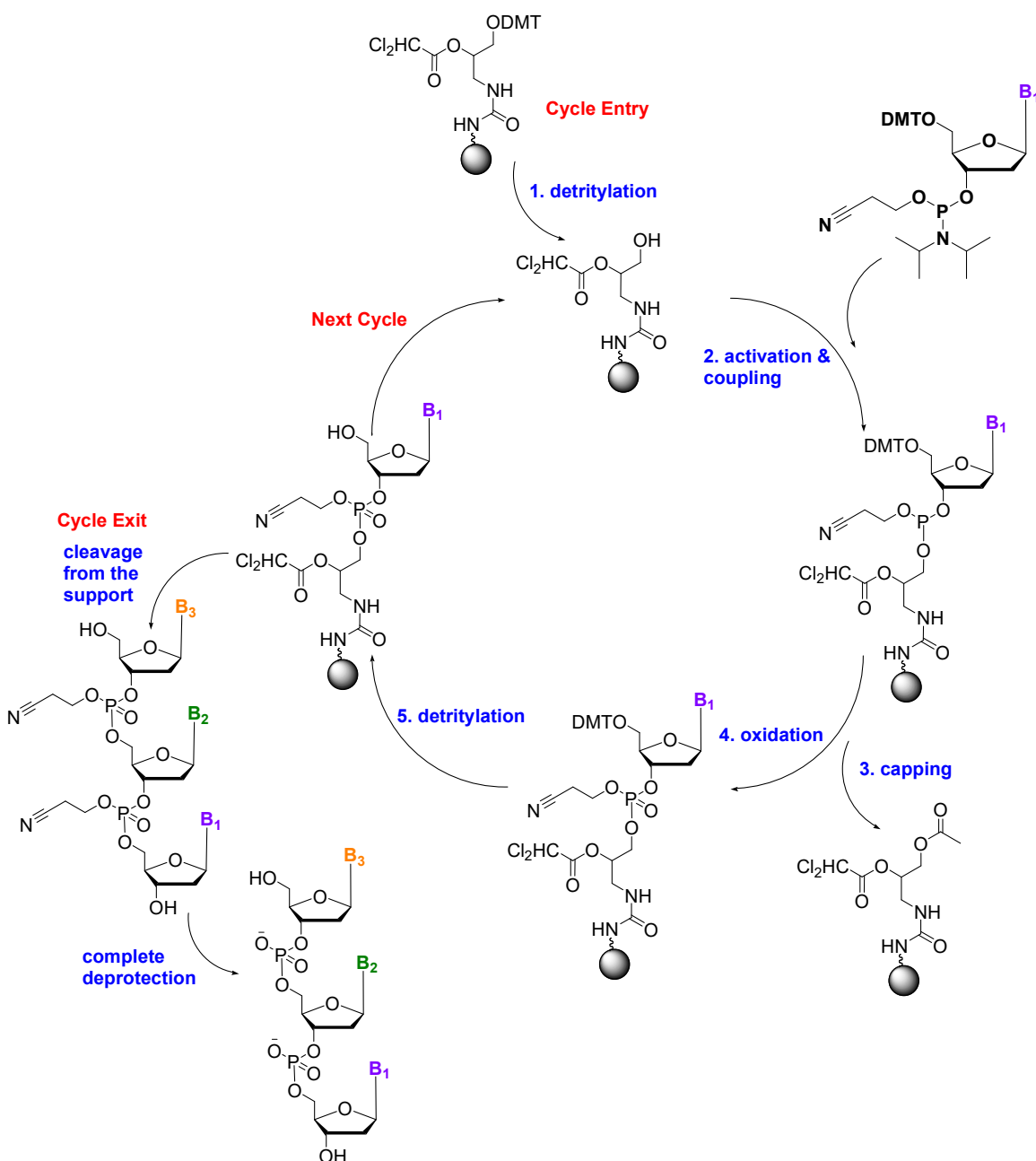
1.6 Solid phase oligonucleotide synthesis

Chemical synthesis of oligonucleotides has long been studied by chemists since 1955.⁹⁵ The first method was phosphite triester method which relied on the use of P(III) chemistry.⁹⁶ Due to inherent sensitivity of the reagents of this method to moisture and air oxidation, and abnormal conditions including $-78\text{ }^{\circ}\text{C}$, the automation of this reaction faced with technical hardships. Later this problem was tackled with the introduction of the phosphoramidite method in 1981.⁹⁷ The compatibility of this method with the automation made this method one of the best and widely used methods for the chemical synthesis of oligonucleotides until now.^{98,99} Several minor revisions were done on the original method and it is used for oligonucleotide synthesis similar to what is shown in the Scheme 1-4.

In the phosphoramidite method, the direction of synthesis is 3' to 5'. In the conventional method, the first nucleotide is fixed on the solid support and the next nucleotides are introduced one by one at each cycle. Recently, universal supports have been introduced to the market which has a DMT protected OH group and the first nucleotide is attached to the

support upon detritylation of the solid support. The structure of the universal support III is illustrated in the Scheme 1-3.

As the first step, DMT protecting group on the universal support is removed by treatment with dichloroacetic acid. Then the first nucleoside is activated using a weak acid like 5-ethylthiotetrazole and a new linkage between 5'-OH of the support and activated



Scheme 1-3: Schematic overview of the chemical synthesis of the oligonucleotide on universal support III.

phosphorous of the first nucleoside is made with 99% yield. In the next step, the unreacted support is deactivated by acetylation of the 5'-OH with acetic anhydride. Then P(III) is oxidized to P(V) with iodine/water. The cycle continues with detritylation of the last nucleoside on the solid support and activation and coupling of the next nucleoside. After completion of the synthesis, the oligonucleotide is removed from the solid support and all the nucleotides are deprotected in a single step of treatment with concentrated ammonium hydroxide for 16 h at 55 °C.

1.7 Objectives of the thesis

In the next two chapters, the studies on the photophysical properties of the pC derivatives are discussed.

In chapter 2, the effect of the nearest neighbours on the quantum yield of the PhpC containing ssDNA and dsDNA are investigated and the results are analyzed based on the nature of the nearest neighbours and their orientation within the ssDNA and dsDNA. Moreover, the possibility of photoinduced electron transfer by pC derivatives is investigated through measurement of the ground state redox potentials by cyclic voltammetry and the calculation of the excited state redox potentials, and the estimation of the free energy change of the pC derivatives with the natural nucleosides.

In chapter 3, the possibility of FRET by two pC derivatives as the donor and acceptor is investigated. Due to their spectral overlap, PhpC is possibly the donor and *p*-NO₂-PhpC the acceptor. The possibility of FRET between pyrene and *p*-NO₂-PhpC is also investigated. In order to do that, the fluorescence intensity of the PhpC and pyrene is plotted against the increasing concentrations of the *p*-NO₂-PhpC and the Stern-Volmer constant and the inverse Stern-Volmer constant is utilized in order to compare the two pairs.

Chapter 2

2 Analysis of the effect of the nearest neighbours on the quantum yield of PhpC upon incorporation into ssDNA and dsDNA and investigation of the underlying mechanism

2.1 Introduction

As discussed earlier PhpC has been utilized in several biological studies. In all of the biological studies conducted, PhpC showed variation in the fluorescence properties. It was found that the fluorescence intensity of PhpC changes with the change in neighbouring nucleosides, the state of hybridization (single or double stranded) and the length of the sequences. These properties may have a dramatic effect on the fluorescence intensity of the PhpC containing probes. Therefore, developing an understanding of the effects of surrounding nucleosides on the fluorescence properties of PhpC and investigation of the underlying mechanism is crucial. The purpose of this study is to provide a guide for the proper design of the PhpC containing oligonucleotides for different applications, either microscopy applications that need the highest fluorescent oligonucleotide sequences, or kinetic/mechanistic investigations which needs oligonucleotides with the biggest difference in fluorescence quantum yield between the different states of hybridizations or different secondary structures. Moreover, the possibility of PET as an underlying mechanism of the different fluorescent intensities of PhpC is investigated.

In this study, the quantum yield of PhpC when incorporated into ssDNA and dsDNA with different nearest neighbours will be analyzed. The sequences of the study are 15-mer DNA containing PhpC in the middle, and different neighbours shown as X and Y, flanked by two symmetric constant regions, 5'-d[ACA CTT XPhpCY TTC ACA]-3' (X, Y = A, G, C, T). This library covers all sixteen possible nearest neighbour variations around the PhpC residue in the single-stranded state. The complementary sequences for the hybridization studies contained all natural nucleosides and G as the complementary base for PhpC.

In order to determine the mechanism of the quenching, the oxidation and reduction potentials of the d-PhpC and two more derivatives; d-*p*-NO₂-PhpC, and *p*-OMe-PhpC are

measured by cyclic voltammetry. Then the mechanism of the quenching was thermodynamically evaluated based on the estimation of the photoinduced electron transfer free energies of the excited state fluorophore and the ground state natural nucleosides.

2.2 Results and discussions

2.2.1 Investigation of the effect of the nearest neighbours on the quantum yield of the ssDNA and dsDNA containing PhpC

In this section, the results of the studies on the photophysical properties of the PhpC upon incorporation into ssDNA and dsDNA is analyzed and the effect of the nature and the orientation of the variations of the nearest neighbours on the quantum yield of PhpC is discussed. The fluorescence quantum yields (Φ_f) of the ssDNA and dsDNA containing PhpC are listed in Table 2-1 and depicted graphically in Figure 2-1 from the highest to the lowest quantum yield for the single stranded state.

Table 2-1: The fluorescence quantum yield of the ssDNA and dsDNA containing PhpC. The highest and the lowest numbers in each column are bolded.

Label	DNA sequence	Φ_f ssDNA	Φ_f dsDNA	Φ_f ssDNA - Φ_f dsDNA
TT	5'-d[ACA CTT T PhpCT TTC ACA]-3'	0.14 ±0.010	0.10 ±0.007	0.04 ±0.017
TA	5'-d[ACA CTT T PhpCA TTC ACA]-3'	0.36 ±0.025	0.11 ±0.004	0.25 ±0.029
AT	5'-d[ACA CTT A PhpCT TTC ACA]-3'	0.45 ±0.030	0.26 ±0.018	0.19 ±0.048
TC	5'-d[ACA CTT T PhpCC TTC ACA]-3'	0.20 ±0.014	0.14 ±0.010	0.06 ±0.024
CT	5'-d[ACA CTT C PhpCT TTC ACA]-3'	0.34 ±0.020	0.10 ±0.005	0.24 ±0.025
TG	5'-d[ACA CTT T PhpCG TTC ACA]-3'	0.19 ±0.013	0.09 ±0.006	0.10 ±0.019
GT	5'-d[ACA CTT G PhpCT TTC ACA]-3'	0.22 ±0.015	0.06 ±0.004	0.16 ±0.019
AA	5'-d[ACA CTT A PhpCA TTC ACA]-3'	0.38 ±0.027	0.24 ±0.002	0.14 ±0.029
AC	5'-d[ACA CTT A PhpCC TTC ACA]-3'	0.29 ±0.020	0.19 ±0.013	0.10 ±0.033
CA	5'-d[ACA CTT C PhpCA TTC ACA]-3'	0.20 ±0.014	0.06 ±0.005	0.14 ±0.019
AG	5'-d[ACA CTT A PhpCG TTC ACA]-3'	0.29 ±0.020	0.09 ±0.004	0.20 ±0.024
GA	5'-d[ACA CTT G PhpCA TTC ACA]-3'	0.17 ±0.012	0.02 ±0.001	0.15 ±0.013
CC	5'-d[ACA CTT C PhpCC TTC ACA]-3'	0.19 ±0.013	0.07 ±0.005	0.12 ±0.018
CG	5'-d[ACA CTT C PhpCG TTC ACA]-3'	0.11 ±0.007	0.09 ±0.006	0.02 ±0.013
GC	5'-d[ACA CTT G PhpCC TTC ACA]-3'	0.18 ±0.013	0.05 ±0.003	0.13 ±0.016
GG	5'-d[ACA CTT G PhpCG TTC ACA]-3'	0.10 ±0.007	0.05 ±0.007	0.05 ±0.014

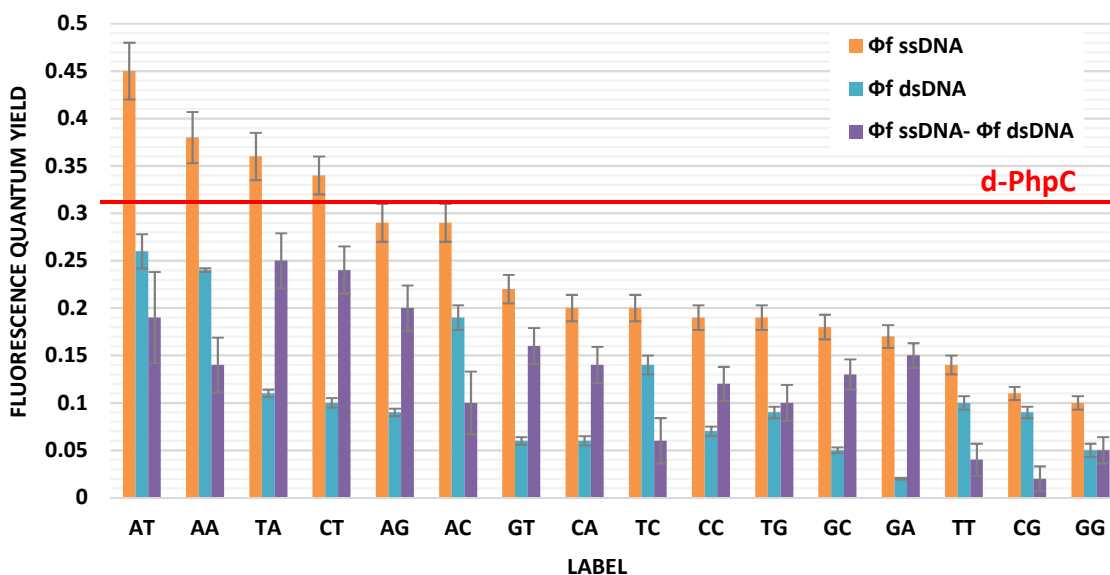


Figure 2-1: The fluorescence quantum yield of the ssDNA (orange) in decreasing order from left to right in conjunction with the quantum yield of the dsDNA (teal) and the quantum yield difference of ssDNA and dsDNA (purple). The red line shows the quantum yield of the free d-PhpC in water ($\Phi_f = 0.31$)

2.2.1.1 Fluorescence quantum yield of the ssDNA containing PhpC

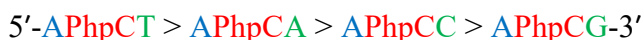
The quantum yield of the ssDNA containing PhpC displayed a broad range from 0.10-0.45. Among all the ssDNA sequences, the quantum yield of those containing AT, AA, TA, AC, AG and CT flanking pairs is greater or very close to the d-PhpC free nucleoside ($\Phi_f = 0.31$).⁷⁰ However, the quantum yield of all other sequences decreases upon incorporation into ssDNA. Five sequences of the six most fluorescent sequences were those in which PhpC is flanked by adenine (AT, AA, TA, AC, and AG) and four of the five least fluorescent sequences have flanking guanine in their neighbourhood (GC, GA, CG, GG).

A brief analysis of the quantum yields of the ssDNA shows that the nature of the neighbouring nucleosides affects the fluorescence quantum yield of the ssDNA containing PhpC. Furthermore, in-depth analysis revealed interesting increasing and decreasing trends of fluorescence quantum yields. To highlight the trends, the obtained results were classified into four groups based on the variation of the adjacent nucleotides (4 nucleotides) and each group were further classified into two subgroups based on the orientation of each

nucleotide (either on the 5' side or 3' side of the PhpC) illustrated as 5'-XPhpCY-3' (Figure 2-2). In all the charts in Figure 2-2 the horizontal and vertical axis are labels and fluorescent quantum yields respectively which are deleted from the chart to save the space.

Here, the findings are explained for adenine as an example:

a) When adenine is placed at the 5' side of the PhpC ($X = A$; 5'-APhpCY-3'), the resulting fluorescence depends on the 3'-nucleotide residue (Y), and follows this order:



In other words; when $X = A$, then $Y = T > A > C > G$. (Figure 2-2A)

b) Similarly, when adenine is placed at the 3' side of the PhpC ($Y = A$; 5'-XPhpCA-3'), the fluorescence varies as follow: 5'-APhpCA > TPhpCA > CPhpCA > GPhpCA-3'

Therefore, when $Y = A$, $X = A > T > C > G$. (Figure 2-2B)

Similar trends were observed for 2'-deoxycytidine (Figure 2-2C and 2-2D) and 2'-deoxyguanosine (Figure 2-2E and 2-2F). However, in the case of thymidine, both subgroups followed the trend; $X, Y = A > C > G > T$ (Figure 2-2G and 2-2H). This observation shows that the fluorescence quantum yield of the PhpC upon incorporation into ssDNA depends on the nature and the orientation of the neighbouring nucleosides. Figure 2-3, summarizes the trends explained earlier. It shows that for example if nucleotide X or Y is T, the resulting fluorescence quantum yields follow this trend: $X/Y = A > C > G > T$.

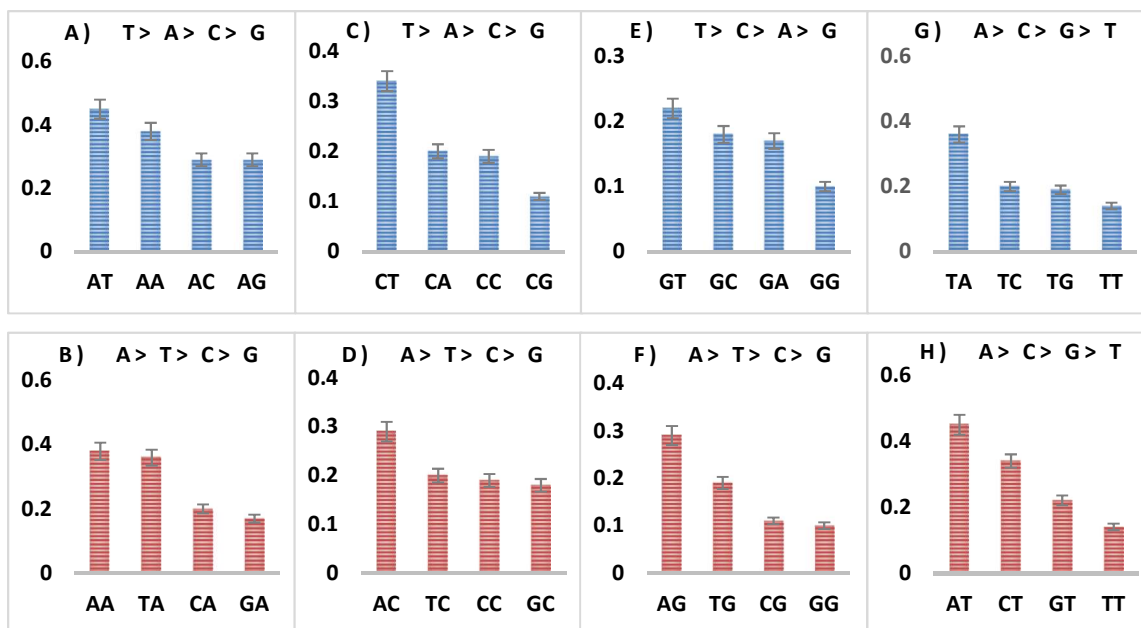


Figure 2-2: Fluorescence quantum yield of ssDNA containing PhpC in decreasing order and the observed trends where: A) X= A; B) Y= A; C) X= C; D) Y= C; E) X= G; F) Y= G; G) X= T; H) Y= T.

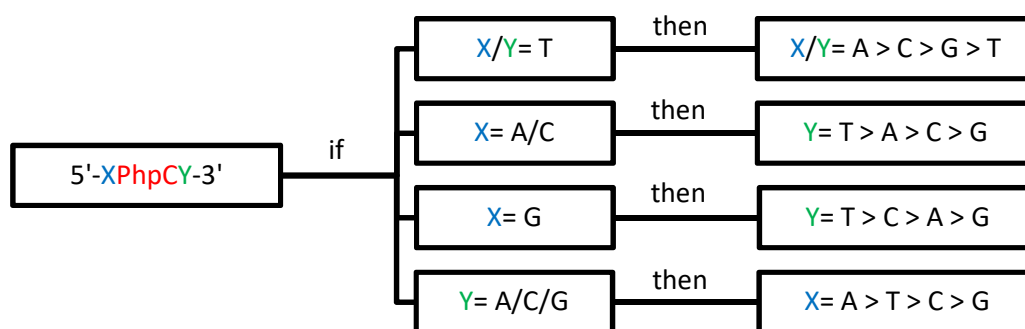


Figure 2-3: Summary of the structure activity relationship of the change in quantum yield of the PhpC upon incorporation into ssDNA with different neighbours

A more careful analysis of the quantum yields of the ssDNA, presented in Table 2-1 and Figure 2-1, revealed that the orientation of the neighbours around PhpC significantly affects the quantum yield. In order to investigate the effect of the orientation on the fluorescent properties of PhpC, every two similar sequences with 5' and 3' orientations were analyzed and their p-value was calculated. In Figure 2-4, the comparison was made between two orientations of each nucleoside and the sequences with no significant difference (at 95% confidence interval) were shown with a star. Figure 2-4 shows that there is a significant difference between 3' and 5' orientations of each two sequences except TG

and GT and there is a consistent trend between the sequences containing A (Figure 2-4A). The analysis shows that the sequences with a 5'-flanking adenine are more fluorescent than those with 3'-flanking adenine.

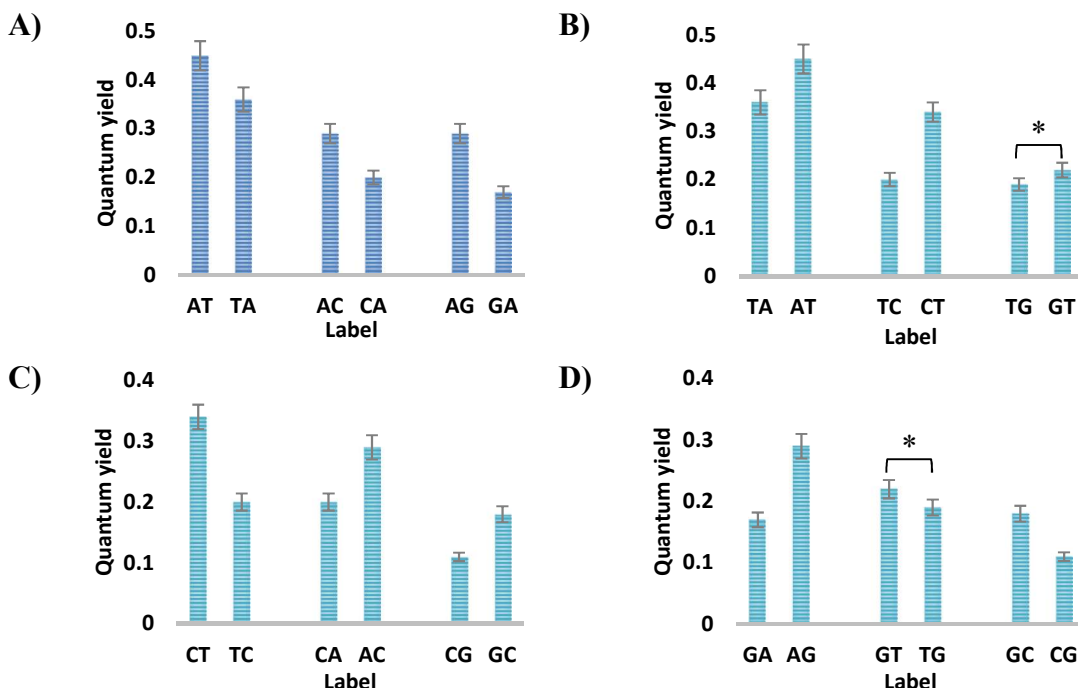


Figure 2-2: Fluorescence quantum yield of the ssDNA containing PhpC flanked by A) 5'-A and 3'-A. B) 3'-T and 5'-T. C) 5'-C and 3'-C. D) 5'-G and 3'-G. The sequences with no significant difference are shown with star (*).

2.2.1.2 Fluorescence quantum yield of the dsDNA containing PhpC

The fluorescence quantum yield of the sixteen DNA sequences containing PhpC was measured upon hybridization into their complementary strand. The numbers are listed in Table 2-1 and depicted graphically in Figure 2-1. The data shows that the fluorescence quantum yield of the all the variations is decreased upon hybridization to the complementary DNA and the decrease is statistically significant ($p < 0.05$). The decrease in the quantum yield varies from 0.25 for TA to 0.02 for CG showing a huge sequence-dependent manner. Figure 2-5 shows the observed trends for dsDNA when A/C/G/T are at either 5'-side or 3'-side of the PhpC. Comparison of the graphs for dsDNA (Figure 2-5) with ssDNA (Figure 2-2) demonstrates that quantum yield of the dsDNA with 3'-A, 3'-C, and 3'-G follows the same trend as ssDNA and the other variations do not have the same

trend in single-stranded and double-stranded form. This observation shows that the degree of the quenching upon hybridization in more extent depends on the nature of the neighbouring nucleoside at the 5' side of the PhpC and in less extent on the neighbouring nucleoside at 3' side. Figure 2-6, summarizes the trends explained earlier. It shows that for example if nucleotide Y is A/T/C/G, the resulting fluorescence quantum yield follows the trend: $X = A > T > C > G$.

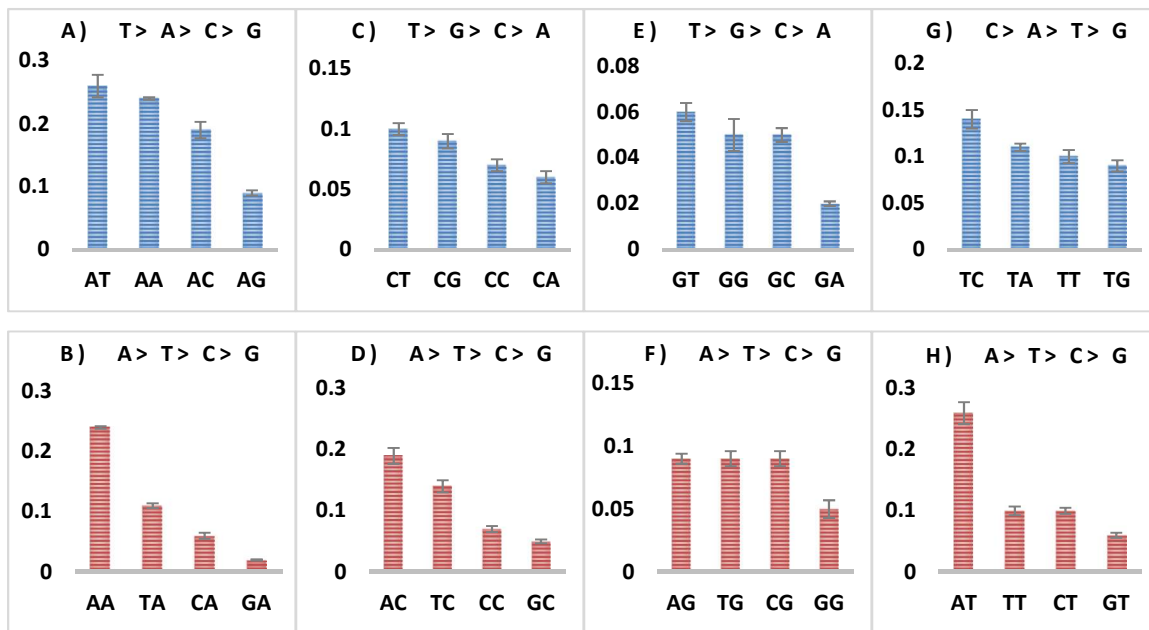


Figure 2-3: Fluorescence quantum yield of dsDNA containing PhpC (5'-XPhpCY-3') to decreasing order and the observed trends where: A) X= A; B) Y= A; C) X= C; D) Y= C; E) X= G; F) Y= G; G) X= T; H) Y= T.

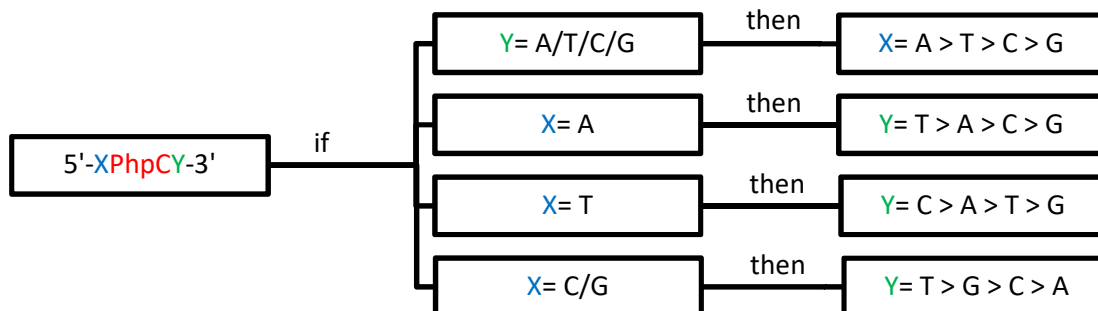


Figure 2-4: Summary of the structure-activity relationship of the change in quantum yield of the PhpC upon hybridization into dsDNA having different neighbours.

A more careful analysis of the quantum yields of the dsDNA, presented in Table 2-1 and Figure 2-1, revealed that same as the single-stranded state, the orientation of the neighbours around PhpC significantly affects its quantum yield in the double-stranded state. The quantum yield of each two similar sequences with different 5' and 3' orientations were analyzed. All the variations showed statistically significant difference between placement at 3' and 5' side of the PhpC however only adenine and guanine showed consistent trends. Sequences with a 5'-flanking adenine are more fluorescent than those with 3'-flanking adenine (Figure 2-7A) and sequences with 3'-flanking guanine are brighter than 5'-flanking guanine (Figure 2-7D).

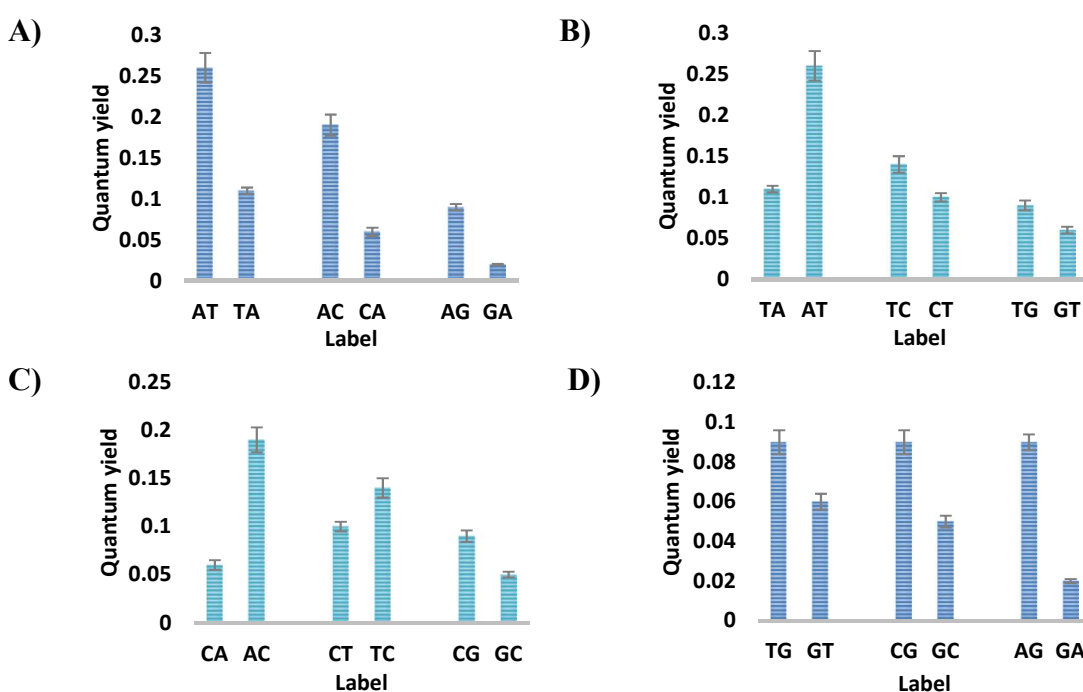


Figure 2-5: Fluorescence quantum yield of the dsDNA containing PhpC flanked by:
A) 5'-A and 3'-A. B) 5'-T and 3'-T. C) 5'-C and 3'-C. D) 3'-G and 5'-G.

Furthermore, hybridization of the PhpC containing DNA with its complementary strand brings three more nucleosides into the vicinity of PhpC. One is the paired guanine and the other two are A/T/C/G at the 5' side or 3' side of PhpC on the complementary strand shown as X' and Y' ($\frac{5'-X\text{PhpC}Y-3'}{3'-X'G'Y'-5'}$). The effect of the placement of a particular nucleoside on the same strand or on the complementary strand is analyzed in Figure 2-8.

In Figure 2-8A, the quantum yield of the sequences containing A at the 3' side of PhpC and on the same strand (AA, TA, CA, GA) are compared with the sequences containing A on the complementary strand (AT, TT, CT, GT) respectively. In Figure 2-8B the sequences containing A at the 5' side of PhpC on the same strand (AT, AA, AC, AG) are compared with the sequences containing A on the complementary strand (TT, TA, TC, TG) respectively (this comparison applies for T as well). The same analysis was done for G and C in Figure 2-8C and 2-8D. The p-value was calculated for every two sequences and for the whole set of the numbers and every two sequences with no statistical difference are shown with a star. It is worth noting that placement of A/T at the 3' side and 5' of PhpC on the same strand or on the complementary strand does not change the quantum yield significantly ($p > 0.05$). Furthermore, placement of C/G at the 3' side of PhpC on the same strand or on the complementary does not change quantum yield significantly ($p > 0.05$) (Figure 2-8C). However, placement of C/G at the 5' side of PhpC on the same strand or on the complementary strand significantly affects the quantum yield (Figure 2-8D).

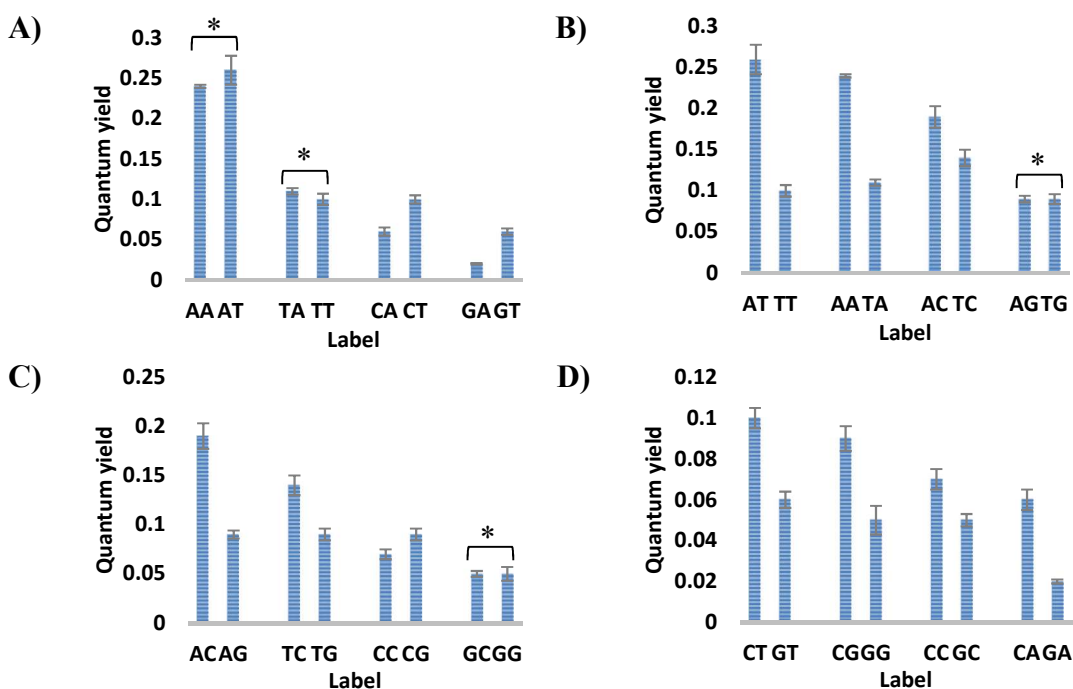


Figure 2-6: Change in the quantum yield of dsDNA containing PhpC with respect to the placement of the nucleosides on the same strand VS. the complementary strand where: A) Y/Y'= A/T; B) Y/Y'= C/G; C) X/X'= A/T; X/X'= C/G. The sequences with no significant difference are shown with star (*).

Moreover, on the dsDNA, guanine as the well-known natural quencher of the PhpC can be found in different numbers around PhpC. Therefore, dsDNA sequences containing PhpC were categorized into three groups based on the number of guanines (1G, 2G, 3G). The quantum yield of the dsDNA containing PhpC is shown in Figure 2-9. The analysis of the variance shows that there is a significant difference between the groups ($p < 0.05$) and generally PhpC is quenched more with increasing the number of guanine in the vicinity.

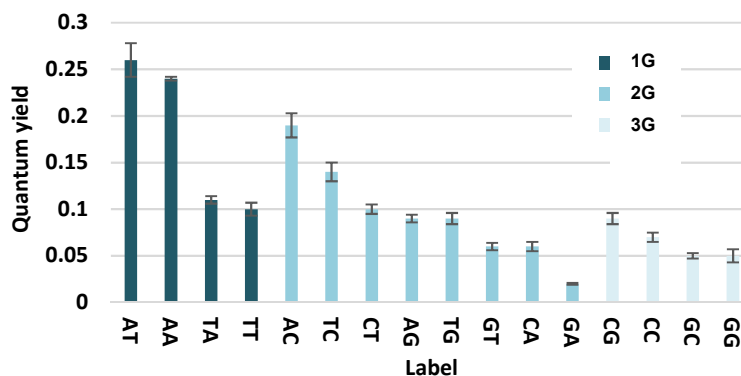


Figure 2-7: Quantum yield of the dsDNA containing PhpC based on the number of guanines around PhpC

Furthermore, guanine can be found in three different positions ($\frac{5'-X\text{PhpC}Y-3'}{3'-X'G Y'-5'}$): 1) in hydrogen bonding with PhpC, 2) as nearest neighbour at the 5' side (X) or 3' side (Y) of PhpC, 3) in hydrogen bonding with the nearest neighbours of PhpC at the 5' side (Y') or 3' side (X') of the PhpC. In all of the sequences PhpC is in hydrogen bonding with guanine and arrangement of guanine in other two positions differ. In addition to the number of guanines, the orientation also affects the quantum yield of PhpC. The observed trend for the quenching of the guanine in different positions is as followed:

$G=Y' > G=X' > G=Y > G=X, Y' > G=X', Y > G=X > G=X, Y' > G=X, Y.$

The trends show that quenching of guanine is more efficient when it is on the same strand with the PhpC and especially when it is on the 5' side of it. Interestingly, PhpC is more quenched when there is one guanine at the 5' side of PhpC compared to the presence of two guanines both on the complementary strand ($G=X', Y'$) and one on the 3' side of PhpC on the same strand and one on the complementary strand ($G=X', Y$).

By only considering the quenching effect of guanine the expected trend does not match with the observed trend (Figure 2-10A). The other influential nucleoside on the photophysical properties of PhpC is adenine. Adenine seems to have a dual effect on the quantum yield of PhpC when it is placed in different positions. From the results, it can be concluded that 3'-A works as a quencher and the 5'-A increases the fluorescence intensity. The trend for this interesting observation is as follows:

$$A=Y < A=Y' < A=X', Y < A=X', Y' < A=X' < A=X < A=X, Y < A=X, Y'$$

The trends show that PhpC is efficiently quenched when adenine is on the 3' side of PhpC on the same strand (Y) compared to the complementary strand (Y'). Moreover, the quenching effect of adenine on the 3' side of PhpC seems to be better than guanine on the 3' side of PhpC (Figure 2-10B).

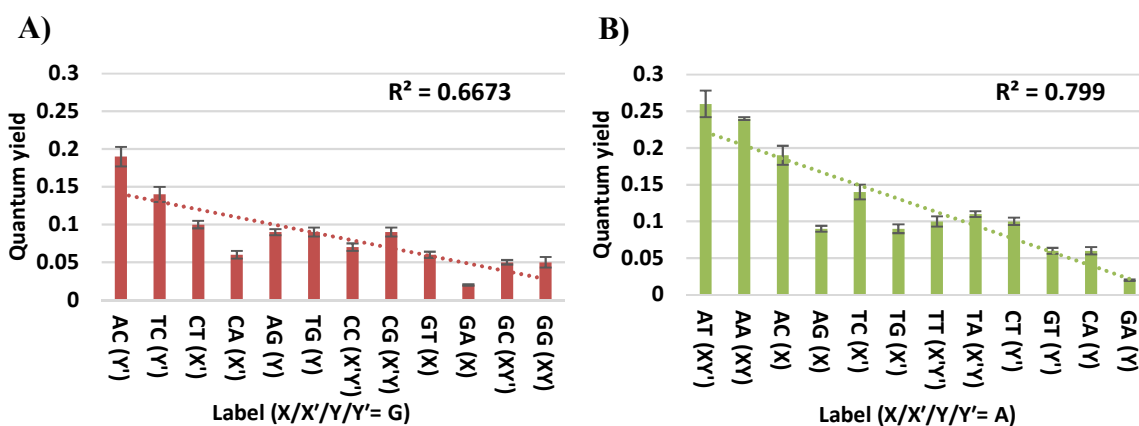


Figure 2-8: The observed trend for the dsDNA sequences containing PhpC based on the influence of neighbouring A) Guanine, and B) Adenine

By considering only one of these rules the expected trends do not match with the experimental values. By combining the two rules for adenine and guanine the observed irregularities in each one of the trends are resolved and the expected trend match the experimental values and have a better correlation (Figure 2-11).

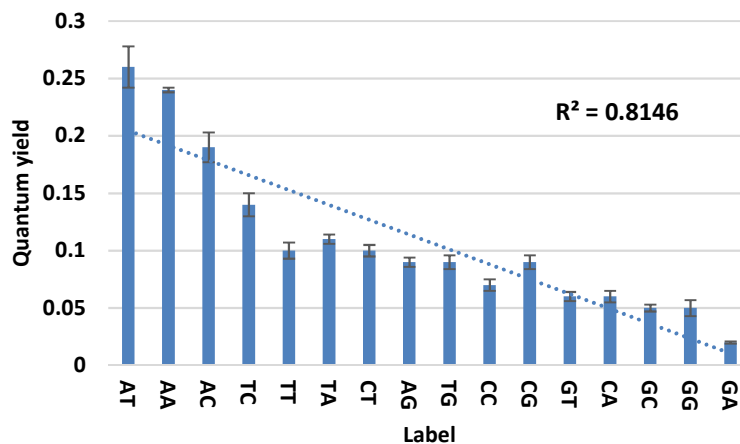


Figure 2-9: The revised trend for the dsDNA sequences by including the effect of the neighbouring guanine and adenine on the quantum yield

Even though more change in the fluorescence quantum yield upon hybridization seems to be very good for the design of the hybridization probes which need the biggest difference in the unhybridized (unquenched) and hybridized (quenched) state, the presence of the background fluorescence in the hybridized state (quenched) is also important. In other words, the decrease in the fluorescence intensity upon hybridization is better to be efficient. Efficient quenching allows going from near zero emission in the hybridized (quenched) state to fluorescence (unquenched) state with acceptable quantum yield. The efficiency of the quenching can be judged by comparing the normalized change in the quantum yield. The normalized change in quantum yield shows the most dramatic change in quantum yield in the ssDNA state upon hybridization into dsDNA and is calculated for each sequence by the equation below where Φ_f ssDNA is the fluorescence quantum yield of the single stranded DNA and Φ_f dsDNA is the fluorescence quantum yield of the double stranded DNA. The more negative normalized quantum yield shows the most dramatic change of the fluorescence quantum yield upon hybridization.

$$\text{Normalized change in quantum yield} = \frac{\Phi_f \text{ dsDNA} - \Phi_f \text{ ssDNA}}{\Phi_f \text{ ssDNA}} \quad \text{Equation 4}$$

Figure 2-12 shows the normalized quantum yield of the designed sequences in increasing order. It shows that GA has the most dramatic change in quantum yield upon hybridization, therefore it is the best sequence for the studies which need the “ON-OFF” state.

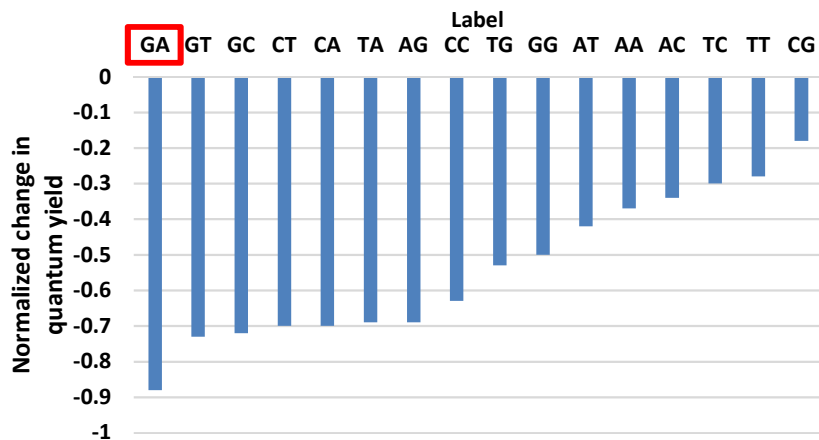


Figure 2-10: Normalized change in quantum yield of ssDNA upon hybridization into dsDNA

2.2.1.3 Optimum design of the fluorescent probes containing PhpC

Studies on the quantum yield of the PhpC in response to different nearest neighbours is done in order to design better fluorescent probes containing PhpC. Herein, best sequences for some of the previously discussed applications of PhpC is recommended.

For the single nucleotide polymorphism (SNP) detection of guanine, the designed probe must have a dramatic change in fluorescence response in different hybridization states. Therefore, GA sequence which has the most negative normalized change in fluorescence quantum yield is the best option. For the monitoring of the nucleic acid trafficking and accumulation, the designed probe must have very high and stable fluorescence response. Therefore, for the ssDNA probes AT, AA, TA, and CT are recommended and for the dsDNA probes AT, AA and AC are recommended. For the hybridization probes, same as the SNP detection the designed probe must have the most dramatic change in fluorescence upon hybridization. Therefore, sequence GA is the best option for this application.

2.2.2 Investigation of the photoinduced electron transfer (PET) of some pC derivatives

In order to understand the origin of fluorescence quenching discussed in the previous section the possibility of the photoinduced electron transfer was investigated. These studies required the measurement of the ground state redox potentials by cyclic voltammetry. The excited state redox potentials were calculated then using the zero-zero energy for the

transition to the lowest excited state of the fluorophore. Using the excited state redox potentials of the fluorophore, the ground state redox potentials of the natural nucleosides, and Rehm-Weller equation the free energy change was calculated. The sign and the magnitude of the free energy change can determine the possibility of the PET.¹⁰⁰

The derivatives which were used in this study are d-PhpC, d-*p*-NO₂-PhpC and *p*-OMe-PhpC. The nitro and methoxy derivative of PhpC was chosen in order to investigate the effect of the electron withdrawing and electron donating groups on the free energy change and the possibility of prediction of the quantum yield of the nitro and methoxy derivatives based on their free energy changes. The d-PhpC and d-*p*-NO₂-PhpC were synthesized and the *p*-OMe-PhpC was provided from the inventory of our lab.

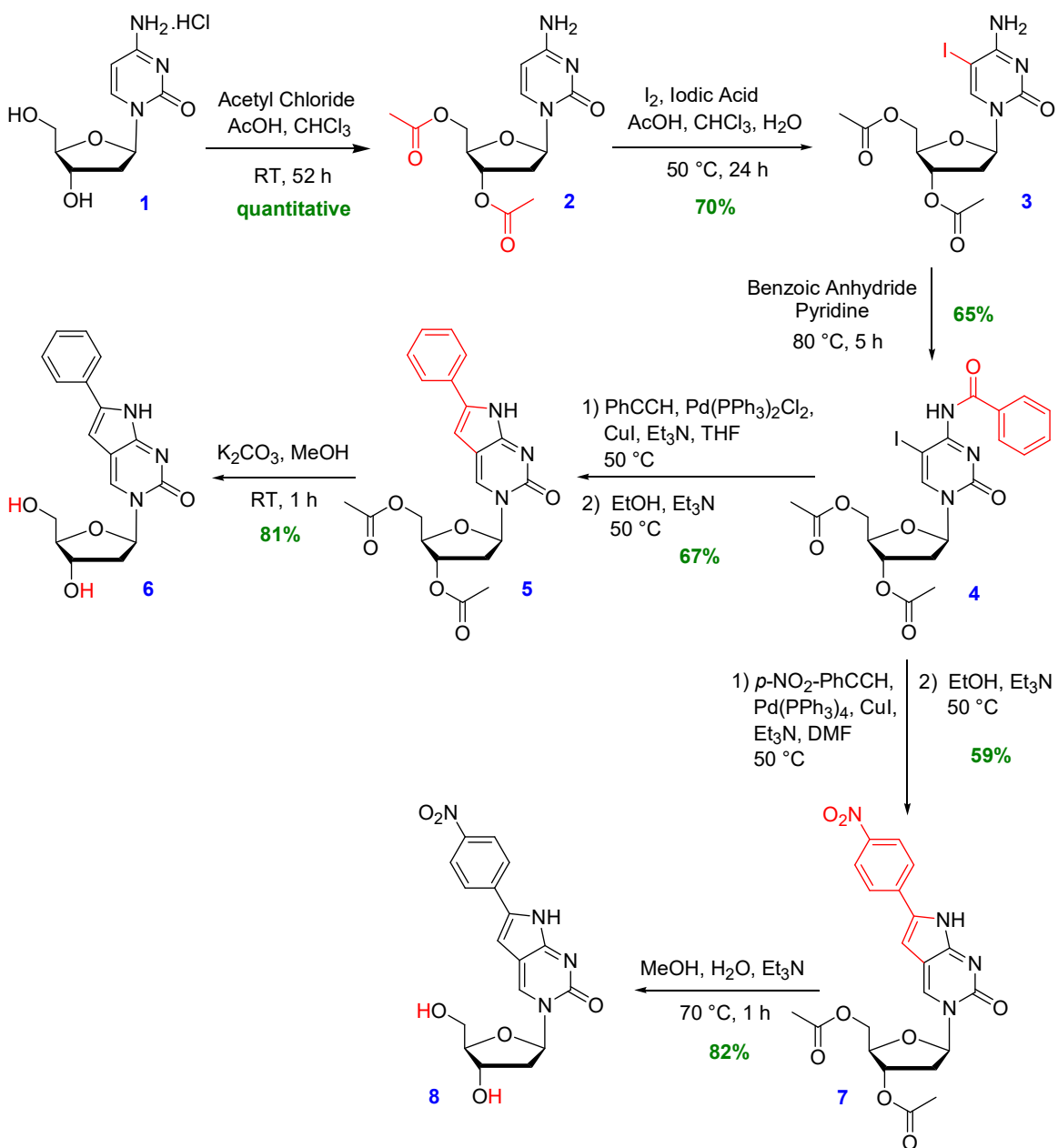
2.2.2.1 Synthesis of the d-PhpC and d-*p*-NO₂-PhpC

The synthesis of d-PhpC and d-*p*-NO₂-PhpC is described in Scheme 2-1. It starts with the acetylation of 2'-deoxycytidine hydrochloride. Then it is iodinated at the 5 position of the pyrimidine ring which provides the handle for the Sonogashira cross-coupling. The protection of the exocyclic amine enables us to perform the cross coupling and consequent cyclization reaction simultaneously. After the Sonogashira cross-coupling and cyclization, the benzoyl group is removed under basic conditions in one pot with the Sonogashira cross-coupling and cyclization. Finally, the protecting groups on the sugar backbone can be removed under basic conditions.^{70,101}

For the synthesis of the d-PhpC, the phenylacetylene was commercially available however the 1-ethynyl-4-nitrobenzene needed for the synthesis of the d-*p*-NO₂-PhpC was prepared by Sonogashira cross-coupling of 1-iodo-4-nitrophenyl and trimethylsilyl(TMS)-acetylene and consequent deprotection of TMS under basic conditions.^{102,103}

The presented route of synthesis in Scheme 2-1 provides compound **4** without any need for tiring purification methods like FCC with reasonable yield (45% through 3 steps). Deprotection of compound **5** was done by K₂CO₃ in methanol and the purification was done by FCC of a highly polar compound. However, deacetylation of the compound **7** was done using triethylamine in methanol without further purification.¹⁰⁴

The purity of the compounds was tested by NMR and mass spectrometry.



Scheme 2-1: Synthesis of the d-PhpC and d-*p*-NO₂-PhpC

2.2.2.2 Cyclic voltammetry

The CV measurements were performed at 25 °C in nonaqueous solutions of 1.0 mM respective pC derivative, using Bioanalytical Systems Inc. (BASi) Epsilon potentiostat and analyzed using BASi Epsilon software. The redox potentials were measured in two electrolyte systems: 0.1 M tetrabutylammonium hexafluorophosphate [nBu₄N][PF₆] dissolved in dry

MeCN and [nBu₄N][PF₆] dissolved in dry DMF. Aprotic solvents were used to avoid complications that arise from follow up protonation reactions that happen either prior to or following electron transfer in protic solvents during the CV run. These two electrolyte systems were used to cover different voltage ranges: 0.1 M [nBu₄N][PF₆]/DMF was useful from -2.50 V to +1.90 V vs normal hydrogen electrode (NHE) and 0.1 M [nBu₄N][PF₆]/MeCN for -2.00 V to +2.30 V vs NHE. The electrode setup consisted of a glassy carbon working electrode, a Pt wire counter electrode, and an Ag wire pseudo-reference electrode. All the samples were stirred and purged with Ar for 5 minutes before the scan and the scan rate was 100 mV/s. The $E_p^{1/2}$ of 1.0 mM ferrocene in the respective electrolyte systems was used as a calibration for voltages measured against the Ag wire as a pseudo-reference electrode to the NHE. The $E_p^{1/2}$ of 1.0 mM ferrocene was 75 mV in 0.1 M [nBu₄N][PF₆]/DMF, and 66 mV in 0.1 M [nBu₄N][PF₆]/MeCN. The shifts to the NHE was calculated based on the $E_p^{1/2}$ for ferrocene against NHE (+0.63 V).¹⁰⁵

2.2.2.3 Ground state redox potentials

The ground state one electron redox potentials of d-PhpC, d-*p*-NO₂-PhpC, and *p*-OMe-PhpC were measured by cyclic voltammetry in freshly distilled MeCN and DMF with 0.1 M [nBu₄N][PF₆] as supporting electrolyte. In order to validate the procedure, the redox potentials of thymidine were measured prior to the measurements of the redox potentials of the pC derivatives with the conditions described earlier. The resulting redox potentials, $E_{OX}^{\circ T} = +2.10 V$, $E_{RED}^{\circ T} = -2.00 V$ were in good agreement with the literature values ($E_{OX}^{\circ T} = +2.11 V$, $E_{RED}^{\circ T} = -2.14 V$).¹⁰⁶

The d-PhpC was readily soluble in DMF and was dissolved in MeCN upon sonication and prolonged stirring. The d-*p*-NO₂-PhpC was readily soluble in DMF however, it did not dissolve in MeCN upon sonication and prolonged stirring consequently did not show any oxidation or reduction peaks in the cyclic voltammogram. The amount of *p*-OMe-PhpC available in the lab was not enough for both redox potentials in DMF and MeCN, therefore it was only measured in DMF since it was predicted that it will not dissolve in MeCN.

The cyclic voltammogram of the d-PhpC, d-*p*-NO₂-PhpC, and *p*-OMe-PhpC in 0.1 M [nBu₄N][PF₆]/DMF and 0.1 M [nBu₄N][PF₆]/MeCN is shown in Figure 2-13 to Figure 2-

16 and the redox potentials are gathered in Table 2-2. The cyclic voltammograms of *d*-PhpC, *d-p*-NO₂-PhpC, and *p*-OMe-PhpC in MeCN and DMF demonstrates irreversible oxidation and reduction potentials similar to natural nucleosides and nucleoside derivatives^{100,106-108}. Irreversible redox potentials are observed due to the production of unstable redox products during the timescale of the run, therefore they only survive during the forward scan with no observable peak during the reverse scan.

Table 2-2: Ground state oxidation and reduction potentials in DMF and MeCN

Sample	Solvent	E_{OX}° (V)	E_{RED}° (V)
d-PhpC	DMF	1.19	-2.26
	MeCN	1.67	-2.20
d-<i>p</i>-NO₂-PhpC	DMF	1.33	-1.64
<i>p</i>-OMe-PhpC	DMF	1.02	< -2.80

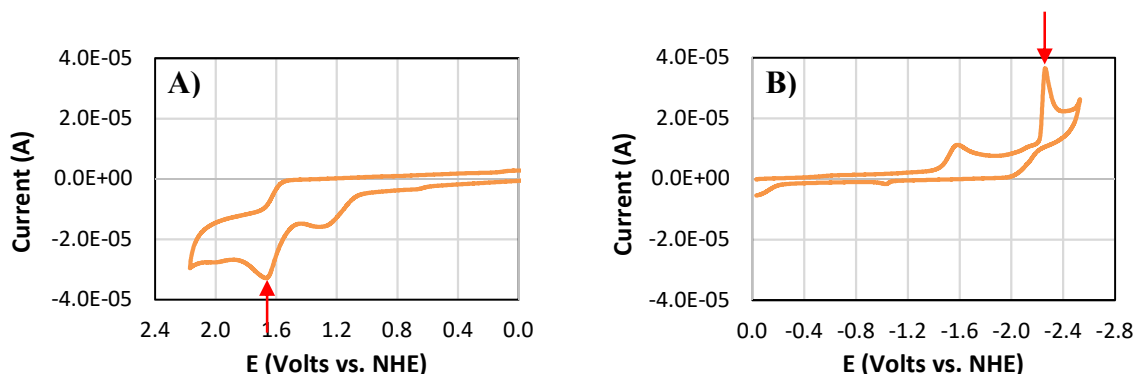


Figure 2-13: A) Oxidation side and B) Reduction side of the CV of *d*-PhpC in [nBu₄N][PF₆]/MeCN

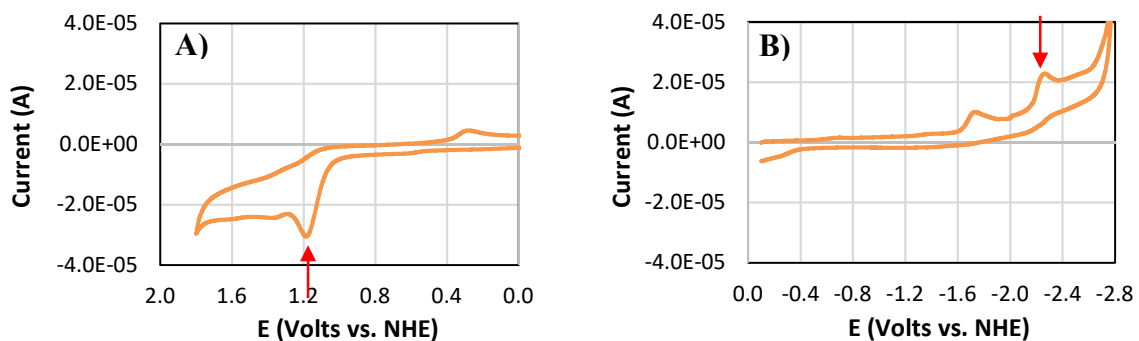


Figure 2-14: A) Oxidation side and B) reduction side of the CV of the *d*-PhpC in [nBu₄N][PF₆]/DMF

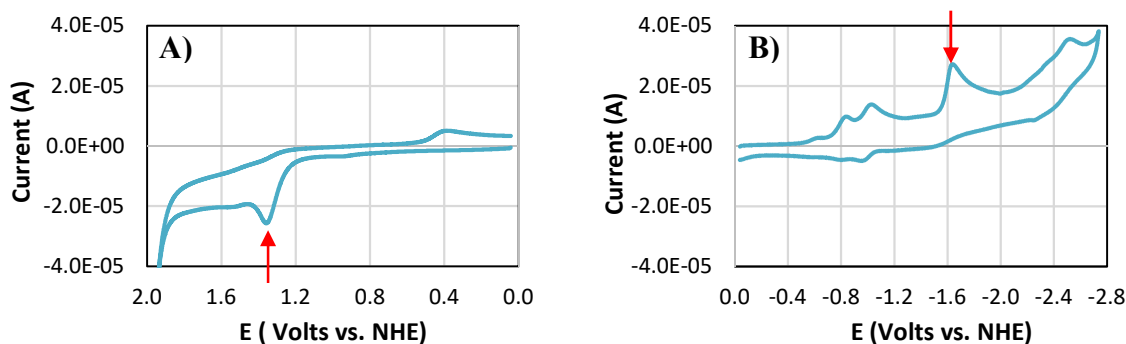


Figure 2-15: A) Oxidation side and B) reduction side of the CV of the *d-p*-NO₂-PhpC in [nBu₄N][PF₆]/DMF

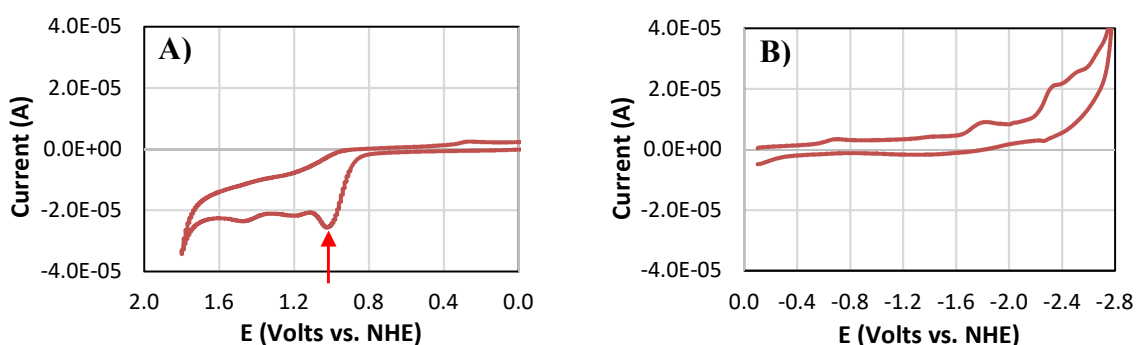


Figure 2-16: A) Oxidation side and B) Reduction side of the CV of the *p*-OMe-PhpC in [nBu₄N][PF₆]/DMF

2.2.2.4 Excited state redox potentials

Excited state oxidation potential $E_{OX}^{\circ*}$, and excited state reduction potential $E_{RED}^{\circ*}$, can be calculated according to equations 5 and 6, where E_{OX}° and E_{RED}° are ground state oxidation and reduction potential of the pC derivatives respectively and E_{00} is the energy difference between the ground state and first excited electronic state which can be calculated according to equation 7, where $h = 4.135667662 \times 10^{-15} \text{ eV} \cdot \text{s}$ is Planck constant, $c = 2.99792458 \times 10^8 \text{ m} \cdot \text{s}^{-1}$ is light velocity, and λ_{abs} and λ_{em} are absorption and emission wavelength of pC derivatives measured in DMF and MeCN.

$$E_{OX}^{\circ*} = E_{OX}^{\circ} - E_{00} \quad \text{Equation 5}$$

$$E_{RED}^{\circ*} = E_{RED}^{\circ} + E_{00} \quad \text{Equation 6}$$

$$E_{00} = \frac{1}{2} hc \left(\frac{1}{\lambda_{abs}} + \frac{1}{\lambda_{em}} \right) \quad \text{Equation 7}$$

The calculated excited state oxidation potential and excited state reduction potentials in DMF and MeCN are as followed:

Table 2-3: Excited state oxidation and reduction potentials in DMF and MeCN. The bolded numbers are used for the estimation of the photoinduced electron transfer.

Sample	Solvent	λ_{abs} (nm)	λ_{em} (nm)	E_{00} (eV)	E_{OX}^* (V)	E_{RED}^* (V)
d-PhpC	DMF	322	444	3.32	-2.13	1.06
	MeCN	320	441	3.34	-1.67	1.14
d-p-NO₂-PhpC	DMF	402	633	2.52	-1.19	0.88
p-OMe-PhpC	DMF	422	444	2.87	-1.85	< 0.07

2.2.2.5 Estimation of photoinduced electron transfer free energies

The fluorescence quenching of the excited state pC derivatives by natural nucleosides via electron transfer can happen through two possible routes. Either the excited state pC derivatives reduce the ground state nucleosides (nucleoside reduction, NRED), or excited state pC derivatives are reduced by the nucleosides (nucleoside oxidation, NOX). The possibility of each route can be judged by the magnitude and the sign of the ΔG° . The photoinduced electron transfer free energies can be calculated using Rehm-Weller equation shown as equations 8 and 9 where ΔG_{NOX}° is the free energy change of the nucleoside oxidation and ΔG_{NRED}° is the free energy change of the nucleoside reduction. $\Delta G^\circ(\epsilon)$ is the Born correction and contains two correction terms based on the Born equation: (I) the interaction energy of radical ions formed after electron transfer with radius r_{ion} in a complex with a center to center distance r_{EC} ; (II) the difference of ion solvation between a solvent of interest, in this case water with a dielectric constant of ϵ_W and an organic solvent with the dielectric constant of ϵ_O . In these experiments, the organic solvents are either DMF or MeCN and the solvent of interest is water. $\Delta G^\circ(\epsilon)$ can be calculated using equation 10. Using standard parameters for $r_{ion} = 3.0 \text{ \AA}$, $r_{EC} = 7.0 \text{ \AA}$, $\epsilon_O = 36.7$ for DMF, $\epsilon_O = 37.5$ for MeCN, and $\epsilon_W = 80.1$ for water, we obtained $\Delta G^\circ(\epsilon) \approx -0.1 \text{ eV}^{106}$. Moreover, the ground state oxidation and reduction potentials of the natural nucleoside ($E_{OX}^{\circ \text{Nucleoside}}$ and

$E_{RED}^{\circ \text{Nucleoside}}$) measured by Seidel and co-workers are shown in Table 2-4¹⁰⁶ and the calculated ΔG_{NOX}° and ΔG_{NRED}° are listed in Table 2-5.

$$\Delta G_{NOX}^{\circ} = E_{OX}^{\circ \text{Nucleoside}} - E_{RED}^{\circ *} + \Delta G^{\circ}(\varepsilon) \quad \text{Equation 8}$$

$$\Delta G_{NRED}^{\circ} = E_{OX}^{\circ *} - E_{RED}^{\circ \text{Nucleoside}} + \Delta G^{\circ}(\varepsilon) \quad \text{Equation 9}$$

$$\Delta G^{\circ}(\varepsilon) = \frac{e^2}{4\pi\epsilon_0} \left[\left(\frac{1}{r_{ion}} - \frac{1}{r_{EC}} \right) \frac{1}{\epsilon_W} - \frac{1}{r_{ion} \epsilon_O} \right] \quad \text{Equation 10}$$

Table 2-4: The oxidation and the reduction potentials of the natural nucleosides

Nucleoside	$E_{OX}^{\circ \text{Nucleoside}}$ (V)	$E_{RED}^{\circ \text{Nucleoside}}$ (V)
G	1.49	< -2.76
A	1.96	-2.45
C	2.14	-2.23
T	2.11	-2.14

Table 2-5: The estimation of the free energy of electron transfer ($\Delta G_{NOX/NRED}^{\circ}$ in eV) for pC derivatives calculated using Rehm-Weller equation

	d-PhpC		d- <i>p</i> -NO ₂ -PhpC		<i>p</i> -OMe-PhpC	
	ΔG_{NOX}°	ΔG_{NRED}°	ΔG_{NOX}°	ΔG_{NRED}°	ΔG_{NOX}°	ΔG_{NRED}°
G	0.33	> 0.99	0.51	> 1.47	> 1.32	0.81
A	0.8	0.68	0.98	1.16	> 1.79	0.5
C	0.98	0.46	1.16	0.94	> 1.97	0.28
T	0.95	0.37	1.13	0.85	> 1.94	0.19

2.2.2.6 Discussion

The ground state oxidation and reduction potential of the pC derivatives in DMF follow these orders:

$$E_{OX}^{\circ} = \text{d-}p\text{-NO}_2\text{-PhpC} > \text{d-PhpC} > p\text{-OMe-PhpC}$$

$$E_{Red}^{\circ} = \text{d-}p\text{-NO}_2\text{-PhpC} > \text{d-PhpC} > p\text{-OMe-PhpC}$$

The electron withdrawing effect of the nitro group on the d-PhpC makes the molecule easier to be reduced and harder to be oxidized. Moreover, the electron donating properties of the methoxy group on the d-PhpC makes the molecule easier to be oxidized and harder to be reduced.

However, the excited state oxidation and reduction potentials of the pC derivatives in DMF does not follow the above-mentioned trends. The excited state d-PhpC is the easiest to oxidize and easiest to reduce and d-*p*-NO₂-PhpC is the hardest to oxidize and *p*-OMe-PhpC hardest to reduce.

$$E_{OX}^{\circ*} = \text{d-}p\text{-NO}_2\text{-PhpC} > p\text{-OMe-PhpC} > \text{d-PhpC}$$

$$E_{RED}^{\circ*} = \text{d-PhpC} > \text{d-}p\text{-NO}_2\text{-PhpC} > p\text{-OMe-PhpC}$$

All the free energy change values for all the pC derivatives are positive. This suggests that the quenching of the pC derivatives does not happen through photoinduced electron transfer and other mechanisms are probably involved. However, there is one experimental error in the calculating of the free energy changes. Since the d-*p*-NO₂-PhpC and d-*p*-OMe-PhpC were not soluble in MeCN, the oxidation potentials of these derivatives in MeCN are not available and the oxidation potential of these derivatives in DMF was used for the calculations. Therefore, the difference could be attributed to the difference in the solvent which could result in different oxidation value for d-*p*-NO₂-PhpC and d-*p*-OMe-PhpC. This is while there is a huge difference in the oxidation potential of d-PhpC in DMF and MeCN (Table 2-5) which could be the case for d-*p*-NO₂-PhpC and d-*p*-OMe-PhpC.

Based on the observed trend for the oxidation potentials of the pC derivatives of the study we can predict that the oxidation potential of the d-*p*-NO₂-PhpC and d-*p*-OMe-PhpC are greater and smaller than 1.67 V respectively. Assuming the E_{00} for the d-*p*-NO₂-PhpC and d-*p*-OMe-PhpC are the same in MeCN and DMF the revised excite state redox potentials are listed in Table 2-6.

Table 2-6: Revised ground state and excited state redox potentials of d-*p*-NO₂-PhpC and *p*-OMe-PhpC are highlighted.

Sample	Solvent	E_{OX}° (V)	E_{RED}° (V)	E_{00} (eV)	$E_{OX}^{*\circ}$ (V)	$E_{RED}^{*\circ}$ (V)
d- <i>p</i> -NO ₂ -PhpC	DMF	1.33	-1.64	2.52	-1.19	0.88
	MeCN	> 1.67	-	2.52	> -0.85	-
<i>p</i> -OMe-PhpC	DMF	1.02	< -2.80	2.87	-1.85	< 0.07
	MeCN	< 1.67	-	2.87	< -1.2	-

Using the revised excited state oxidation potentials, the revised free energy changes are calculated in Table 2-7. By looking at the numbers we can see that none of the possible photoinduced electron transfer events are favorable.

Table 2-7: The revised free energy changes ($\Delta G_{NOX/NRED}^{\circ}$ in eV) of d-*p*-NO₂-PhpC and *p*-OMe-PhpC are highlighted.

	d- <i>p</i> -NO ₂ -PhpC		<i>p</i> -OMe-PhpC	
	ΔG_{NOX}°	ΔG_{NRED}°	ΔG_{NOX}°	ΔG_{NRED}°
G	0.51	> 1.81	> 1.32	< 1.46
A	0.98	> 1.5	> 1.79	< 1.15
C	1.16	> 1.28	> 1.97	< 0.93
T	1.13	> 1.19	> 1.94	< 0.84

For the comparison purpose, the free energies of electron transfer for 2-aminopurine (2-AP), 8-vinyladenine (8-VA), and four pteridine derivatives are collected in Table 2-8.^{100,107,108} All of these modified nucleosides have negative values for their free energy change of the NOX with guanine meaning photoinduced electron transfer between excited state modified nucleoside and the guanine is possible through reduction of the excited state modified nucleoside and oxidation of the guanine. All of them have utilized the procedure which was used in the present study, therefore, the validity of the method is proved before.

Table 2-8: The estimation of the free energies ($\Delta G_{NOX/NRED}^{\circ}$ in eV) of the 2-AP, 8-VA, 6-MAP, DMAP, 3-MI, and 6-MI

	E_{Ox}° (V)	E_{Red}° (V)	E_{00} (eV)	E_{Ox}^{*} (V)	E_{Red}^{*} (V)		ΔG_{NOX}°		ΔG_{NRED}°
8-VA ¹⁰⁰	1.43 (DCM)	-2.11 (MeCN)	3.73	-2.31 (DCM)	1.62 (MeCN)	G	-0.2	G	0.32
			(MeCN)			A	0.27	A	0.01
			3.74			C	0.45	C	-0.21
			(DCM)			T	0.42	T	-0.3
2-AP ¹⁰⁸	1.71 (MeCN) 1.58 (DMF)	-2.13 (MeCN) -2.27 (DMF)	3.73	-2.02 (MeCN)	1.44 (DMF)	G	-0.05	G	0.64
			(MeCN)			A	0.42	A	0.33
			3.71			C	0.6	C	0.11
			(DMF)			T	0.57	T	0.02
6-MAP ¹⁰⁷	1.95 (MeCN)	-1.97 (MeCN)	3.47	-1.52 (MeCN)	1.92 (DMF)	G	-0.53	G	1.14
		-1.46, -2.37 (DMF)	(MeCN)			A	-0.06	A	0.83
			3.38			C	0.12	C	0.61
			(DMF)			T	0.09	T	0.52
DMAP ¹⁰⁷	1.88 (MeCN)	-2.04 (MeCN)	3.43	-1.55 (MeCN)	1.89 (DMF)	G	-0.50	G	1.11
		-1.50, -2.42 (DMF)	(MeCN)			A	-0.03	A	0.8
			3.39			C	0.15	C	0.58
			(DMF)			T	0.12	T	0.49
3-MI ¹⁰⁷	1.79 (MeCN) 1.68 (DMF)	-1.76 (MeCN)	3.29	-1.50 (MeCN)	1.83 (DMF)	G	-0.44	G	1.16
		-1.44, -1.96 (DMF)	(MeCN)			A	0.03	A	0.85
			3.27			C	0.21	C	0.62
			(DMF)			T	0.18	T	0.54
6-MI ¹⁰⁷	1.65 (MeCN) 1.54 (DMF)	-1.85 (MeCN)	3.13	-1.48 (MeCN)	1.41 (DMF)	G	-0.02	G	1.18
		-1.68, -1.96 (DMF)	(MeCN)			A	0.45	A	0.87
			3.09			C	0.63	C	0.65
			(DMF)			T	0.6	T	0.56

Similar investigations were done on the influence of the nearest neighbors on the fluorescent properties of tC by Wilhelmson and co-workers.⁴² The minimal changes in the quantum yield, lifetime, and the absorption and emission wavelengths of tC in ssDNA and dsDNA was attributed to photoinduced electron transfer (PET). In order to investigate the possibility of PET, the one-electron redox potentials of tC in sodium phosphate buffer (pH= 5.5) were measured and the free energy changes were calculated. The results showed that PET between the reduced excited state tC and oxidized guanine is thermodynamically favorable ($\Delta G_{NOX}^{\circ} = -0.5$ eV), nevertheless, tC did not show a great amount of quenching

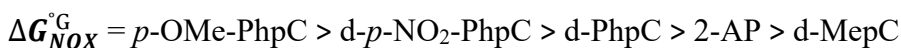
in incorporation into ssDNA and dsDNA. The free energy change for tC was even lower than 2-AP as one example of the established fluorophore which undergoes PET. The excited state reduction potentials of 2-AP in the phosphate buffer was calculated as +1.5 V¹⁰⁹ which was greater than oxidation potential of guanine +1.3 V (measured in 100 mM phosphate buffer, pH= 7)¹¹⁰ showing the possibility of PET ($\Delta G_{NOX}^{\circ} = -0.2$ eV). This contrast in the results could be attributed to the follow-up reactions including prototropic equilibria in aqueous solutions which affect the redox potentials of the bases. Therefore, the measurement of the redox potentials of the nucleosides in aprotic solvents like DMF and MeCN is very important.¹⁰⁶

There is no report of the experimental reduction and oxidation potential of the d-MepC in the literature. However, there are some reports based on DFT calculations. The predictions of the ground state and excited state redox potentials of d-MepC and 2-AP are listed in Table 2-9.¹¹¹

Table 2-9: The computational values of the redox potentials of d-MepC and 2-AP and the estimation of the free energy changes ($\Delta G_{NOX/NRED}^{\circ}$ in eV).

	E_{Ox}° (V)	E_{Red}° (V)	E_{00} (eV)	$E_{Ox}^{*\circ}$ (V)	$E_{Red}^{*\circ}$ (V)		ΔG_{NOX}°		ΔG_{NRED}°
d-MepC	1.64	-2.11	3.55	-1.9	1.4	G	0.1	G	1.0
2-AP	1.88	-2.46	3.6	-1.8	1.2	G	0.4	G	1.1

It is worth noting that computational studies in the literature showed that nucleobase oxidation (NOX) of d-MepC with guanine is more favorable than 2-AP and experimental studies in the present study showed that nucleobase oxidation (NOX) of 2-AP with guanine is more favorable than PhpC.



Nevertheless, the calculation of the free energy changes was done by using the experimental redox potentials of guanine, and it might introduce some errors into the calculations. The free energy changes $\Delta G_{NOX/NRED}^{\circ}$ of d-MepC and 2-AP were recalculated based on the computational redox potentials of guanine and are compared with the experimental free energy changes of 2-AP in previous studies and d-PhpC, d-*p*-NO₂-PhpC,

and *p*-OMe-PhpC in this study (Table 2-10). It is shown that ΔG_{NOX}° of 2-AP is only slightly lower than the ΔG_{NOX}° of MepC. Considering the error between the ΔG_{NOX}° of 2-AP in the experimental study and computational study, we can conclude that:

$$\Delta G_{NOX}^{\circ} = p\text{-OMe-PhpC} > d\text{-}p\text{-NO}_2\text{-PhpC} > d\text{-PhpC} > d\text{-MepC} > 2\text{-AP}$$

This trend is in more agreement with the fluorescent studies of the d-PhpC, d-MepC and 2-AP. Since the quantum yield of 2-AP is extensively reduced upon incorporation into single-stranded oligonucleotides and is further reduced upon duplex formation by the order of 10-100 magnitude,⁶² while d-MepC is quenched 60% upon incorporation into single-stranded and 75% upon hybridization into double-stranded oligonucleotides.¹¹² Moreover, the quantum yield of the d-PhpC upon incorporation into ssDNA was shown to increase or decrease depending on the neighbouring nucleotide and decreases 6-83% upon hybridization into dsDNA.

Table 2-10: The revised estimation of the free energy changes of ($\Delta G_{NOX/NRED}^{\circ}$ in eV) d-MepC and 2-AP and comparing with the free energy change ($\Delta G_{NOX/NRED}^{\circ}$ in eV) of pC derivatives of the study.

	Condition	E_{Ox}° (V)	E_{Red}° (V)	E_{00} (eV)	$E_{Ox}^{*\circ}$ (V)	$E_{Red}^{*\circ}$ (V)		ΔG_{NOX}°		ΔG_{NRED}°
2-AP	Experimental study	1.71	-2.27	3.72	-2.02	1.44	G	-0.05	G	0.64
2-AP	Computational study	1.88	-2.46	3.7	-1.82	1.24	G	0.58	G	0.59
d-MepC	Computational study	1.64	-2.11	3.2	-1.56	1.09	G	0.73	G	0.85
d-PhpC	Experimental study			3.33	-1.67	1.06	G	0.33	G	> 0.99
d-<i>p</i>-NO₂-PhpC	Experimental study	> 1.67	-1.64	2.53	> -0.85	0.88	G	0.51	G	> 1.81
<i>p</i>-OMe-PhpC	Experimental study			2.88			G	1.01	G	0.81<X<1.46

2.3 Conclusion

The present study shows how the fluorescence quantum yield of PhpC is affected by its nearest neighbours upon incorporation into single- and double-stranded DNA. The fluorescent quantum yield of the PhpC upon incorporation into ssDNA is decreased except for AT, AA, TA, and CT sequences which displayed a slight increase in the quantum yield.

In general, adenine has the smallest effect on PhpC fluorescence quenching, and guanine is the main quencher of the PhpC. Moreover, the orientation of neighbours around PhpC significantly affects its quantum yield in single-stranded form. For example, the quenching effect of guanine and adenine is higher when it is placed at the 3'-side of PhpC compared to the 5'-side. Thus, the fluorescence quantum yield of PhpC within ssDNA is highly affected by the nature of the nearest neighbours and the orientation of the bases around PhpC.

The data also indicates that the fluorescence quantum yield of the PhpC is always decreased upon hybridization into the complementary strand and the degree of the quenching depends on the nature and the orientation of the nearest neighbours. For example, having a guanine at the 5' side of PhpC usually provides the biggest difference between the fluorescence of single- and double-stranded forms. Moreover, the quenching effect of guanine can be assessed by its place around the PhpC and it follows this trend: $G=Y' > G=X' > G=Y > G=X', Y' > G=X', Y > G=X > G=X, Y' > G=X, Y$. Furthermore, adenine in the dsDNA exhibits a dual nature when it is placed in different positions. Generally, 3'-A works as a quencher and 5'-A as fluorescence enhancer and it follows this trend: $A=Y < A=Y' < A=X', Y < A=X', Y' < A=X' < A=X < A=X, Y < A=X, Y'$. Combining these two trends results in the very good prediction of the experimental trends.

Furthermore, the measurement of the ground state redox potentials of the pC derivatives and the calculation of the excited state redox potentials and the estimation of the free energy changes revealed that the photoinduced electron transfer of the pC derivatives and the natural nucleosides are not favorable. The variations in the quantum yield can be attributed to other mechanisms of quenching including Dexter exchange or heavy atom effect. Another possible explanation is that the protonation of the nucleobases might play a role in the photophysical events. Since the protonation of the nucleosides was avoided in this study to avoid other events including proton and electron transfer and to solely investigate the photoinduced electron transfer events. Moreover, the hydrogen bonding and the phosphodiester bond between the nucleosides might play a role in the photophysical events. Furthermore, π -stacking of the bases is another possible reason for the quenching of PhpC.

Chapter 3

3 Study of the possibility of FRET by pC derivatives as fluorescent donor and acceptor

3.1 Introduction

Molecular beacons (MBs) are single-stranded oligonucleotides first introduced by Tyagi and Kramer in 1996¹¹³ and consist of a stem-and-loop structure with a fluorophore and a quencher component on opposite ends (Figure 3-1). They are hybridization probes and can report the presence of a specific sequence of nucleic acids. The loop region is called probe region and is designed to be complementary to the target sequence. Two ends of the oligonucleotide are called stem region and are designed to be complementary to each other. In the absence of the target sequence, molecular beacons are closed by the stem and the fluorophore and quencher are in close proximity of each other. Therefore, the fluorescence is quenched by FRET. However, in the presence of target sequence, the probe region hybridizes with the target and because of the conformational changes the fluorophore and the quencher will be far apart enough to reduce or eliminate FRET.¹¹⁴⁻¹¹⁸

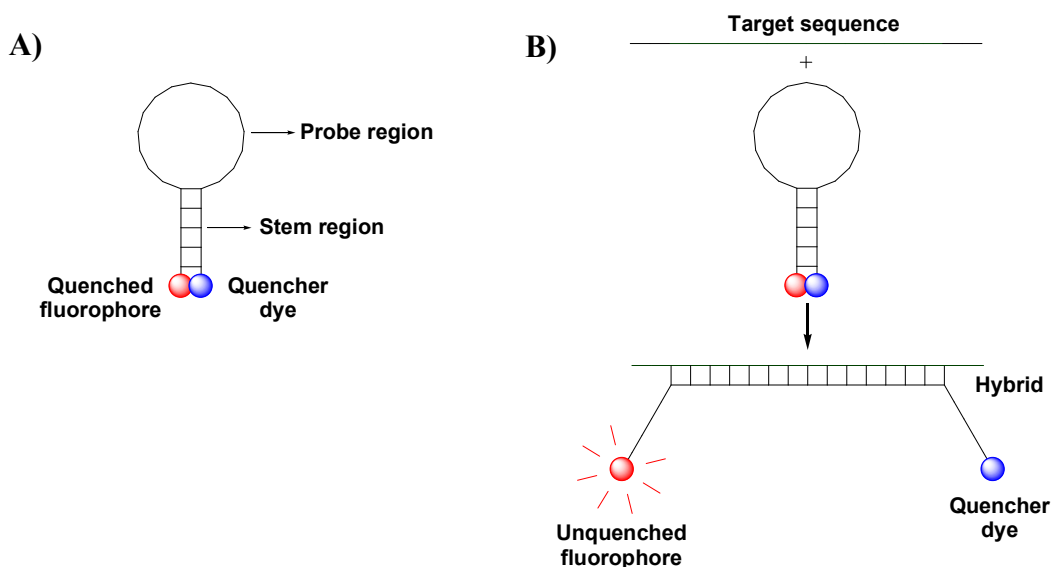


Figure 3-1: A) Molecular beacons in the absence of target sequence and B) in the presence of target sequence.

MBs have been used in a variety of different applications. Besides the selectivity and sensitivity of the MBs, their ability in the detection of the target oligonucleotide in solution

and in situations where it is not possible or desirable to isolate the probe-target hybrids from an excess of the unhybridized probes is very impressive. These properties enable the use of MBs for in vitro detection of bacteria and viruses, human disease diagnostics, gene expression studies, gene profiling, SNP detection, DNA and RNA monitoring during PCR and DNA/RNA ligation and self-assembly. Although one of the biggest advantages of the MBs is in-solution detection ability, they are utilized in microarrays as well.¹¹⁵

The first molecular beacon designed by Kramer and Tyagi was 25-nucleotide long sequence shown in Figure 3-2. The fluorophore and the quencher are 5-(2'-aminoethyl)aminonaphthalene-1-sulfonic acid (EDANS) and 4-(4'-dimethylaminophenylazo) benzoic acid (DABCYL), respectively, which are covalently bonded with a relatively long linker to the 5' and 3' ends of the sequence. Upon excitation of EDANS with UV light of 336 nm wavelength, it emits fluorescence of 490 nm wavelength. On the other hand, DABCYL is a non-fluorescent chromophore whose absorption spectrum overlaps with the emission spectrum of EDANS. DABCYL absorbs the radiant energy emitted by EDANS and dissipates it as heat. Therefore, this MB is dark when it is unhybridized and upon hybridization into the target strand, it Fluoresces. Going from no fluorescence to fluorescence upon hybridization shows very good quenching efficiency for DABCYL and EDANS as a FRET pair.¹¹³

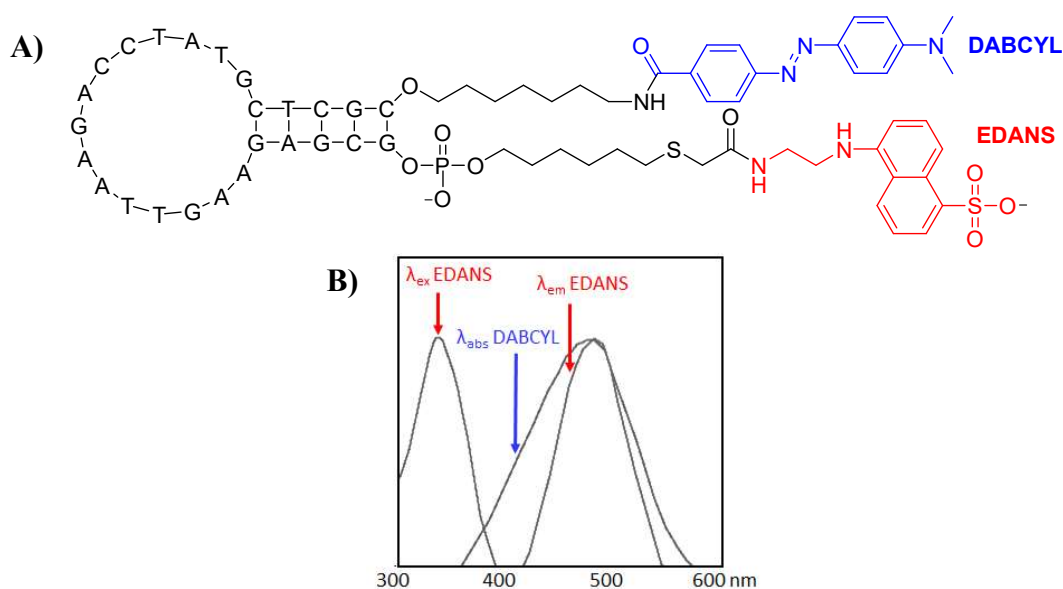


Figure 3-2: A) The structure of the first molecular beacon designed by Kramer and Tyagi. B) The spectral overlap between EDANS and DABCYL

The designed MB showed great specificity towards the target sequence and even one nucleotide deletion, insertion or mismatch in the probe region led to very low fluorescence in comparison to the matched sequence. This study showed that there is a 25-fold increase in fluorescence upon hybridization of the MB into the target sequence¹¹³. However, previous studies showed that covalently linked EDANS and DABCYL have a 200-fold decrease in fluorescence intensity.¹¹⁹ The decrease in the quenching efficiency of DABCYL in the designed molecular beacon, and in other words presence of the background fluorescence in the unhybridized state, could be due to relatively long alkyl linkers, or due to the transient unraveling of the ends of the stem hybrid. Therefore, it is suggested that fluorophore can be quenched even more by shortening the linker, utilizing the fluorescently labeled nucleosides instead of the covalently bonded fluorophore and quencher, and putting the fluorophore and the quencher at the stem region to reduce the effects of unraveling.¹¹³

The first molecular beacon with isomorphous fluorescent nucleosides was designed by Martí and co-workers in 2006.¹²⁰ The designed molecular beacon was quencher-free and contained one fluorophore in the stem and one fluorophore in the loop region. They utilized 2-aminopurine (2-AP) in the loop and methyl-pyrrolocytidine (MepC) in the stem region. MepC and 2-AP have emission wavelength at 461 nm and 370 nm respectively and their fluorescence intensity depends on the state of hybridization. In the hybridized state, their fluorescence is quenched, and in the unhybridized state their fluorescence is unquenched. Therefore, in the unhybridized state of the molecular beacon, MepC produces less fluorescence at 461 nm than 2-AP at 370 nm. However, in the hybridized state 2-AP produces less fluorescence at 370 nm than MepC at 461 nm. As a result, this molecular beacon produces ratiometric fluorescence intensity for 2-AP and MepC in the hybridized and unhybridized states (Figure 3-3).

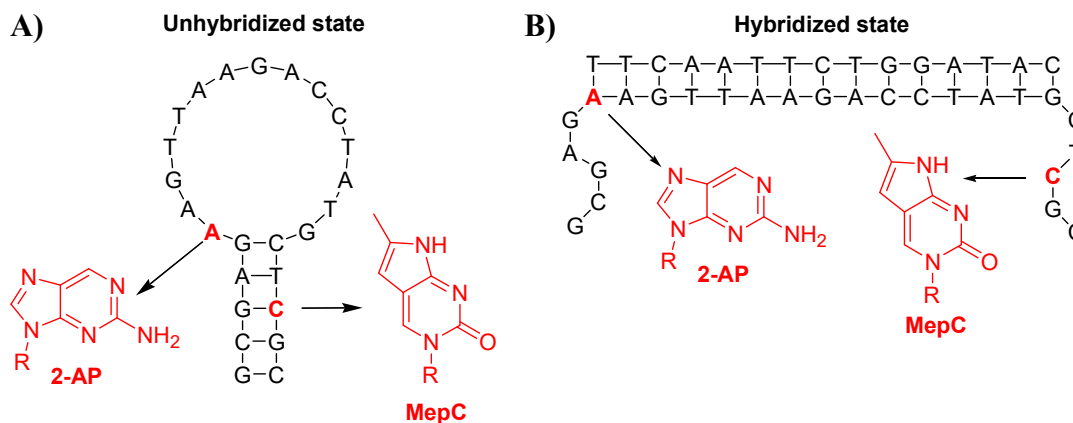


Figure 3-3: The structure of the molecular beacon containing 2-AP and MepC in A) unhybridized state and B) hybridized state

The molecular beacon intended to synthesize in this chapter contains isomorphous fluorescent nucleosides as donor and acceptor of the FRET pair and they are placed in the stem region. The donor is PhpC and the acceptor is *p*-NO₂-PhpC. The photophysical studies show that emission of the PhpC is well overlapped with the absorption of *p*-NO₂-PhpC and it is predicted that upon placement of these derivatives in the stem region of the molecular beacons, PhpC is quenched by *p*-NO₂-PhpC. Moreover, *p*-NO₂-PhpC is fluorescent and emits light at 538 nm. The design of the novel pairs of fluorophores and quenchers is very important because it allows simultaneous use of several molecular beacons, each of which emits light of a different wavelength or can be excited by light of a different wavelength in order to identify and quantify multiple targets at the same time¹²¹. *D-p*-NO₂-PhpC keeps its hydrogen bonding face with guanine similar to *d*-PhpC. The advantage of synthesizing a base pairing competent quencher is that it can be incorporated anywhere in an oligonucleotide strand and should not compromise duplex stability. Moreover, since we can incorporate this intrinsic quencher into the stem region of molecular beacons, more accurate FRET measurements can be obtained compared to traditional molecular beacon constructs where the quencher is attached via a long linker.

This chapter focuses on the synthesis and the quenching studies of *d-p*-NO₂-PhpC as the acceptor in the FRET pair with *d*-PhpC and pyrene as the donor of the FRET pair. Comparison between the quenching of PhpC and pyrene by *p*-NO₂-PhpC will give a better understanding of the quenching effect of *p*-NO₂-PhpC to different fluorophores.

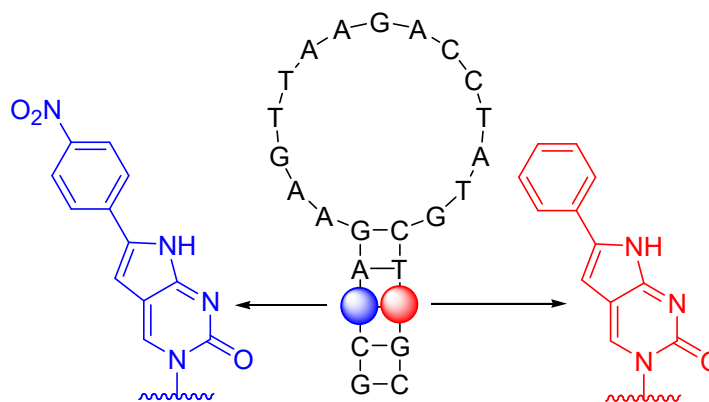


Figure 3-4: The designed molecular beacon containing PhpC and *p*-NO₂-PhpC

3.2 Results and discussion

3.2.1 Spectroscopic Properties of d-*p*-NO₂-PhpC, and d-PhpC

D-*p*-NO₂-PhpC exhibits an absorption and emission maximum at 403 and 538 nm in EtOH respectively. The molar extinction coefficient of this compound in EtOH at 403 nm was calculated to be 26000 M⁻¹ cm⁻¹. On the other hand, d-PhpC has absorption and emission maxima at 369 and 447 nm respectively and its molar extinction coefficient and quantum yield are reported 3500 M⁻¹ cm⁻¹ and 0.40, respectively in EtOH.⁷⁰

3.2.2 Quenching studies of d-PhpC and pyrene by d-*p*-NO₂-PhpC

In order to determine viable FRET pairs for use in molecular beacons, fluorescence quenching experiments were performed between d-*p*-NO₂-PhpC as an acceptor and the d-PhpC and pyrene as a donor. These fluorophores were chosen as a donor since their emission spectra overlap with the absorption spectrum of d-*p*-NO₂-PhpC.

Therefore, in a 1 μM solution of the d-PhpC in EtOH varying concentrations of the d-*p*-NO₂-PhpC was added and irradiated at 369 nm and the emission spectra were obtained. Figure 3-5 illustrates the emission spectra of the d-PhpC with 0-26 nM concentrations of d-*p*-NO₂-PhpC. Clearly, there is a decrease in the fluorescence emission of the fluorophore with increasing concentrations of the quencher. Similarly, a 1 μM solution of pyrene in EtOH was combined with varying concentrations of d-*p*-NO₂-PhpC. Figure 3-7

demonstrates a decrease in fluorescence emission of the fluorophore with increasing concentrations of the d-*p*-NO₂-PhpC.

Furthermore, the Stern-Volmer plot was constructed based on the ratio of the fluorescence intensity of the quencher free fluorophore and the fluorescence intensity of the increasing concentrations of the quencher (I_0/I) as Y axis and the concentration of the quencher as X axis. The Stern-Volmer quenching constant, K_{SV} is the slope of the resulting line. The K_{SV} value for the quenching of d-PhpC by d-*p*-NO₂-PhpC was approximately 27000 M⁻¹ (Figure 3-6). The K_{SV} value for the quenching of pyrene by d-*p*-NO₂-PhpC was 22000 M⁻¹ (Figure 3-8).

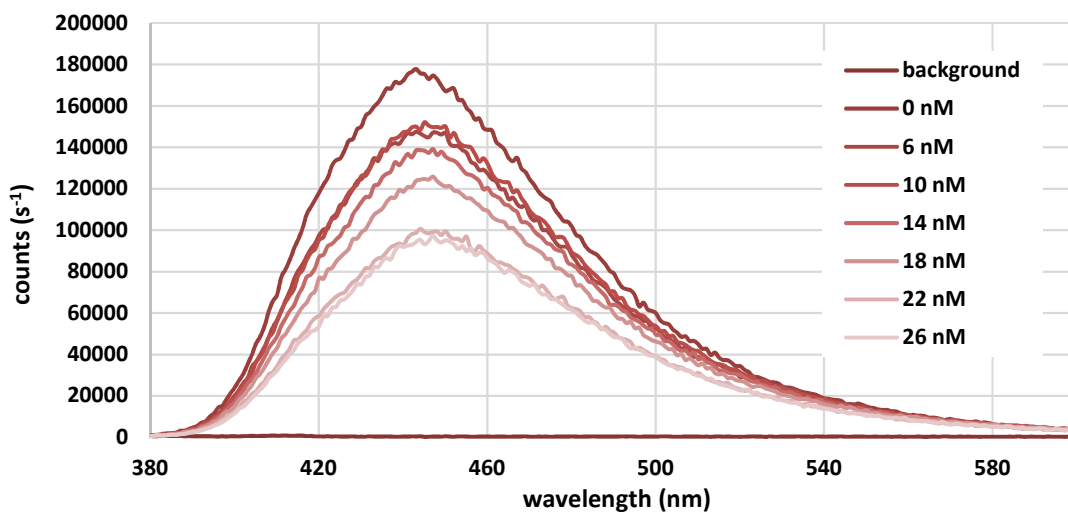


Figure 3-5: Quenching spectra of d-PhpC by d-*p*-NO₂-PhpC in EtOH

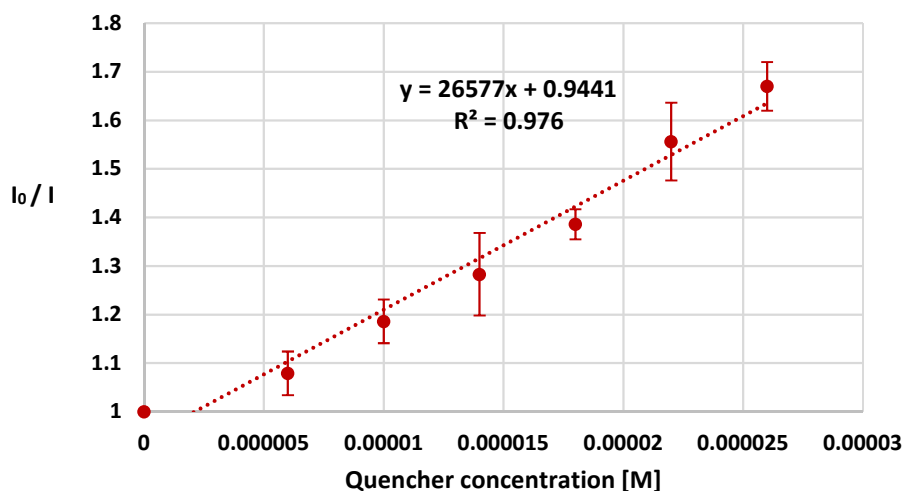


Figure 3-6: Stern-Volmer plot for the quenching of d-PhpC by d-*p*-NO₂-PhpC

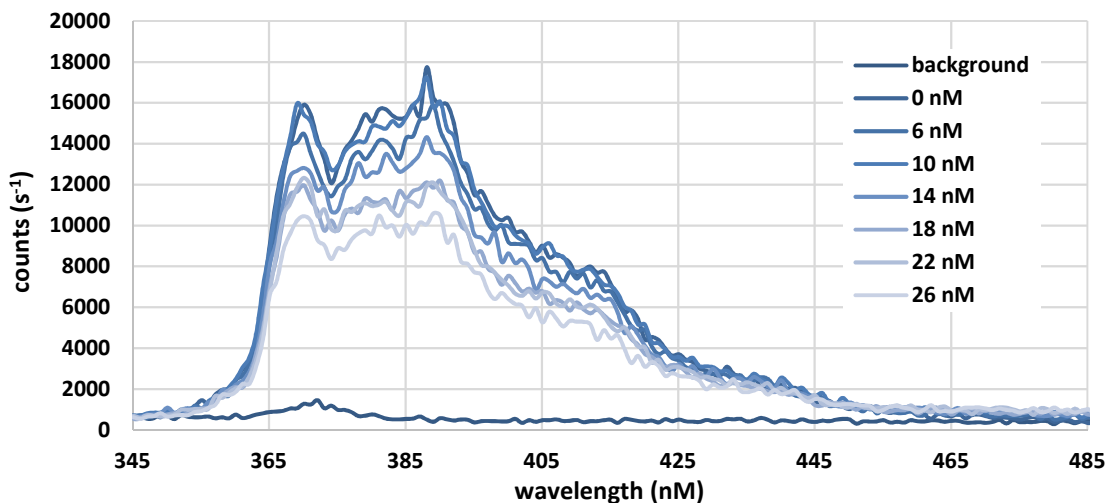


Figure 3-7: Quenching spectra of Pyrene by *d-p*-NO₂-PhpC in EtOH

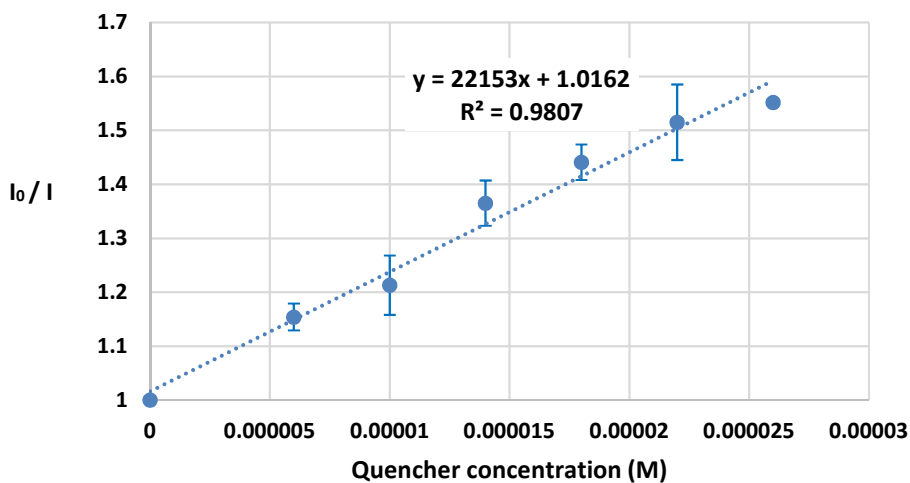


Figure 3-8: Stern-Volmer plot for the quenching of pyrene by *d-p*-NO₂-PhpC

The K_{sv} value indicates the sensitivity of a fluorophore to a quencher.¹⁵ The comparison of the obtained K_{sv} values for *d*-PhpC and *d-p*-NO₂-PhpC, and pyrene and *d-p*-NO₂-PhpC suggest that *d*-PhpC is more sensitive to quenching from *d-p*-NO₂-PhpC than pyrene. Moreover, the inverse of the Stern-Volmer quenching constant, K_{sv}^{-1} , is the concentration of the quencher at which 50% of the intensity of the fluorophore is quenched. The K_{sv}^{-1} value for the quenching of *d*-PhpC with *d-p*-NO₂-PhpC was determined to be 37 μ M. The K_{sv}^{-1} value for the quenching of pyrene with *d-p*-NO₂-PhpC was determined to be 45 μ M (Table 3-1). These values suggest that *d*-PhpC is quenched with a lower concentration of

d-p-NO₂-PhpC than pyrene and therefore, *d*-PhpC and *d-p*-NO₂-PhpC act as a better FRET pair than pyrene and *d-p*-NO₂-PhpC.

Table 3-1: The K_{SV} and K_{SV}^{-1} of the *d*-PhpC and *d-p*-NO₂-PhpC, and pyrene and *d-p*-NO₂-PhpC as FRET pairs.

Fluorophore \ Quencher	<i>d-p</i> -NO ₂ -PhpC	
	K_{SV} (M ⁻¹)	K_{SV}^{-1} (μM)
<i>d</i> -PhpC	27000	37
pyrene	22000	45

3.3 Conclusion

The design of the molecular beacons containing donor and acceptor of the FRET in the stem region possibly decreases the background fluorescent in the unhybridized state of the molecular beacon. Moreover, utilizing pC derivatives which are hydrogen bonding competent fluorescent nucleosides possibly improves the hybridization of the stem region in the unhybridized state consequently decreases the background fluorescent. Furthermore, incorporation of PhpC and *p*-NO₂-PhpC as a novel FRET pair into molecular beacons allows simultaneous use of molecular beacon containing this novel pair along with other molecular beacons with differently labeled fluorophores and quencher for the simultaneous detection of several target sequences in one pot.

The fluorescent studies in this chapter show that emission of the PhpC is well overlapped with the absorption of *p*-NO₂-PhpC and PhpC is quenched with increasing concentrations of *p*-NO₂-PhpC. In order to get a better understanding of the quenching of PhpC by *p*-NO₂-PhpC, the same study was done on the quenching of pyrene as one of the well-known fluorescence substances and *p*-NO₂-PhpC. The results show that *p*-NO₂-PhpC is a better quencher of PhpC than pyrene since the inverse Stern-Volmer constant (K_{SV}^{-1}) of PhpC and *p*-NO₂-PhpC pair is smaller than the pyrene and *p*-NO₂-PhpC.

Chapter 4

4 Future studies

The interesting properties of the PhpC and the pC derivatives can be utilized in the vast areas of the research. Furthermore, understanding the fluorescence properties of PhpC in response to different nearest neighbours helps to develop more efficient hybridization probes. One idea to improve the photophysical properties of the PhpC in response to different neighbours is to use “insulators”. Insulators are nucleobases or moieties that could perturb the π -stacking of the nucleobases in some extent and decrease the effects of the nearest neighbours. Some examples of the moieties which can be used as insulators are terphenyl nucleosides (TP), 5,6-dihydro-2'-deoxythymidine (DHT) and a glycolic abasic site (Ab). These moieties could be placed in between the PhpC and different natural nucleobases and the measurement of their quantum yield shows whether the insulator works or not.

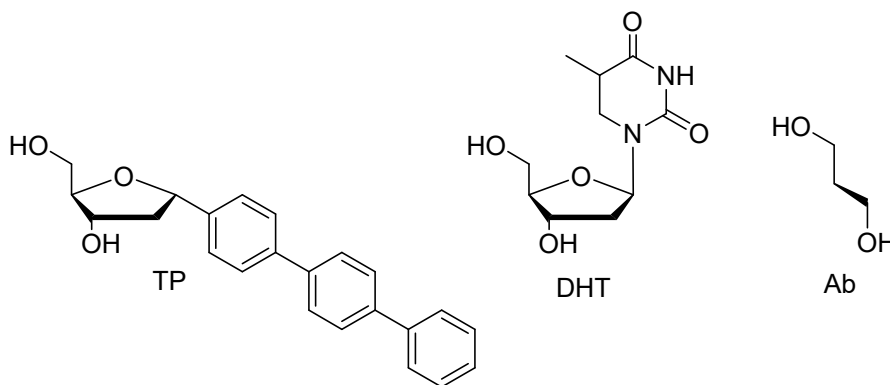


Figure 4-1: Chemical structure of some examples of the insulators

Even though the experimental results of the redox potentials showed that the photoinduced electron transfer of the pC derivatives are unfavorable the analysis of these derivatives by DFT calculations can help to enlighten the exact mechanism of the quenching.

Lastly, the incorporation of the PhpC and *p*-NO₂-PhpC into oligonucleotides as intrinsic FRET pairs is recommended since the quenching studies demonstrated that the PhpC is efficiently quenched by *p*-NO₂-PhpC.

Experimental

Synthesis of 3',5'-di-*O*-acetyl-2'-deoxycytidine (2)

2'-Deoxycytidine hydrochloride (9.5 g, 36 mmol) was suspended in AcOH (100 mL) and a solution of 30 mL acetyl chloride in 80 mL chloroform was added. The reaction mixture was stirred at room temperature for 52 hours until the suspension turned to clear yellowish solution. The volatiles were removed using rotary evaporator and the remaining were dissolved in methanol to quench remaining acetyl chloride. Upon evaporation of the methanol, the white solid was obtained. The solid was left under high vacuum overnight to yield the desired product with sufficient purity to be carried out to the next step. Yield: quantitative. R_f : 0.77 (MeOH:DCM 1:9). $^1\text{H NMR}$ (600 MHz, DMSO- d^6) δ : 10.17 (s, 1H), 8.98 (s, 1H), 8.01 (d, $J=7.63$, 1H), 6.29 (d, $J=7.63$, 1H), 6.07 (t, 1H), 5.18 (s, 1H), 4.22-4.26 (m, 3H), 2.39-2.48 (m, 2H), 2.05 (s, 3H), 2.03 (s, 3H).⁷⁰

Synthesis of 5-iodo-3',5'-di-*O*-acetyl-2'-deoxycytidine (3)

3',5'-Di-*O*-acetyl-2'-deoxycytidine (12.56 g, 36 mmol) was dissolved in 55 mL of water and I_2 (5.42 g, 21.34 mmol), iodic acid (1.58 g, 8.97 mmol), CHCl_3 (55 mL) and AcOH (80 mL) was added to the solution. The reaction mixture was heated to 50 °C and stirred for 24 hours. The volatiles were removed under vacuum and the residue was dissolved in 400 mL DCM. The solution was washed once with 400 mL 10% sodium thiosulphate and once with 400 mL saturated sodium bicarbonate. The organic phase was dried over sodium sulfate and was filtered. Using a rotary evaporator, the DCM was evaporated and the residue was placed under high vacuum overnight to be dried further. The desired product was yielded as a yellowish solid with sufficient purity to be used in next step. Yield: 70%. R_f = 0.61 (MeOH:DCM 0.5:9.5). $^1\text{H NMR}$ (600 MHz, DMSO- d^6) δ : 7.94 (s, 1H), 7.92 (br, s, 1H), 6.73 (br, s, 1H), 6.11 (t, 1H), 5.17 (br, s, 1H), 4.19- 4.28 (m, 3H), 2.29- 2.37 (m, 2H), 2.09 (s, 3H), 2.05 (s, 3H).⁷⁰

Synthesis of N⁴-benzoyl-5-iodo-3',5'-di-*O*-acetyl-2'-deoxycytidine (4)

5-Iodo-3',5'-di-*O*-acetyl-2'-deoxycytidine (11.09 g, 25.36 mmol) was dissolved in 100 mL pyridine and benzoic anhydride (8.6 g, 38 mmol) was added. The reaction mixture was stirred at 90 °C for 5 hours. After completion of the reaction the volatiles was removed using rotary evaporator and upon addition of 150 mL methanol the off-white solid precipitated. The filtration of the solid gave the desired product. Yield: 67 %. $R_f = 0.5$ (MeOH:DCM 0.2:9.8). ¹H NMR (600 MHz, DMSO-*d*⁶) δ : 12.83 (br, s, 1H), 8.23 (s, 3H), 7.62 (t, 1H), 7.53 (t, 2H), 6.12 (t, 1H), 5.20 (s, 1H), 4.27-4.32 (m, 3H), 2.53-2.58 (m, 1H), 2.40 (br, s, 1H), 2.13 (s, 3H), 2.07 (s, 3H).⁷⁰

Synthesis of 3',5'-di-*O*-acetyl-2'-deoxy-6-phenylpyrrolocytidine (5)

A 50 mL RB-flask was charged with N⁴-benzoyl-5-iodo-3',5'-di-*O*-acetyl-2'-deoxycytidine (1 g, 1.84 mmol) and 12 mL of dry THF was added. The solution was placed in dry ice/acetone bath (-78 °C) and degassed several times to remove any oxygen and moisture present in the solution. Then Pd(PPh₃)₂Cl₂ (130 mg, 0.185 mmol), CuI (70 mg, 0.37 mmol) and triethylamine (0.51 mL, 3.696 mmol) was added to the solution and degassed again. Lastly, phenylacetylene (0.6 mL, 5.54 mmol) was added to the reaction mixture. The mixture was stirred at 50 °C, under a nitrogen atmosphere, and in darkness for overnight. After 18 hours, TLC showed the complete consumption of the starting material, then 40 mL of anhydrous ethanol and 1 mL of triethylamine was added to the reaction mixture to remove the benzoyl group of the amine. The mixture was stirred for another 24 hours at 50 °C under nitrogen atmosphere and in darkness. After completion of the reaction, the mixture was concentrated using a rotary evaporator and the residue was dissolved in 100 mL of DCM. The solution was transferred to a separatory funnel and was washed with 5% EDTA (3×100 mL). The organic phase was dried using anhydrous sodium sulfate and concentrated. The residue was dry packed into a silica gel column and eluted using DCM, later replaced with DCM: MeOH 96:4. Yield: 67%. $R_f = 0.4$ (MeOH:DCM 0.5:9.5). ¹H NMR (600 MHz, DMSO-*d*⁶) δ : 11.83 (s, 1H), 8.45 (s, 1H), 7.84 (d, 2H), 7.45 (t, 2H), 7.35 (t, 1H), 6.78 (s, 1H), 6.31 (s, 1H), 5.24 (s, 1H), 4.33 (s, 3H), 2.54-2.58 (m, 1H), 2.34-2.39 (m, 1H), 2.09 (s, 3H), 2.06 (s, 3H).⁷⁰

Synthesis of 2'-deoxy-6-phenylpyrrolocytidine (6)

An RB-flask was charged with 3',5'-di-*O*-acetyl-2'-deoxy-6-phenylpyrrolocytidine (1 g, 2.43 mmol), K₂CO₃ (335 mg, 2.43 mmol) and methanol (20 mL). The suspension was stirred for 30 minutes at room temperature. The murky solution was concentrated and upon addition of 1 M HCl, a yellow solid precipitated out. The solids were collected and washed with water several times and dried overnight. Yield: 81%. ¹H NMR (DMSO-*d*⁶) δ : 11.77 (br, s, 1H), 8.71 (s, 1H), 7.83 (d, *J*= 7.63, 2H), 7.44 (t, *J*= 7.63, 2H), 7.34 (t, 1H), 6.74 (s, 1H), 6.27 (t, 1H), 5.27 (d, 1H), 5.13 (t, 1H), 4.26 (s, 1H), 3.91 (s, 1H), 3.62-3.72 (m, 2H), 2.35-2.39 (m, 1H), 2.02-2.07 (m, 1H).⁷⁰

Synthesis of 3',5'-di-*O*-acetyl-2'-deoxy-6-(*p*-nitro)phenylpyrrolocytidine (7)

A 50 mL RB-flask was charged with N⁴-benzoyl-5-iodo-3',5'-di-*O*-acetyl-2'-deoxycytidine (440 mg, 0.81 mmol), *p*-NO₂-phenylacetylene (180 mg, 1.2 mmol) and 5 mL of dry DMF was added. The solution was placed in dry ice/acetone bath (-78 °C) and degassed several times to remove any oxygen and moisture present in the solution. Then Pd(PPh₃)₄ (93 mg, 0.081 mmol) and CuI (31 mg, 0.162 mmol) were added and degassed again. Lastly, triethylamine (0.23 mL, 1.626 mmol) was added to the solution. The mixture was stirred at 50 °C, under a nitrogen atmosphere, and in darkness for overnight. After 12 hours, TLC showed the complete consumption of the starting material, then 10 mL of anhydrous ethanol and 0.5 mL of triethylamine was added to the reaction mixture and stirred for another 24 hours at 50 °C under nitrogen atmosphere and in darkness. After completion of the reaction, the mixture was concentrated using rotary evaporator and the residue was dissolved in 100 mL of DCM. The solution was transferred to a separatory funnel and was washed with 5% EDTA (3×100 mL). The organic phase was dried using anhydrous sodium sulfate and concentrated. The residue was dry packed into a silica gel column and eluted using DCM, later replaced with DCM: MeOH 96:4. Then the oily product was dissolved in the mixture of MeOH and ET₃N and poured into cold stirring hexanes. Yield: 59%. ¹H NMR (600 MHz, DMSO-*d*⁶) δ : 12.06 (s, 1H), 8.60 (s, 1H), 8.28 (d, 2H), 8.10 (d, 2H), 7.10 (s, 1H), 6.28 (m, 1H), 5.24 (m, 1H). ¹³C NMR (600 MHz, DMSO-*d*⁶) δ : 170.17, 170.06,

160.21, 153.55, 146.42, 138.03, 136.69, 125.75 (2×C), 124.20 (2×C), 109.17, 101.50, 87.66, 82.25, 74.15, 63.63, 38.01, 20.79, 20.64.

Synthesis of 2'-deoxy-6-(*p*-nitro)phenylpyrrolocytidine (8)

A 25 mL RB-flask was charged with 3',5'-di-*O*-acetyl-2'-deoxy-6-(*p*-nitro)phenylpyrrolocytidine (100 mg, 0.22 mmol), triethylamine (0.22 mL, 1.53 mmol), 2 mL MeOH and 2 mL water. After 1 hour stirring at 70 °C, the volatiles was removed by rotary evaporator and trituration with methanol gave the desired product as an orange solid. Yield: 82%. ¹H NMR (600 MHz, DMSO-*d*⁶) δ: 12.01 (s, 1H), 8.86 (s, 1H), 8.28 (d, *J* = 9.0, 2H), 8.09 (d, *J* = 9.0, 2H), 7.07 (s, 1H), 6.24 (t, 1H), 5.27 (d, 1H), 5.15 (t, 1H), 4.26 (m, 1H), 3.92 (m, 1H), 3.70 (m, 2H), 2.39 (m, 1H), 2.05 (m, 1H).¹⁰¹

Synthesis of 1-ethynyl-4-nitrobenzene

An oven-dried 50 mL RB flask was charged with 1-iodo-4-nitrophenyl (2 g, 8 mmol), Pd(PPh₃)₂Cl₂ (300 mg, 0.4 mmol) and CuI (80 mg, 0.4 mmol) and dissolved in 25 mL triethylamine. The reaction mixture was degassed and nitrogenated three times. Lastly, TMS-acetylene (1.5 mL, 10 mmol) was added to the mixture and degassed and nitrogenated again. The reaction mixture was stirred at room temperature in the N₂ atmosphere and in darkness. After 24 hours TLC showed the complete consumption of the starting material. The volatiles was removed using rotary evaporator and the remaining was suspended in hexane and was passed through cellite and washed with hexane. The filtrate was concentrated and suspended in 20 mL methanol and K₂CO₃ (8 mmol, 1.1 g) was added and stirred for 2 hours at room temperature. After completion of the reaction, it was concentrated and dry packed into a short column and eluted with Hex:EtOAc 9:1. Yield: 91%. ¹H NMR (600 MHz, CDCl₃) δ: 8.20 (d, 2H), 7.66 (d, 2H), 3.37 (s, 1H).¹⁰²

References

- (1) Dahm, R. *J. Hum. Genet.* **2008**, *122*, 565-581.
- (2) Altmann, R. *Arch. Anat. Physiol. Abt. Physiol.* **1889**, *1889*, 524-536.
- (3) Portugal, F.; Cohen, J. *A century of DNA: A History of the Discovery of the Structure and Function of the Genetic Substance*, The MIT Press, Cambridge, **1977**.
- (4) Levene, P. *J. Biol. Chem.* **1919**, *40*, 415-424.
- (5) Levene, P.; London, E. *J. Biol. Chem.* **1929**, *83*, 793-802.
- (6) Todd, A. R. *Proc. Natl. Acad. Sci.* **1954**, *40*, 748-755.
- (7) Watson, J. D.; Berry, A. *DNA: The secret of life*, Knopf, **2009**.
- (8) Zamenhof, S.; Brawerman, G.; Chargaff, E. *Biochim. Biophys. Acta.* **1952**, *9*, 402-405.
- (9) Watson, J.; Crick, F. *Nature* **1953**, *171*, 737-738.
- (10) Crick, F. *Nature* **1970**, *227*, 561-563.
- (11) Berg, J. M.; Tymoczko, J. *Stryer: Biochemistry*, WH Freeman and Company, **2002**, *5*, 306-307.
- (12) Arnott, S. *Trends Biochem. Sci.* **2006**, *31*, 349-354.
- (13) Dickerson, R. E.; Drew, H. R.; Conner, B. N.; Wing, R. M.; Fratini, A. V.; Kopka, M. L. *Science* **1982**, *216*, 475-485.
- (14) Travers, A.; Muskhelishvili, G. *FEBS J.* **2015**, *282*, 2279-2295.
- (15) Lackowicz, J. R. *Principle of Fluorescence Spectroscopy* 3rd ed., Springer Science+ Business Media, New York, **2006**, 277-351.
- (16) Wilhelmsson, M.; Tor, Y. *Fluorescent Analogs of Biomolecular Building Blocks: Design and Applications*, John Wiley & Sons, **2016**, 174-207.
- (17) Sinkeldam, R. W.; Greco, N. J.; Tor, Y. Fluorescent analogs of biomolecular building blocks: design, properties, and applications. *Chem. Rev.* **2010**, *110*, 2579-2619.
- (18) Tanpure, A. A.; Pawar, M. G.; Srivatsan, S. G. *Isr. J. Chem.* **2013**, *53*, 366-378.
- (19) Matarazzo, A.; Hudson, R. H. *Tetrahedron* **2015**, *71*, 1627-1657.
- (20) Dodd, D.; Hudson, R. *Mini-Rev. Org. Chem.* **2009**, *6*, 378-391.
- (21) Seela, F.; Budow, S.; Peng, X. *Curr. Org. Chem.* **2012**, *16*, 161-223.

- (22) Barbatti, M. *Photoinduced Phenomena in Nucleic Acids I*, Springer International Publishing, **2014**, 209-243.
- (23) Wilhelmsson, L. M. *Q. Rev. Biophys.* **2010**, *43*, 159-183.
- (24) Wang, S.; Guo, J.; Ono, T.; Kool, E. T. *Angew. Chem. Int. Ed.* **2012**, *51*, 7176-7180.
- (25) Guo, J.; Wang, S.; Dai, N.; Teo, Y. N.; Kool, E. T. *Proc. Natl. Acad. Sci.* **2011**, *108*, 3493-3498.
- (26) Tan, S. S.; Kim, S. J.; Kool, E. T. *J. Am. Chem. Soc.* **2011**, *133*, 2664-2671.
- (27) Koo, C.-K.; Samain, F.; Dai, N.; Kool, E. T. *Chem. Sci.* **2011**, *2*, 1910-1917.
- (28) Wilson, J. N.; Gao, J.; Kool, E. T. *Tetrahedron* **2007**, *63*, 3427-3433.
- (29) Gao, J.; Strässler, C.; Tahmassebi, D.; Kool, E. T. *J. Am. Chem. Soc.* **2002**, *124*, 11590-11591.
- (30) Kwon, H.; Jiang, W.; Kool, E. T. *Chem. Sci.* **2015**, *6*, 2575-2583.
- (31) Kwon, H.; Chan, K. M.; Kool, E. T. *Org. Biomol. Chem.* **2017**, *15*, 1801-1809.
- (32) Hawkins, M. E.; Balis, F. M. *Nucleic Acids Res.* **2004**, *32*, e62.
- (33) Costa, J. A.; Leal-Pinto, E.; Henderson, S. C.; Zabel, T.; Hawkins, M. E.; Hanss, B. *Pteridines* **2012**, *23*, 81-89.
- (34) Lin, K.-Y.; Jones, R. J.; Matteucci, M. *J. Am. Chem. Soc.* **1995**, *117*, 3873-3874.
- (35) Wilhelmsson, L. M.; Holmén, A.; Lincoln, P.; Nielsen, P. E.; Nordén, B. *J. Am. Chem. Soc.* **2001**, *123*, 2434-2435.
- (36) Wilhelmsson, L. M.; Sandin, P.; Holmén, A.; Albinsson, B.; Lincoln, P.; Nordén, B. *J. Phys. Chem. B* **2003**, *107*, 9094-9101.
- (37) Sandin, P.; Börjesson, K.; Li, H.; Mårtensson, J.; Brown, T.; Wilhelmsson, L. M.; Albinsson, B. *Nucleic Acids Res.* **2007**, *36*, 157-167.
- (38) Börjesson, K.; Sandin, P.; Albinsson, B.; Mårtensson, J.; Brown, T.; Wilhelmsson, L. M. *Nucleic Acids Symp. Ser. (Oxf)*, *52*, 3-4.
- (39) Preus, S.; Kilså, K.; Wilhelmsson, L. M.; Albinsson, B. *Phys. Chem. Chem. Phys.* **2010**, *12*, 8881-8892.
- (40) Preus, S.; Börjesson, K.; Kilså, K.; Albinsson, B.; Wilhelmsson, L. M. *J. Phys. Chem. B* **2009**, *114*, 1050-1056.
- (41) Engman, K. C.; Sandin, P.; Osborne, S.; Brown, T.; Billeter, M.; Lincoln, P.; Nordén, B.; Albinsson, B.; Wilhelmsson, L. M. *Nucleic Acids Res.* **2004**, *32*, 5087-5095

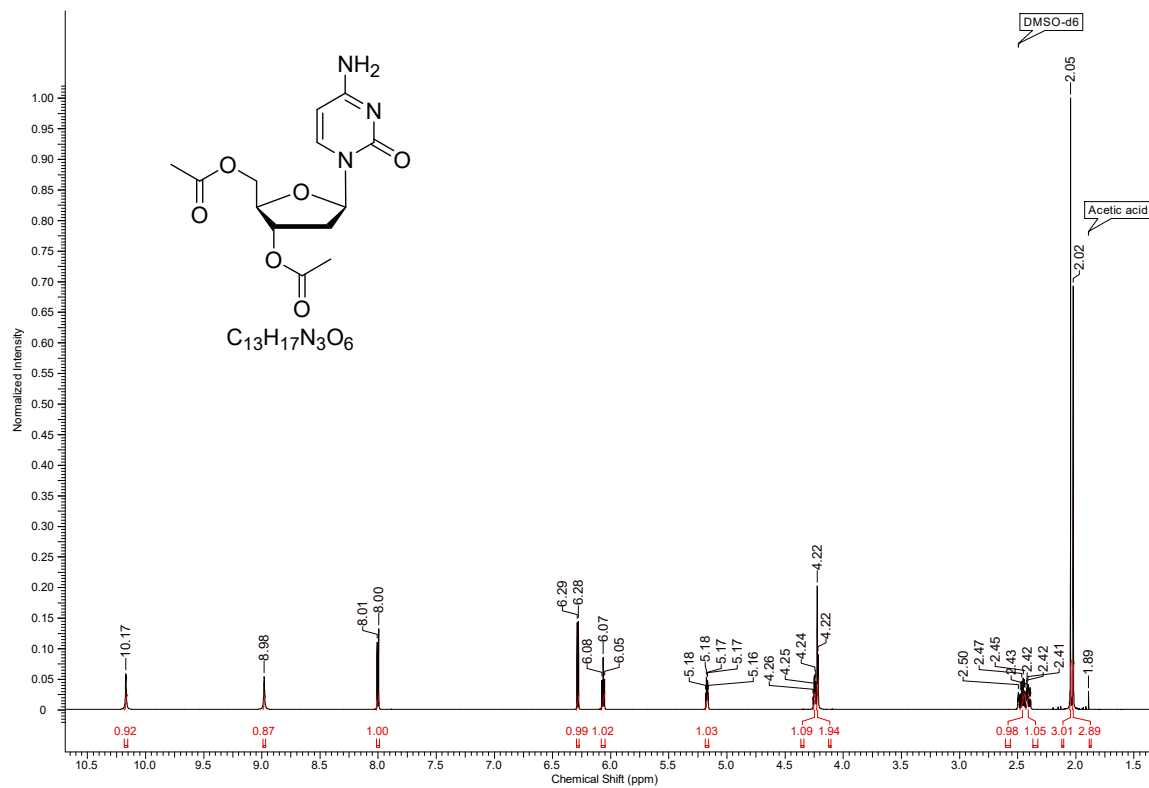
- (42) Sandin, P.; Wilhelmsson, L. M.; Lincoln, P.; Powers, V. E.; Brown, T.; Albinsson, B. *Nucleic Acids Res.* **2005**, *33*, 5019-5025.
- (43) Sandin, P.; Stengel, G.; Ljungdahl, T.; Börjesson, K.; Macao, B.; Wilhelmsson, L. M. *Nucleic Acids Res.* **2009**, *37*, 3924-3933.
- (44) Stengel, G.; Purse, B. W.; Wilhelmsson, L. M.; Urban, M.; Kuchta, R. D. *Biochemistry* **2009**, *48*, 7547-7555.
- (45) Stengel, G.; Gill, J. P.; Sandin, P.; Wilhelmsson, L. M.; Albinsson, B.; Nordén, B.; Millar, D. *Biochemistry* **2007**, *46*, 12289-12297.
- (46) Walsh, J. M.; Bouamaied, I.; Brown, T.; Wilhelmsson, L. M.; Beuning, P. J. *J. Mol. Biol.* **2011**, *409*, 89-100.
- (47) Preus, S.; Jønck, S.; Pittelkow, M.; Dierckx, A.; Karpkird, T.; Albinsson, B.; Wilhelmsson, L. M. *Photochem. Photobiol. Sci.* **2013**, *12*, 1416-1422.
- (48) Börjesson, K.; Sandin, P.; Wilhelmsson, L. M. *Biophys. Chem.* **2009**, *139*, 24-28.
- (49) Füchtbauer, A. F.; Preus, S.; Börjesson, K.; McPhee, S. A.; Lilley, D. M.; Wilhelmsson, L. M. *Sci. Rep.* **2017**, *7*, 2393-2401.
- (50) Börjesson, K.; Preus, S.; El-Sagheer, A. H.; Brown, T.; Albinsson, B.; Wilhelmsson, L. M. *J. Am. Chem. Soc.* **2009**, *131*, 4288-4293.
- (51) Posse, V.; Hoberg, E.; Dierckx, A.; Shahzad, S.; Koolmeister, C.; Larsson, N.-G.; Wilhelmsson, L. M.; Hällberg, B. M.; Gustafsson, C. M. *Nucleic Acids Res.* **2014**, *42*, 3638-3647.
- (52) Shi, Y.; Dierckx, A.; Wanrooij, P. H.; Wanrooij, S.; Larsson, N.-G.; Wilhelmsson, L. M.; Falkenberg, M.; Gustafsson, C. M. *Proc. Natl. Acad. Sci.* **2012**, *109*, 16510-16515.
- (53) Dumat, B.; Larsen, A. F.; Wilhelmsson, L. M. *Nucleic Acids Res.* **2016**, *44*, e101.
- (54) Sellrie, F.; Lenz, C.; Andersson, A.; Wilhelmsson, L. M.; Schenk, J. A. *Talanta* **2014**, *124*, 67-70.
- (55) Okamoto, A.; Saito, Y.; Saito, I. *J. Photochem. Photobiol. C: Photochem. Rev.* **2005**, *6*, 108-122.
- (56) Okamoto, A.; Tanaka, K.; Fukuta, T.; Saito, I. *J. Am. Chem. Soc.* **2003**, *125*, 9296-9297.
- (57) Okamoto, A.; Tainaka, K.; Saito, I. *Tetrahedron Lett.* **2003**, *44*, 6871-6874.
- (58) Dziuba, D.; Jurkiewicz, P.; Cebecauer, M.; Hof, M.; Hocek, M. *Angew. Chem. Int. Ed.* **2016**, *55*, 174-178.
- (59) Dziuba, D.; Pohl, R.; Hocek, M. *Bioconjugate Chem.* **2014**, *25*, 1984-1995.
- (60) Suzuki, A.; Saito, M.; Katoh, R.; Saito, Y. *Org. Biomol. Chem.* **2015**, *13*, 7459-7468.

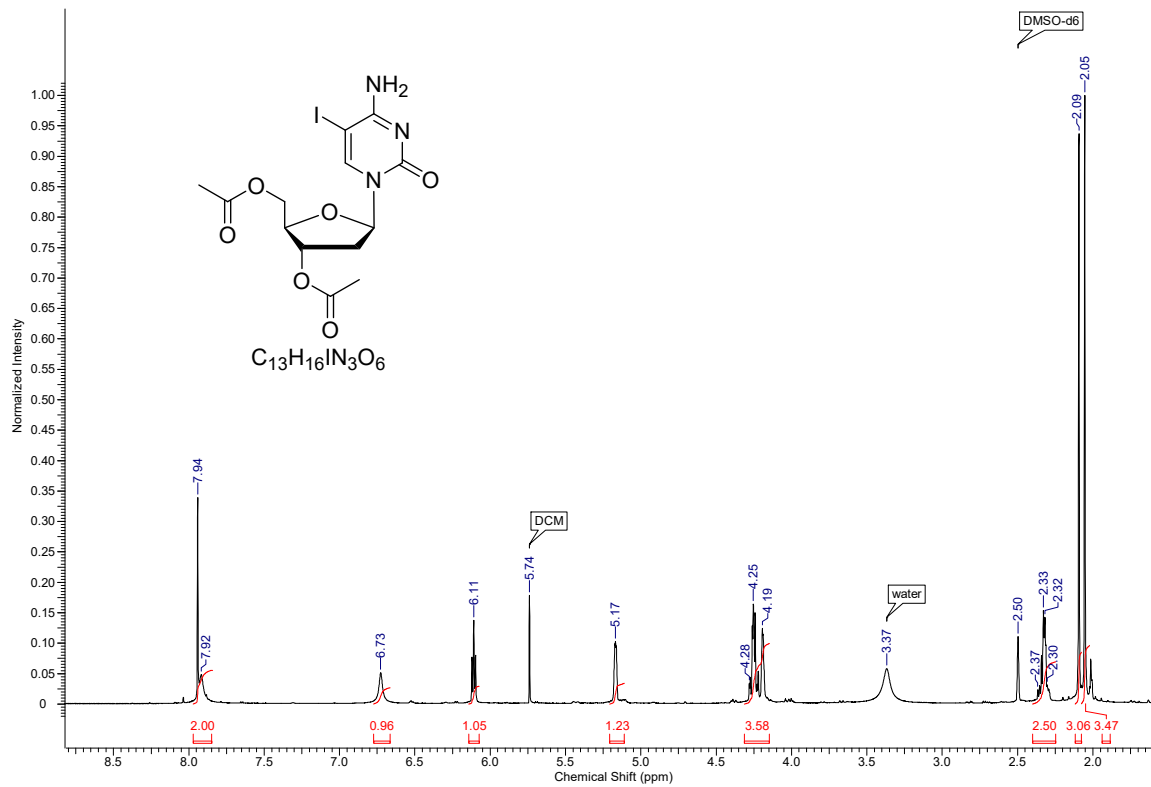
- (61) Ward, D.; Reich, E.; Stryer, L. *J. Biol. Chem.* **1969**, *244*, 1228-1237.
- (62) Jones, A. C.; Neely, R. K. *Q. R. Biophys.* **2015**, *48*, 244-279.
- (63) Shin, D.; Sinkeldam, R. W.; Tor, Y. *J. Am. Chem. Soc.* **2011**, *133*, 14912-14915.
- (64) Sholokh, M.; Sharma, R.; Shin, D.; Das, R.; Zaporozhets, O. A.; Tor, Y.; Mély, Y. *J. Am. Chem. Soc.* **2015**, *137*, 3185-3188.
- (65) Park, S.; Otomo, H.; Zheng, L.; Sugiyama, H. *Chem. Commun.* **2014**, *50*, 1573-1575.
- (66) Noé, M. S.; Ríos, A. C.; Tor, Y. *Org. Lett.* **2012**, *14*, 3150-3153.
- (67) Inoue, H.; Imura, A.; Ohtsuka, E. *Nippon Kagaku Kaishi* **1987**, 1214-1220.
- (68) Woo, J.; Meyer, R. B.; Gamper, H. B. *Nucleic Acids Res.* **1996**, *24*, 2470-2475.
- (69) Berry, D. A.; Jung, K.-Y.; Wise, D. S.; Sercel, A. D.; Pearson, W. H.; Mackie, H.; Randolph, J. B.; Somers, R. L. *Tetrahedron Lett.* **2004**, *45*, 2457-2461.
- (70) Elmehriki, A. A.; Suchý, M.; Chicas, K. J.; Wojciechowski, F.; Hudson, R. H. *Artif. DNA: PNA & XNA* **2014**, *5*, e29174.
- (71) Hudson, R. H.; Dambeniaks, A. K.; Viirre, R. D. *Synlett* **2004**, *2004*, 2400-2402.
- (72) Hudson, R. H.; Dambeniaks, A. K.; Moszynski, J. M. *Proc. SPIE 5969, Photonic Applications in Biosensing and Imaging* **2005**, 59690J.
- (73) Hudson, R. H.; Ghorbani-Choghamarani, A. *Synlett* **2007**, *2007*, 0870-0873.
- (74) Wahba, A. S.; Esmacili, A.; Damha, M. J.; Hudson, R. H. *Nucleic Acids Res.* **2009**, *38*, 1048-1056.
- (75) Wilhelmsson, M.; Tor, Y. *Fluorescent Analogs of Biomolecular Building Blocks: Design and Applications*, John Wiley & Sons, **2016**, 174-207.
- (76) Seela, F.; Schweinberger, E.; Xu, K.; Sirivolu, V. R.; Rosemeyer, H.; Becker, E.-M. *Tetrahedron* **2007**, *63*, 3471-3482.
- (77) Koh, Y.-H.; Shim, J. H.; Girardet, J.-L.; Hong, Z. *Bioorg. Med. Chem. Lett.* **2007**, *17*, 5261-5264.
- (78) Leonard, P.; Ingale, S. A.; Ding, P.; Ming, X.; Seela, F. *Nucleosides, Nucleotides and Nucleic Acids* **2009**, *28*, 678-694.
- (79) Aucagne, V.; Amblard, F.; Agrofoglio, L. A. *Synlett* **2004**, *2004*, 2406-2408.
- (80) Sniady, A.; Durham, A.; Morreale, M. S.; Marcinek, A.; Szafert, S.; Lis, T.; Brzezinska, K. R.; Iwasaki, T.; Ohshima, T.; Mashima, K. *J. Org. Chem.* **2008**, *73*, 5881-5889.
- (81) Yu, C.; Yowanto, H.; Wan, Y.; Meade, T. J.; Chong, Y.; Strong, M.; Donilon, L. H.; Kayyem, J. F.; Gozin, M.; Blackburn, G. F. *J. Am. Chem. Soc.* **2000**, *122*, 6767-6768.

- (82) Rao, M. S.; Esho, N.; Sergeant, C.; Dembinski, R. *J. Org. Chem.* **2003**, *68*, 6788-6790.
- (83) Sonogashira, K.; Tohda, Y.; Hagihara, N. *Tetrahedron Lett.* **1975**, *16*, 4467-4470.
- (84) Sonogashira, K. *J. Organomet. Chem.* **2002**, *653*, 46-49.
- (85) Wahba, A. S.; Damha, M. J.; Hudson, R. H. *Nucleic Acids Symp. Ser. (Oxf)* **2008**, *52*, 399-400.
- (86) Wahba, A. S.; Azizi, F.; Deleavey, G. F.; Brown, C.; Robert, F.; Carrier, M.; Kalota, A.; Gewirtz, A. M.; Pelletier, J.; Hudson, R. H. *ACS Chem. Biol.* **2011**, *6*, 912-919.
- (87) Wahba, A. S.; Esmacili, A.; Damha, M. J.; Hudson, R. H. *Nucleic Acids Res.* **2010**, *38*, 1048-1056.
- (88) Wojciechowski, F.; Hudson, R. H. *J. Am. Chem. Soc.* **2008**, *130*, 12574-12575.
- (89) Wojciechowski, F.; Hudson, R. H. *Nucleic Acids Symp. Ser. (Oxf)* **2008**, *52*, 401-402.
- (90) Hu, J.; Dodd, D. W.; Hudson, R. H.; Corey, D. R. *Bioorg. Med. Chem. Lett.* **2009**, *19*, 6181-6184.
- (91) Torres, A. G.; Fabani, M. M.; Vigorito, E.; Williams, D.; Al-Obaidi, N.; Wojciechowski, F.; Hudson, R. H.; Seitz, O.; Gait, M. J. *Nucleic Acids Res.* **2011**, *40*, 2152-2167.
- (92) Yang, H.; Mei, H.; Seela, F. *Chem. Eur. J.* **2015**, *21*, 10207-10219.
- (93) Ming, X.; Ding, P.; Leonard, P.; Budow, S.; Seela, F. *Org. Biomol. Chem.* **2012**, *10*, 1861-1869.
- (94) Saito, Y.; Shinohara, Y.; Bag, S. S.; Takeuchi, Y.; Matsumoto, K.; Saito, I. *Tetrahedron* **2009**, *65*, 934-939.
- (95) Michelson, A.; Todd, A. R. *J. Chem. Soc.* **1955**, 2632-2638.
- (96) Letsinger, R. L.; Lunsford, W. B. *J. Am. Chem. Soc.* **1976**, *98*, 3655-3661.
- (97) Beaucage, S.; Caruthers, M. *Tetrahedron Lett.* **1981**, *22*, 1859-1862.
- (98) Beaucage, S. L.; Caruthers, M. H. *Curr. Protoc. Nucleic Acid Chem.* **2000**, 3.3.1-3.3.20.
- (99) Shivalingam, A.; Brown, T. *Biochem. Soc. Trans.* **2016**, *44*, 709-715.
- (100) Narayanan, M.; Kodali, G.; Singh, V. R.; Velvadapu, V.; Stanley, R. J. *J. Photochem. Photobiol.* **2012**, *249*, 9-14.
- (101) Suchy, M.; Ettles, C.; Wisner, J. A.; Matarazzo, A.; Hudson, R. H. *J. Org. Chem.* **2016**, *81*, 8415-8425.
- (102) Feng, Y.-S.; Xie, C.-Q.; Qiao, W.-L.; Xu, H.-J. *Org. Lett.* **2013**, *15*, 936-939.

- (103) Sharber, S. A.; Baral, R. N.; Frausto, F.; Haas, T. E.; Müller, P.; Thomas III, S. W. *J. Am. Chem. Soc.* **2017**, *139*, 5164-5174.
- (104) Meier, L.; Monteiro, G. C.; Baldissera, R. A.; Sá, M. M. *J. Braz. Chem. Soc.* **2010**, *21*, 859-866.
- (105) Pavlishchuk, V. V.; Addison, A. W. *Inorg. Chim. Acta* **2000**, *298*, 97-102.
- (106) Seidel, C. A.; Schulz, A.; Sauer, M. H. *J. Phys. Chem.* **1996**, *100*, 5541-5553.
- (107) Narayanan, M.; Kodali, G.; Xing, Y.; Hawkins, M. E.; Stanley, R. J. *J. Phys. Chem. B* **2010**, *114*, 5953-5963.
- (108) Narayanan, M.; Kodali, G.; Xing, Y.; Stanley, R. J. *J. Phys. Chem. B* **2010**, *114*, 10573-10580.
- (109) Kelley, S. O.; Barton, J. K. *Science* **1999**, *283*, 375-381.
- (110) Kelley, S. O.; Barton, J. K. *Chemistry & Biology*. **1998**, *5*, 413-425.
- (111) Nguyen, Q. L.; Spata, V. A.; Matsika, S. *Phys. Chem. Chem. Phys.* **2016**, *18*, 20189-20198.
- (112) Tinsley, R. A.; Walter, N. G. *RNA* **2006**, *12*, 522-529.
- (113) Tyagi, S.; Kramer, F. R. *Nat. Biotechnol.* **1996**, *14*, 303-308.
- (114) Han, S.-X.; Jia, X.; Ma, J.-l.; Zhu, Q. *Arch. Immunol. Ther. Exp.* **2013**, *61*, 139.
- (115) Zheng, J.; Yang, R.; Shi, M.; Wu, C.; Fang, X.; Li, Y.; Li, J.; Tan, W. *Chem. Soc. Rev.* **2015**, *44*, 3036-3055.
- (116) Tyagi, S.; Kramer, F. R. *F1000 Med. Rep.* **2012**, *4*, 10.
- (117) Huang, K.; Martí, A. A. *Anal. Bioanal. Chem.* **2012**, *402*, 3091-3102.
- (118) Mhlanga, M. M.; Tyagi, S. *Nat. Protoc.* **2006**, *1*, 1392.
- (119) Wang, G. T.; Matayoshi, E.; Huffaker, H. J.; Krafft, G. A. *Tetrahedron Lett.* **1990**, *31*, 6493-6496.
- (120) Martí, A. A.; Jockusch, S.; Li, Z.; Ju, J.; Turro, N. J. *Nucleic Acids Res.* **2006**, *34*, e50.
- (121) Tyagi, S.; Bratu, D. P.; Kramer, F. R. *Nat. Biotechnol.* **1998**, *16*, 49-53.

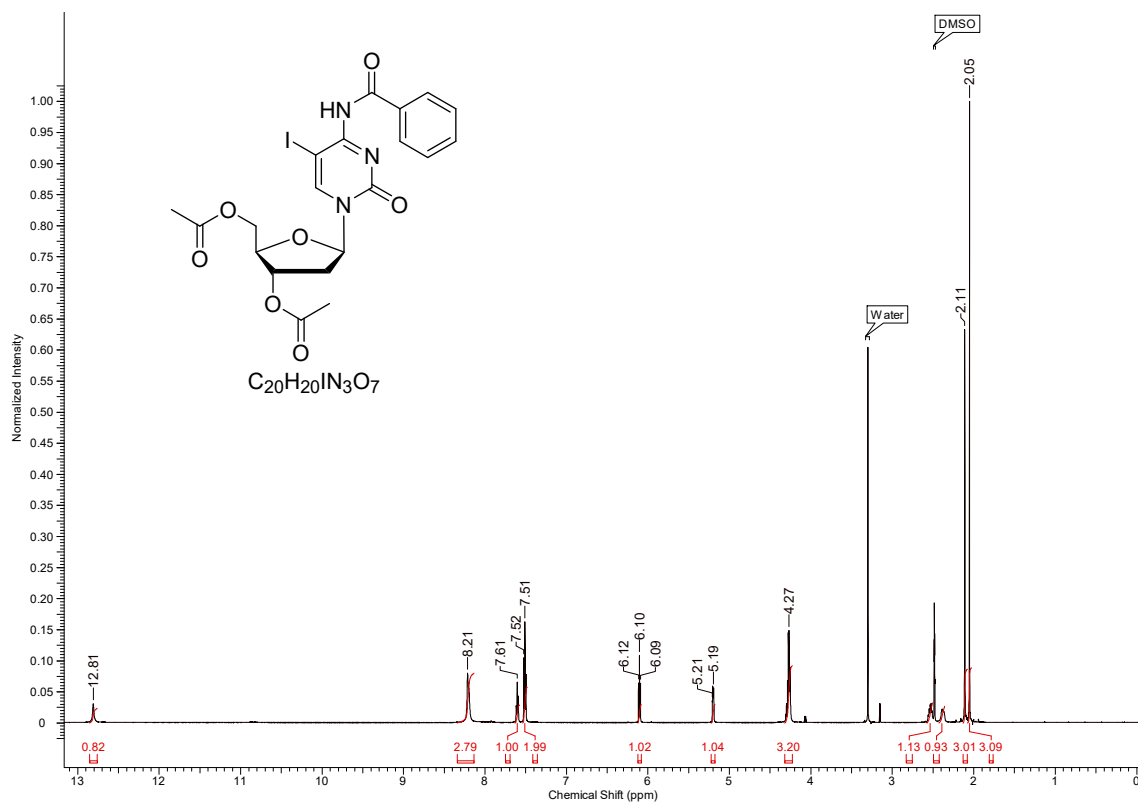
Appendices

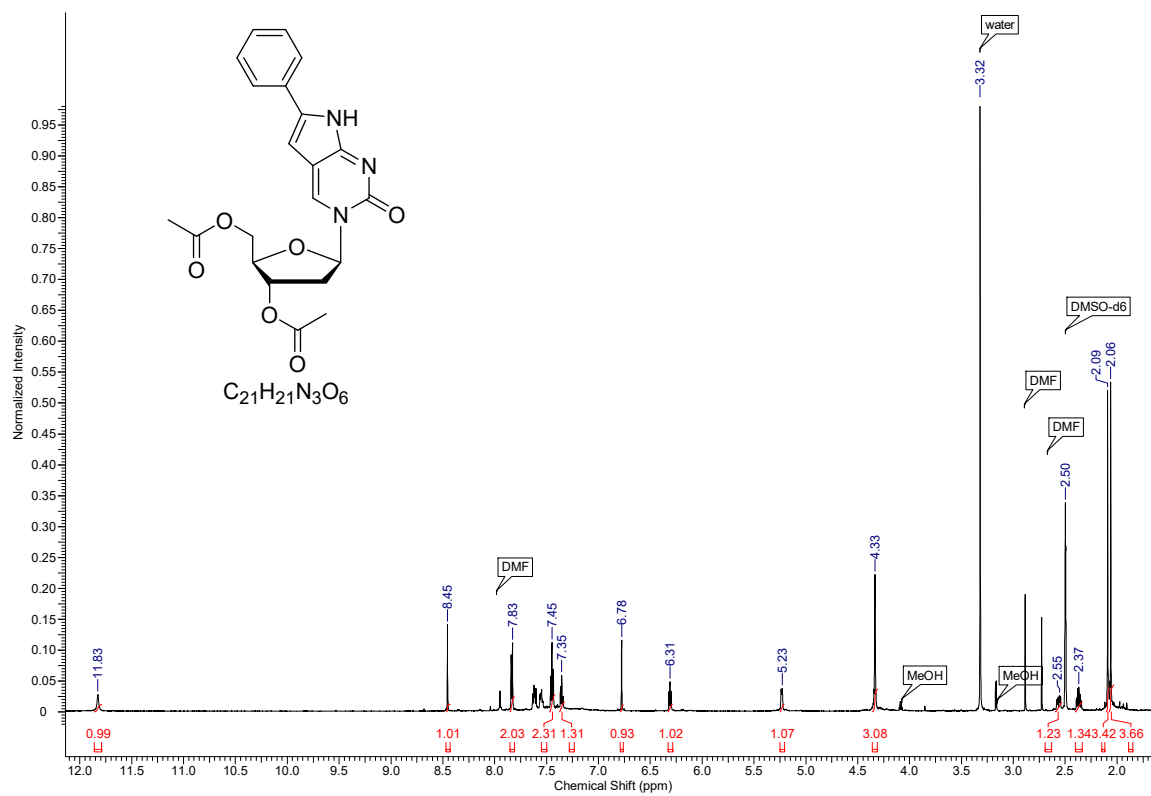
Appendix 1: ^1H NMR spectra 3',5'-di-*O*-acetyl-2'-deoxycytidine (2)

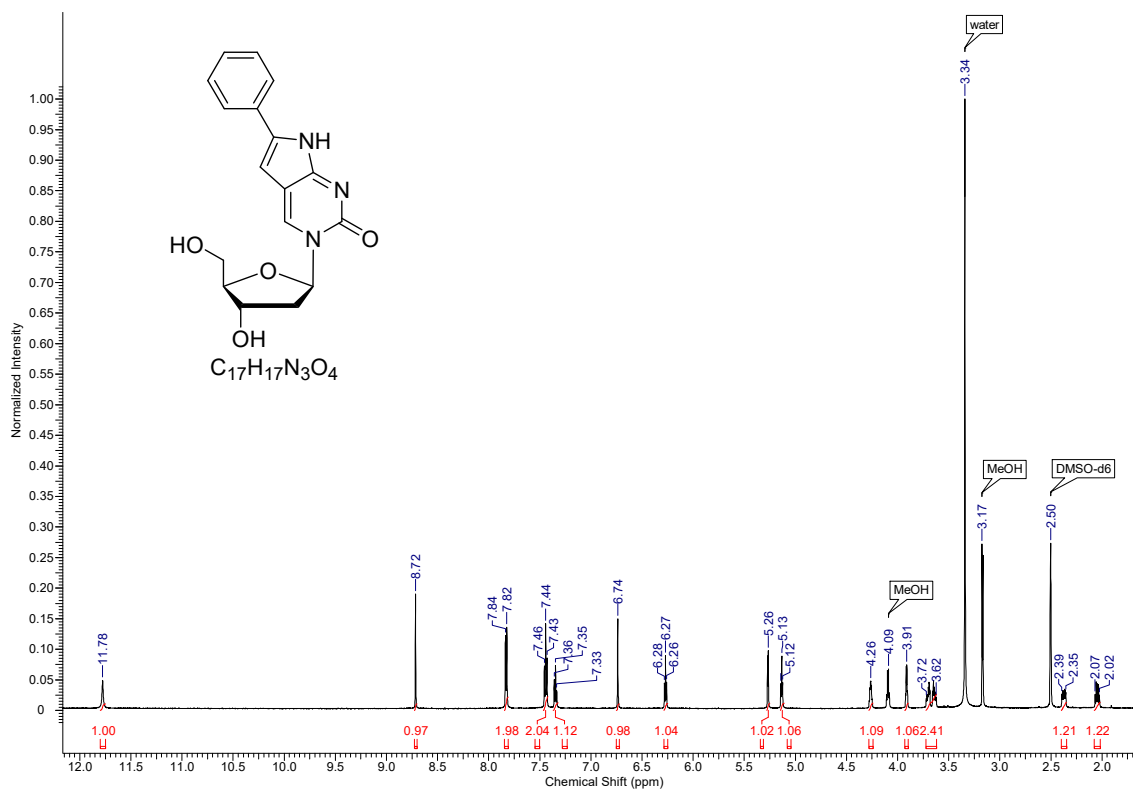
Appendix 2: ^1H NMR spectra 5-iodo-3',5'-di-*O*-acetyl-2'-deoxycytidine (3)

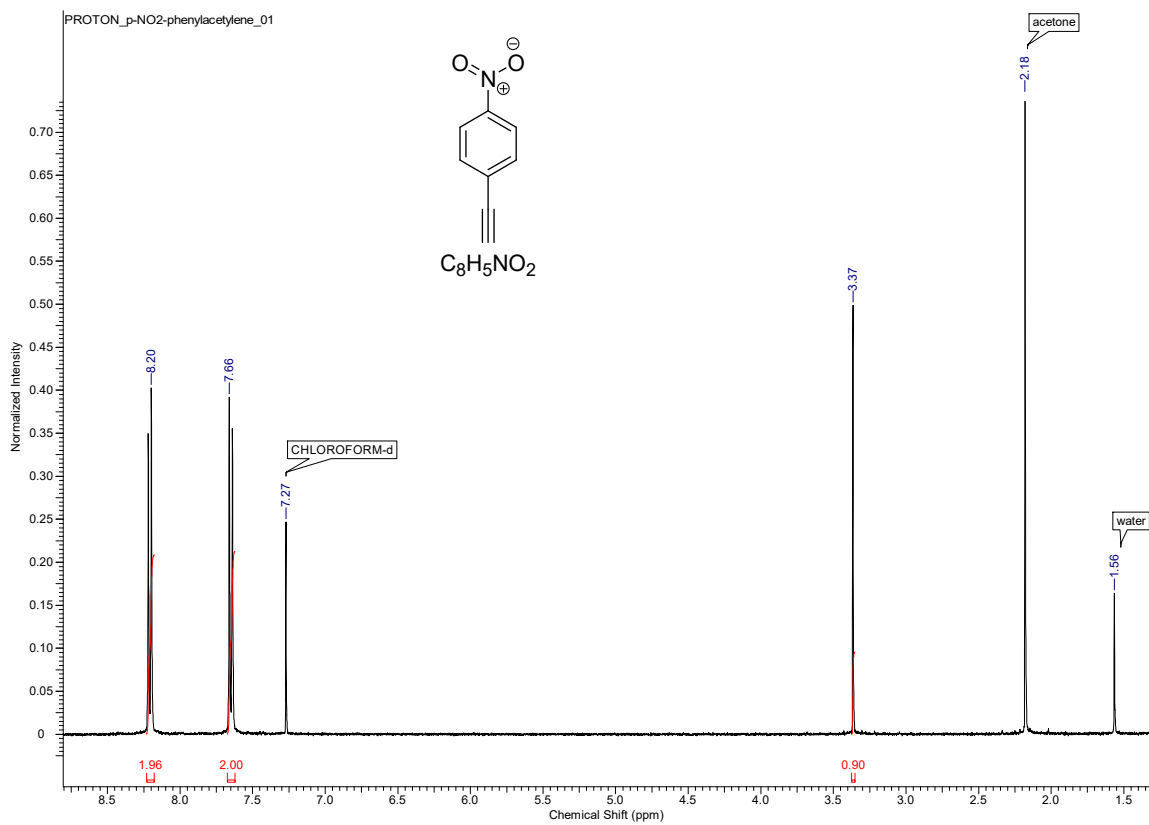
Appendix 3: ^1H NMR spectra N^4 -benzoyl-5-iodo-3',5'-di-*O*-acetyl-2'-deoxycytidine

(4)

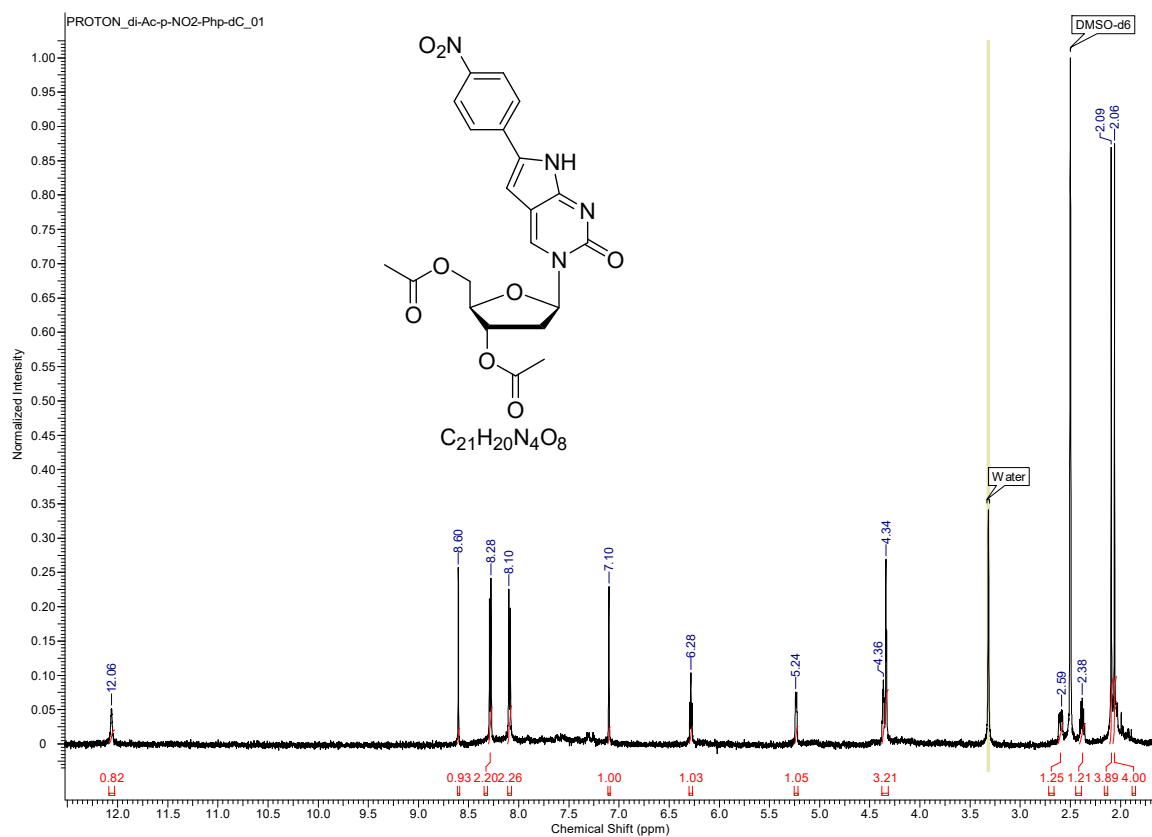


Appendix 4: ¹H NMR spectra 3',5'-di-O-acetyl-2'-deoxy-6-phenylpyrrolocytidine (5)

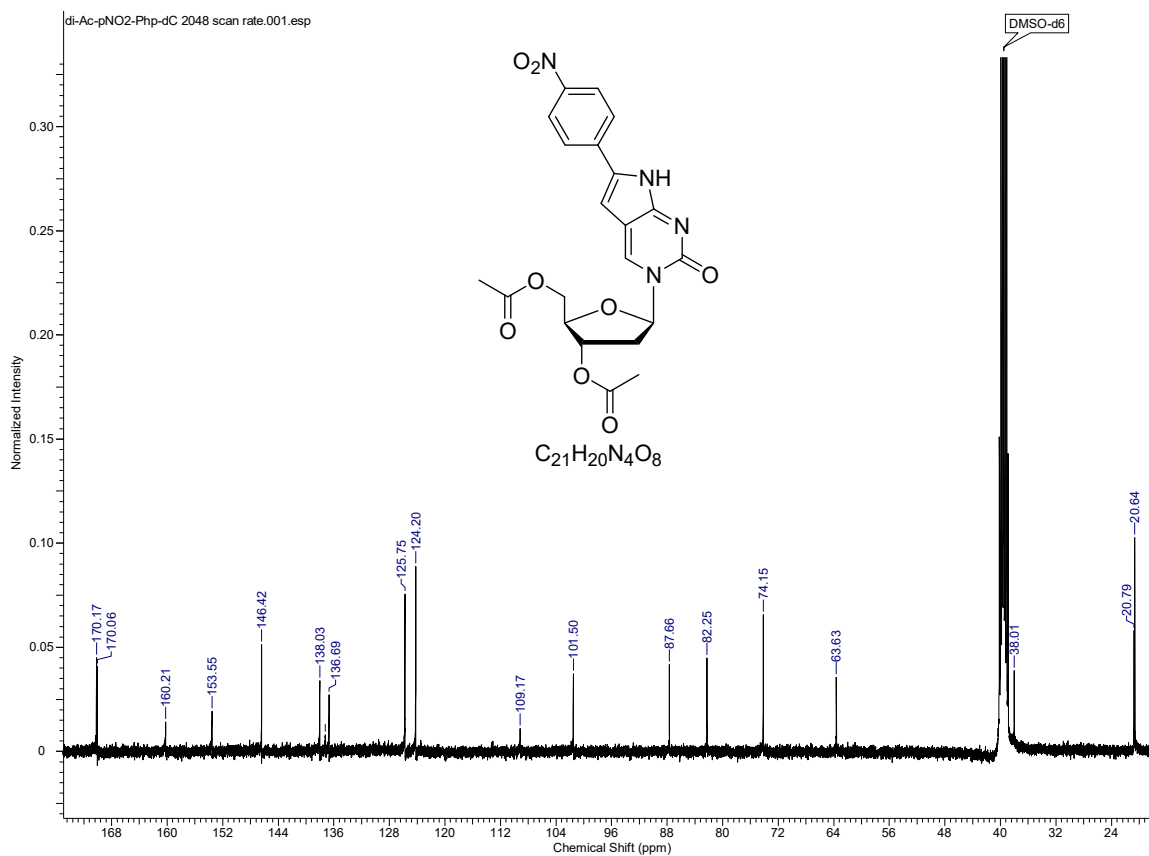
Appendix 5: ^1H NMR spectra 2'-deoxy-6-phenylpyrrolocytidine (6)

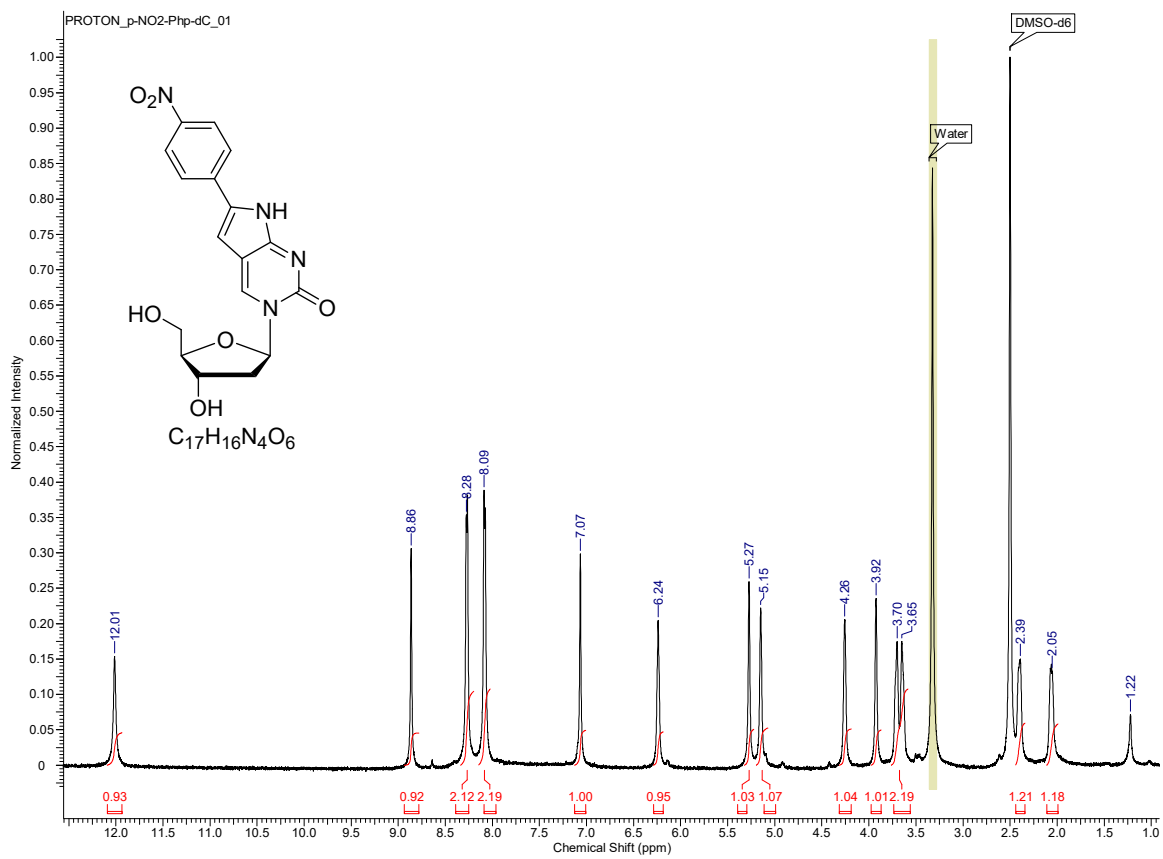
Appendix 6: ^1H NMR spectra 1-ethynyl-4-nitrobenzene

Appendix 7: ¹H NMR spectra 3',5'-di-*O*-acetyl-2'-deoxy-6-(*p*-nitro)phenylpyrrolocytidine (7)



Appendix 8: ^{13}C NMR spectra 3',5'-di-*O*-acetyl-2'-deoxy-6-(*p*-nitro)phenylpyrrolocytidine (7)



Appendix 9: ^1H NMR spectra 2'-deoxy-6-(*p*-nitro)phenylpyrrolocytidine (8)

Appendix 10: The copyright permission

OXFORD UNIVERSITY PRESS LICENSE TERMS AND CONDITIONS

Oct 04, 2017

This Agreement between Atefeh rouhi ("You") and Oxford University Press ("Oxford University Press") consists of your license details and the terms and conditions provided by Oxford University Press and Copyright Clearance Center.

License Number	4201990880244
License date	Oct 04, 2017
Licensed content publisher	Oxford University Press
Licensed content publication	Nucleic Acids Research
Licensed content title	A single-label phenylpyrrolocytidine provides a molecular beacon-like response reporting HIV-1 RT RNase H activity
Licensed content author	Wahba, Alexander S.; Esmaeili, Abbasali
Licensed content date	Nov 20, 2009
Type of Use	Thesis/Dissertation
Institution name	
Title of your work	Synthesis and Photophysical Studies of Pyrrolocytosine Derivatives
Publisher of your work	n/a
Expected publication date	Jan 2018
Permissions cost	0.00 CAD
Value added tax	0.00 CAD
Total	0.00 CAD
Requestor Location	

Publisher Tax ID	GB125506730
Billing Type	Invoice
Billing Address	

Total	0.00 CAD
Terms and Conditions	

Appendix 11: The copyright permission

ELSEVIER LICENSE TERMS AND CONDITIONS

Oct 04, 2017

This Agreement between Atefeh rouhi ("You") and Elsevier ("Elsevier") consists of your license details and the terms and conditions provided by Elsevier and Copyright Clearance Center.

License Number	4202000602539
License date	Oct 04, 2017
Licensed Content Publisher	Elsevier
Licensed Content Publication	Trends in Biochemical Sciences
Licensed Content Title	Historical article: DNA polymorphism and the early history of the double helix
Licensed Content Author	Struther Arnott
Licensed Content Date	Jun 1, 2006
Licensed Content Volume	31
Licensed Content Issue	6
Licensed Content Pages	6
Start Page	349
End Page	354
Type of Use	reuse in a thesis/dissertation
Intended publisher of new work	other
Portion	figures/tables/illustrations
Number of figures/tables/illustrations	1
Format	both print and electronic
Are you the author of this Elsevier article?	No
Will you be translating?	No
Original figure numbers	I am going to use figure 1.
Title of your thesis/dissertation	Synthesis and Photophysical Studies of Pyrrolocytosine Derivatives
Expected completion date	Jan 2018
Estimated size (number of pages)	1
Requestor Location	
Total	0.00 CAD

Curriculum Vitae

Name: Atefeh Rouhi

Post-secondary Education and Degree: Shahid Beheshti University of Medical Science
Tehran, Tehran, Iran
Jan 2007- Oct 2013 Pharm.D.

The University of Western Ontario
London, Ontario, Canada
2015-2017 M.Sc.

Honours and Awards:

Related Work Experience: Teaching Assistant
The University of Western Ontario
Sep 2015- Sep 2017

Research Assistant
The University of Western Ontario
Sep 2015- Sep 2017

Publications: Azizi, F. Rouhi, A. Damha, M. J. Hudson, R. H. E. The effect of the nearest neighbours on the fluorescent properties of PhpC upon incorporation into single stranded and double stranded DNA and the investigation of the possibility of photoinduced electron transfer, *J. Photochem. Photobiol. A.* **2017**, in progress.